GEOMATICS
ENGINEERING

UCGE Reports
Number 20074

Department of Geomatics Engineering

Kinematic Attitude Determination from GPS

(URL: http://www.geomatics.ucalgary.ca/graduatetheses)

by

Ahmed El-Mowafy

1995

SCHULICH
School of Engineering
UNIVERSITY OF CALGARY

THE UNIVERSITY OF CALGARY

KINEMATIC ATTITUDE DETERMINATION FROM GPS

by

AHMED EL-MOWAFY

A THESIS
SUBMITTED TO THE FACULTY OF GRADUATE STUDIES
IN PARTIAL FULFILMENT OF THE REQUIREMENTS FOR THE DEGREE
OF DOCTOR OF PHILOSOPHY

DEPARTMENT OF GEOMATICS ENGINEERING

CALGARY, ALBERTA
DECEMBER, 1994

© Ahmed El-Mowafy 1994

THE UNIVERSITY OF CALGARY

FACULTY OF GRADUATE STUDIES

The undersigned certify that they have read, and recommend to the Faculty of Graduate Studies for acceptance, a dissertation entitled "Kinematic Attitude Determination from GPS" submitted by Ahmed El-Mowafy in partial fulfillment of the requirements for the degree of Doctor of Philosophy.

K.P. Schwarz.

Supervisor, Dr. K.P. Schwarz
Department of Geomatics Engineering

JAR Blais

Dr. J.A.R Blais
Department of Geomatics Engineering

ME Cannon

Dr. M.E. Cannon
Department of Geomatics Engineering

Dr. P. Gu
Department of Mechanical Engineering

David E. Wells

Dr. David E. Wells
University of New Brunswick

Date: 19-12-1994

ABSTRACT

Attitude determination for real-time kinematic applications using simultaneous GPS phase measurements from multiple antennas has been investigated in this thesis. Three techniques for attitude determination are presented and analyzed. These techniques are: indirect determination using the transformation matrix between the body frame and the local-level frame, determination from vector orientation in the local-level frame, and a new approach of direct determination of attitude parameters from phase measurements. A technique of solving the multi-antenna baselines as a network to enhance attitude determination accuracy has been formulated and analyzed. Factors affecting system accuracy have been investigated. Since real-time kinematic applications are the major interest, emphasis is placed on developing ambiguity resolution techniques capable of determining the ambiguities from a single epoch of data, within the time interval between successive outputs. Two schemes are presented. In the first, a statistical criterion is used in identifying the correct ambiguities. In the second, the known geometry of the antenna configuration is used for the same purpose. The performance of attitude determination and ambiguity resolution techniques has been tested on land and in airborne mode. An accurate inertial system was used as an independent reference in both cases. Test results show that attitude parameters can be determined with an accuracy of a few arcminutes for baselines of 3 m length. Test results also show that the presented instantaneous ambiguity resolution techniques are reliable and can be applied for real-time applications.

ACKNOWLEDGEMENTS

I would like to express my deepest appreciation to my distinguished supervisor, Professor Klaus-Peter Schwarz, for his continued support, encouragement and guidance throughout my Ph.D. program.

Thanks also go to Mr. Jan Skaloud, and Mr. N. El-Sheimy for their assistance in data collection, and Dr. Ming Wei for providing some of the software used in this study. Appreciation is also extended to Professor J.A.R Blais for the many fruitful discussions, and to other members of my Examining Committe, Drs. M.E. Cannon, D. Wells and P. Gu for their helpful suggestions. Mr. T. Labach is thanked for preparing the truck and airplane photographs in the manuscript. Special thanks are extended to faculty members and my graduate students colleagues who have made the course of my graduate studies both fruitful and enjoyable through discussions and fellowship.

The financial support of this research by an NSERC operating grant and NSERC strategic grant of Dr. Klaus-Peter Schwarz, and Graduate assistantships and awards is gratefully acknowledged.

Finally, special thanks go to my mother Nawal, my wife Naglaa and my son Ehab for their support, encouragement and patience.

TABLE OF CONTENTS

Page

APPROVAL PAGE ii

ABSTRACT iii

ACKNOWLEDGEMENTS iv

TABLE OF CONTENTS v

LIST OF TABLES xi

LIST OF FIGURES xiii

NOTATION xix

CHAPTER

1. INTRODUCTION 1

    1.1 Background, Motivation and Objective 1

    1.2 Thesis Outline 4

2. CONCEPTS 7

    2.1 Definition of Attitude 7

    2.2 Coordinate Frames Used in Attitude Determination 8

    2.3 Parameterization of the Attitude 10

    2.4 The Concept of Attitude Determination Using GPS Measurements 15

    2.5 Realization of the Rigid Body Assumption 17

    2.6 Applications of the GPS Multi-Antenna Attitude Determination System .. 19

3. GPS ATTITUDE DETERMINATION TECHNIQUES 20

    3.1 GPS Observables and the Observation Equations 20

        3.1.1 Carrier Phase Single Differences 22

        3.1.2 Estimation of the Receiver-to-Satellite Unit Vectors 23

3.1.3 Carrier Phase Double Differences 25

3.2 Attitude Determination Using the Transformation Matrix between the Body Frame and the Local-Level Frame 26

3.2.1 Determination of the Transformation Matrix 27

3.2.2 Determination of Relative Antenna Coordinates in the Body Frame 29

3.2.3 Determination of Relative Antenna Coordinates in the Local-Level Frame 33

3.2.4 Attitude Determination Using a Least-Squares Approach 36

3.3 Attitude Determination from Vector Orientation in the Local-Level Frame 41

3.3.1 Determination of Attitude Parameters 41

3.3.2 Roll Determination in a General Antenna Configuration 43

3.3.3 Singularity of the Solution and Attitude Recovery 45

3.4 Direct Determination of Attitude Parameters from Phase Measurements . 45

3.4.1 The Direct Observation Equations 45

3.4.2 Determination of Attitude Parameters 48

4. FIRST ASSESSMENT OF FACTORS AFFECTING ATTITUDE DETERMINATION ACCURACY 50

4.1 Measurement Errors 50

4.1.1 Multipath 50

4.1.1.1 Characterization of Multipath 54

4.1.1.2 Software and Hardware Multipath Minimization Techniques 55

4.1.1.3 Effect of Multipath on Attitude Determination 59

4.1.2 Receiver noise (Carrier Tracking Loop) 60

4.1.2.1 Equation of Receiver Noise 60

4.1.2.2 Tuning of the Carrier Phase Bandwidth 62

4.1.3 Antenna Phase Centre Variation 63

4.2 Operational Factors 64

4.2.1 Baseline Length 64

4.2.2 Satellite Number and Geometry 66

4.2.3 Antenna Configuration 72

4.2.3.1 Choosing Antenna Locations with Significant Height Differences 72

4.2.3.2 Optimal Antenna Configuration 74

4.2.3.3 Testing the Optimal Antenna Configuration 80

5. COMPARISON BETWEEN DIFFERENT ATTITUDE DETERMINATION TECHNIQUES 83

5.1 Conceptual Comparison 83

5.2 Practical Comparison Based on Field Testing 86

5.2.1 Test Methodology 86

5.2.2 Test Design and Description 87

5.2.3 Considerations for the Comparison of the 3DF and INS 90

5.2.4 Analysis of Results 92

6. ESTIMATION PROCEDURES AND THE NETWORK APPROACH 100

6.1 GPS Carrier Phase Observation Equations in the Network Adjustment Approach 101

6.2 The Constraint Equations 103

6.3 The Constrained Least-Squares Approach 105

6.4 The Weight Matrix 107

6.5 Design Matrices 109

6.6 General Remarks 110

6.7 Comparison between Solving the Multi-Antenna System Baseline-by-Baseline and as a Small Network 112
6.7.1 Conceptual Comparison 112
6.7.2 Practical Comparison Based on Field Testing 113
6.7.2.1 Test Methodology 114
6.7.2.2 Static Testing on the Roof of the Engineering Building 114
6.7.2.3 Static and Kinematic Van Tests 118
7. AMBIGUITY RESOLUTION TECHNIQUES 121
7.1 Existing Methods of Ambiguity Resolution 121
7.2 Initial Estimation of the Carrier Phase Ambiguity 124
7.3 Initial Estimation of the Antenna Baseline 126
7.4 Using Redundant Antennas for Reliable Initial Vector Estimation 128
7.5 Least-Squares Ambiguity Determination with An Optimum Search Region 133
7.6 Using a Primary Group Consisting of Measurements of Two Phase Double Differences and the Baseline Length 136
7.7 Enhancing the Speed of Ambiguity Resolution 138
7.8 Enhancing Robustness of Finding the Correct Ambiguities Using Known Ones 142
7.9 Acceptance of the Correct Ambiguity Set 143
7.9.1 Statistical Tests 143
7.9.2 Conjugate Ambiguity Test 145
7.9.3 Testing Ambiguity Consistency Using A Moving Average Technique 147
7.10 Ambiguity Resolution Using the Known Baseline Geometry 148
8. TESTING OF THE MULTI-ANTENNA SYSTEM 153
8.1 Test Objectives and Methodology 153

8.2 Test Design 154
8.3 Test Description 155
8.3.1 Description of the First Series of Van Tests 155
8.3.2 Description of the Second Series of Van Tests 157
8.3.3 Description of the Airborne Test 159
8.4 Analysis of Ambiguity Resolution 162
8.4.1 Ambiguity Resolution in the First Series of Van Tests 162
8.4.2 Ambiguity Resolution in the Second Series of Van Tests 166
8.4.3 Ambiguity Resolution in the Airborne Test 167
8.5 Analysis of Attitude Determination Performance 172
8.5.1 Attitude Results in the First Series of Van Tests 172
8.5.1.1 Static Test Results 172
8.5.1.2 Kinematic Test Results 175
8.5.2 Attitude Results in the Airborne Test 178
8.5.2.1 Static Results 178
8.5.2.2 Kinematic Results 179
8.5.3 Comparison between Attitude Determination Performance
on Land and in Airborne Tests 182
9. CONCLUSIONS AND RECOMMENDATIONS 183
9.1 Conclusions 183
9.2 Recommendations 188
REFERENCES 190
APPENDIX A: ATTITUDE PARAMETERIZATION 199
A.1 Cayley Axis/angle 199
A.2 Euler Symmetric Parameters (quaternions) 200
A.3 Gibbs Vector 201
A.4 Euler Angles 202

APPENDIX B: THE ATTITUDE MATRIX FOR THE 12 POSSIBLE EULER ANGLE REPRESENTATIONS 205
B.1 Type I Representation 205
B.2 Type II Representation 206

APPENDIX C: DETAILED ATTITUDE RESULTS 208
C.1 Truck Results 208
C.1.1 Static Results 208
C.1.2 Kinematic Results 209
C.2 First Series of Van Tests 210
C.2.1 Static Results 210
C.2.2 Kinematic Results 211
C.3 Second Series of Van Tests 213
C.4 Airborne Results 214
C.4.1 Static Results 214
C.4.2 Kinematic Results 215

8.5 Performance of ambiguity resolution using the known geometry of the antenna configuration 167
8.6 Performance of ambiguity resolution in airborne mode 172
8.7 rms of attitude differences for the static and kinematic runs 175
8.8 rms of attitude components in static and kinematic tests 179

LIST OF TABLES

Table **Page**

2.1 Attitude accuracy requirement for some major applications 19
4.1 Attitude determination accuracy using different numbers of satellites 67
4.2 Comparing optimal and standard antenna configurations 82
5.1 rms of (INS-3DF) differences using different attitude determination techniques 98
5.2 Variance ratio of attitude differences using different attitude determination techniques 99
6.1 rms values for attitude parameters using different methods for the multi-antenna baseline estimation (test 1) 116
6.2 rms values for attitude parameters using different methods for the multi-antenna baseline estimation (test 2) 117
6.3 Variance ratio between different methods in roof tests 118
6.4 rms values for attitude parameters using different methods for the multi-antenna baseline estimation (static van test) 119
6.5 rms values for attitude parameters using different methods for the multi-antenna baseline estimation (kinematic van test) 119
6.6 Variance ratio between different methods in van tests 120
8.1 Number of epochs and ambiguity success rate 162
8.2 Overall performance of different techniques of testing for correct ambiguity resolution 164
8.3 Basic differences in the search approach between different techniques 165
8.4 Ambiguity computation time ratio between the first method and the second and the third 165

LIST OF FIGURES

Figure **Page**

2.1 Euler angles with respect to the body frame 10

2.2 Determination of the roll angle 12

2.3 Spherical triangle of rotations of the z axis of the body frame 14

2.4 The concept of determining the attitude of antenna baselines in the local-level frame using GPS measurements 16

3.1 Carrier phase measurements and range errors 22

3.2 Baseline-to-satellite vectors 23

3.3 Satellite unit vector components 24

3.4 Determining antenna coordinates in the body frame 30

3.5 An orthogonal multi-antenna configuration 42

3.6 General antenna configuration on the platform 43

3.7 Antenna baseline orientation in the local-level frame 47

4.1 Multipath effect on carrier phase 52

4.2 Orientation error and baseline length 65

4.3 Phase single difference 68

4.4 Changes in the observation angle and the measured phase single difference 68

4.5 Changes in baseline-to-satellite observation angle with changes in baseline-to-satellite geometry 71

4.6 Increasing the baseline length due to elevating one of the baseline antennas 73

4.7a Small S/N ratio with low antenna 74

4.7b High S/N ratio with high antenna 74

4.8a Upright orthogonal antenna triad 79

4.8b Inverted orthogonal antenna triad (optimal) 79

4.9 Test configuration of optimal antenna distribution 80

5.1 The use of redundant antennas for attitude determination 86

5.2 Test vehicle with INS and 3DF 88

5.3 Mounting of INS and 3DF in test vehicle 89

5.4 Test traverse 89

5.5a Static 3DF roll 92

5.5b Static INS roll 92

5.6 Static heading difference 92

5.7 Static pitch difference 92

5.8 Static roll difference 93

5.9a Kinematic 3DF roll 93

5.9b Kinematic INS roll 93

5.10 Kinematic heading difference 94

5.11 Kinematic pitch difference 94

5.12 Kinematic roll difference 94

5.13 Attitude differences between the direct approach and the vector orientation approach 95

5.13a Kinematic heading difference 95

5.13b Kinematic pitch difference 95

5.13c Kinematic roll difference 95

5.14 Attitude differences between the transformation matrix approach and the vector orientation approach 97

5.14a Kinematic heading difference 97

5.14b Kinematic pitch difference 97

5.14c Kinematic roll difference 97

6.1 Antenna configuration as a small network 103

6.2 First test configuration 115

6.3 Second test configuration 115

7.1 Phase measurements and ambiguities 125

7.2 Antenna configurations for fast ambiguity resolution 130

7.2a Minimum antenna configuration with small roll angle 130

7.2b Roll-independent antenna configuration 130

7.2c Sequential antenna configuration for large baselines 130

7.2d Overdetermined attitude estimation with small roll angle 130

7.3 Flowchart of ambiguity search procedure 134

7.4 Flowchart of the second method 139

7.5 Flowchart of the third method 139

7.6 General antenna layout 149

7.7 Flowchart of the ambiguity search using the known geometry 151

8.1 Layout of the antennas for heading and pitch 156

8.2 Layout of the antennas for roll determination 156

8.3 Test traverse of the first van test 156

8.4 Test van 158

8.5 Antenna configuration 158

8.6 Test traverse of the second segment of van tests 159

8.7 Airplane used in test (KING AIR 90) 160

8.8 Antenna configuration on the airplane 160

8.9 Flight trajectory 161

8.10 Phase difference of satellite 19 at antenna 1 170

8.11 Phase difference of satellite 19 at antenna 3 170

8.12 Phase difference of satellite 31 at antenna 1 170

8.13 Phase difference of satellite 31 at antenna 3 171

8.14 Difference of phase double difference between satellites 19 and 31 171

8.15a Static 3DF pitch 173

8.15b Static INS pitch 173

8.16 Static heading difference test (1) 174
8.17 Static pitch difference test (1) 174
8.18 Static heading difference test (2) 174
8.19 Static pitch difference test (2) 174
8.20 Static roll difference 174
8.21a Kinematic 3DF pitch 175
8.21b Kinematic INS Pitch 175
8.22 Kinematic heading difference test(1) 176
8.23 Kinematic pitch difference test(1) 176
8.24 Kinematic heading difference test(2) 176
8.25 Kinematic pitch difference test(2) 176
8.26 Kinematic roll difference 176
8.27a 3DF static heading results 178
8.27b 3DF static pitch results 178
8.28 Static (INS-3DF) heading 179
8.29 Static (INS-3DF) pitch 179
8.30a 3DF kinematic heading results 180
8.30b 3DF kinematic pitch results 180
8.31 Kinematic (INS-3DF) heading 180
8.32 Kinematic (INS-3DF) pitch 180
A.1 The body frame and the reference frame 203

Truck Attitude Results

Static Results

C.1 3DF heading 208
C.2 3DF pitch 208
C.3 3DF roll 209

Kinematic Results

C.4 3DF heading 209
C.5 INS heading 209
C.6 3DF pitch 209
C.7 INS pitch 209
C.8 3DF roll 210
C.9 INS roll 210

First Series of Van Test Attitude Results

Static Results

C.10 3DF heading - test (1) 210
C.11 3DF pitch - test (1) 210
C.12 3DF heading - test (1) 211
C.13 3DF pitch - test (2) 211
C.14 3DF roll 211

Kinematic Results

C.15 3DF heading - test (1) 211
C.16 INS heading - test (1) 211
C.17 3DF pitch - test (1) 212
C.18 INS pitch - test (1) 212
C.19 3DF heading - test (2) 212
C.20 INS heading - test (2) 212
C.21 3DF pitch - test (2) 212
C.22 INS pitch - test (2) 212
C.23 3DF roll 213
C.24 INS roll 213

Second Series of Van Test Attitude Results

C.25 3DF heading 213

C.26 3DF pitch 213

C.27 3DF roll 214

Airborne Results

Static Results

C.28 3DF heading 214

C.29 3DF pitch 214

Kinematic Results

C.30 3DF heading 215

C.31 INS heading 215

C.32 3DF pitch 215

C.33 INS pitch 215

NOTATION

i) Symbols

A	the design matrix of partial derivatives
b	antenna baseline length
$\bar{\mathbf{b}}$	antenna baseline vector
B_w	carrier tracking loop bandwidth
c	speed of light
CL	variance-covariance matrix of the observations
$C\hat{\chi}$	variance-covariance matrix of the unknowns
$\hat{\delta}$	vector of corrections of the unknowns
$\delta\Delta\phi$	error in phase single difference
$\bar{\mathbf{e}}$	unit vector
ϕ	single measurement carrier phase
Φ	geodetic latitude of a point
η	yaw
φ	roll
l	observation vector
λ	carrier phase wavelength
Λ	geodetic longitude of a point
n	single carrier phase measurement ambiguity
θ	pitch
T	attitude matrix, direction cosine matrix and transformation matrix
T_j^i	transformation matrix from the frame i to the frame j

v	vector of corrections of the observations
w	misclosure vector
χ	unknown vector
ψ	heading (azimuth)

ii) Operators

Δ	between antennas single difference
∇	between satellites single difference
$\Delta\nabla$	double difference

iii) Point Coordinates in Different Frames

(x,y,z)	coordinates of a point in the body frame
(E,N,U)	coordinates of a point in the local-level frame
(X,Y,Z)	coordinates of a point in the WGS-84 frame

iv) Acronyms

C/A code	Clear/Acquisition code
P code	Precise code
GPS	Global Positioning System
INS	Inertial Navigation System
C/N_o	carrier-to-noise ratio
S/N	signal-to-noise ratio
HDOP	Horizontal Dilution of Precision
VDOP	Vertical Dilution of Precision
PDOP	Position Dilution of Precision
AZDOP	Azimuth Dilution of Precision
El-DOP	Elevation angle Dilution of Precision
WGS-84	World Geodetic System 1984

v) Conventions

1. Vectors are represented by lower case letters.
2. Matrices are represented by capital letters.
3. Transformation between coordinate frames in a sequence is performed as follows:

$$T_k^{\,i} = T_k^{\,j}\ T_j^{\,i}$$

where the subscript frame index of the first rotation matrix on the right hand side ($T_j^{\,i}$) cancels with the superscript index of the following rotation matrix ($T_k^{\,j}$).

CHAPTER 1

INTRODUCTION

1.1 Background, Motivation and Objective

The feasibility of achieving cm-accuracy level in relative positioning using the Global Positioning System (GPS), see for instance (Remondi,1984), (Leick,1990) and (Hofmann-Wellenhof,1992), has encouraged applications other than positioning and navigation for this satellite-based radio navigation system. One important application is attitude determination, i.e. the orientation of a moving vehicle, ship or aircraft with respect to a well-defined reference system. The main principle in obtaining attitude from GPS is the determination of baseline vectors between antennas mounted on the vehicle. The vectors are defined in the GPS reference frame, and thus orientation is with respect to that frame. Since two or more antennas have to be used on the moving vehicle, these systems have become known as multi-antenna attitude determination systems.

Due to the short baselines used, errors common to satellites and antennas as well as atmospheric propagation errors can be eliminated or greatly reduced when differencing the measurements. Thus, accuracy at the millimetre level in the baseline vectors can be achieved. This transforms into attitude determination accuracy of a few arcminutes. With this accuracy the system is of interest for many kinematic applications. The feasibility of the attitude determination systems for kinematic applications has been shown in different areas, on land (Cannon et al, 1992), (El-Mowafy and Schwarz, 1994a), in shipborne mode (Lu et al.,1993), (Diefes et al.,1993a,b), (Lachapelle el al.,1994), (Kuhl et al.,1994) and (McMillan,1994), and in airborne mode (Van Graas and Brassch,1991), (Cohen and Parkinson,1992), (Cannon et al.,1994), (Sun,1994) and (Schade and Cramer,1994).

Two concepts have been used so far to extract orientation information from the baseline vectors. In both, the GPS determined antenna baseline vectors are first transformed from the WGS-84 frame to the local-level frame, and then either a transformation matrix or vector orientation in the local-level frame is used to determine the attitude. For instance, (Ferguson et al.,1991), (Brown,1992), (Cohen et al.,1992) and (Lachapelle et al.,1994) used the transformation matrix approach, and (Brown and Ward,1990), (Knight and Hatch,1990), and (Brown,1992) used the vector orientation approach. So far, a direct approach that relates the differenced phase measurements to attitude parameters has not been used. Except for an accuracy comparison in (Lu et al, 1993), there has not been a comprehensive comparison of different methods for attitude determination. No attempt has been made to show the strengths and weaknesses of different techniques with a view to implementation considerations for different kinematic applications. The first objective of this study is therefore to address these issues and to analyze algorithm modeling concepts, methodologies, assumptions, and performances. Such a study will help to clarify and enhance model reliability, robustness and accuracy of GPS attitude determination.

The second objective is to compare the generally used technique of treating antenna baselines individually, i.e. solving them baseline-by-baseline, with a method that treats them as a geometric network. In cases where the antenna positions do not experience significant relative movements, multiple antenna baselines can be taken as fixed on the moving vehicle and geometric constraints can be applied to this configuration. For real-time applications, where the number of measurements available is limited, such information is vital. Solving the baselines as a network becomes then an attractive approach that can provide better accuracy and reliability.

To assess system performance, factors affecting its accuracy have to be investigated. Measurement errors, such as multipath, affect the accuracy achievable. Operational factors such as baseline length, satellite number and geometry, and the selected antenna configuration greatly govern system accuracy. Work in this area by (Ferguson et al.,1992), (Brassch,1992), (Jurgens et al.,1992) and (Comp,1993) indicates the need for further research. Without analyzing these factors it is hard to understand and improve system performance in different environments.

To achieve the needed accuracy, carrier phase is the only type of GPS measurements that can be used. The main difficulty in using carrier phase measurements is the resolution of the unknown whole number of cycles, called the phase ambiguity. Moreover, since in kinematic applications and in navigation, a real-time solution is required, i.e. the ambiguities must be resolved instantaneously. The term “instantaneously” will be used here and in the following as meaning that the ambiguities are solved from data of a single epoch within the time interval given by the data rate. It does not mean that a real-time solution has been implemented. Although the technique of static initialization, applied in DGPS, can be used initially, it cannot be applied if re-initialization of the ambiguities is needed during motion. Resolving ambiguities using "on the fly" techniques applied for DGPS, e.g. Frei et al. (1993), is too slow for most kinematic applications. However, the constraints given by the antenna configuration can be used to accelerate ambiguity resolution for multi-antenna systems to achieve an instantaneous solution. This approach is based on previous work by (Hatch,1989) and (Jurgens et al.,1991 and 1992) and has been adopted here with view to real-time applications.

The overall objective of this thesis is to propose and analyze methods and techniques for reliable kinematic attitude determination. Different techniques for attitude determination have been developed, implemented and compared to show their performance in different environments. Factors affecting system accuracy will be investigated to assess their effect on attitude determination. A network solution has been developed and tested to evaluate the expected gain in accuracy. Reliable instantaneous ambiguity resolution algorithms will be developed and tested in different environments, including land and airborne tests. Finally, attitude determination accuracy will be assessed for these environments.

1.2 Thesis Outline

In Chapter 2, fundamental aspects of attitude determination are briefly reviewed. Attitude of a rigid body is defined and the coordinate frames used in attitude representation are described. Then, the definition of attitude parameters used throughout this study, i.e. heading, pitch and roll, is given. The concept of using GPS phase measurements for attitude determination of a rigid body using a multi-antenna system is outlined. A discussion of how well the rigid body assumption can be realized is given. The chapter concludes by reviewing possible applications of attitude determination from GPS.

In Chapter 3, mathematical methodologies of attitude determination using GPS phase measurements are derived. First, GPS observables are described, and differencing techniques to reduce common errors at different antennas are reviewed. Three techniques for attitude determination are presented, namely attitude determination using the transformation matrix between the body frame and the geodetic local-level frame, attitude determination from direct vector orientation in the local-level frame, and a new approach of direct determination of attitude parameters from phase measurements. The concept, development and implementation of each technique are given in detail.

Chapter 4 concentrates on investigating and analyzing the main factors affecting accuracy of attitude determination by use of a multi-antenna system. These factors are categorized in two groups. The first is related to errors in GPS measurements, including multipath, receiver noise and antenna phase centre variation. The focus in this section is on multipath as the major error source. The second group includes operational factors such as baseline length, satellite number and geometry, and antenna configuration. The effect of each factor on accuracy of attitude determination is assessed. The chapter concludes by proposing an optimal antenna configuration. This configuration is tested to assess its usefulness.

Chapter 5 focuses on the comparison between the different attitude determination techniques presented. The advantages and disadvantages of each technique are investigated in terms of initialization requirement, implementation, computation time needed, and flexibility of choosing antenna locations. The theoretical comparison is verified by field tests. The output of each method is compared to that of an accurate inertial system, as an independent reference.

In Chapter 6, a new approach for solving the multi-antenna baselines as a small network is presented. This approach has advantages over a baseline-by-baseline solution because it constrains the known geometry of the antenna configuration, and considers the correlation between antenna baselines. The constrained least-squares adjustment approach is implemented and described in detail. Finally, a theoretical and practical comparison between solving the baselines one by one and as a network is performed, to demonstrate the benefits of using the network approach.

Since the instantaneous ambiguity determination is the key element in solving the attitude in real-time kinematic applications, Chapter 7 focuses on developing reliable instantaneous ambiguity resolution techniques. First, existing techniques are briefly reviewed. Then, two efficient approaches are discussed in detail. In the first, the correct ambiguities are identified as the ones giving minimum variance of the measurements, in the second the known geometry of the antenna configuration is used to determine the correct ambiguities. The theory behind each technique is given followed by a detailed description. Different factors and algorithms that can enhance computational speed and reliability of finding the correct ambiguities are presented.

In Chapter 8, the proposed ambiguity resolution techniques are tested in different operational environments. Tests on land and in an airborne mode have been performed. Although the data were processed in post mission, the techniques developed are applicable to the real-time case. From test results, the capability and reliability of achieving an instantaneous solution is shown. The performance and accuracy of attitude determination in kinematic environments are investigated and compared.

Conclusions and recommendations for further research are presented in Chapter 9.

CHAPTER 2

CONCEPTS

This chapter paves the way to subsequent chapters by briefly discussing some important concepts underlying this thesis. Attitude, its parameterization, and the coordinate frames used in its determination are defined. The concept of attitude determination using GPS measurements is then stated and the realization of the rigid body assumption made in deriving the attitude model is discussed.

2.1 Definition of Attitude

The attitude of a rigid body is defined as its orientation in space with respect to a well defined and stable reference coordinate system. A rigid body is a body with finite dimensions, which maintains the property that the relative positions of all its points, defined in a coordinate frame fixed within the body, remain the same under rotations and translations. The orientation of the rigid body is defined by three non-collinear points within the body which often are chosen in such a way that they represent the orientation of its main longitudinal and transverse axes (centre lines). In practice, the orientation of the rigid body is obtained by determining a coordinate frame that coincides or is parallel to these axes. Such a frame will be called the body frame.

An example of a well-defined reference system is the Conventional Terrestrial (CT) system. Since this study is concerned with attitude determination using the Global Positioning System (GPS), the World Geodetic System 1984 (WGS-84) can be used as a realization of the CT system. On the other hand, in navigation as well as in classical surveying, local attitude determination is important. In this case, the geodetic local-level frame with respect to the ellipsoid of the WGS 84 is usually chosen as the reference coordinate frame. Therefore, in this study, the attitude will be defined with respect to this frame. Determining the attitude in the local-level frame from the one obtained in the WGS-84 frame can be achieved by defining the relation between the two coordinate frames. This is done by specifying the position of the origin of the local-level frame and the orientation of its axes in the WGS-84 frame.

2.2 Coordinate Frames Used in Attitude Determination

I- The body frame:

The body frame is a frame defined within the rigid body. It consists of an orthogonal triad of three axes. The body frame can be defined as follows:

x : pointing to the right side of the rigid body when looking forward (transverse axis).
y : pointing forward along the longitudinal axis of the rigid body.
z : pointing up, perpendicular to the x-y plane.
origin : intersection of the x, y and z axes.

The system is a right-handed system.

II- The local-level frame:

The definition of the local-level frame used in this study is as follows:

origin : identical to the origin of the body frame to eliminate the need to determined the shift vector between the two origins.
E : pointing East in the plane of the ellipsoidal horizon.

N : pointing towards geodetic North, i.e. in the North direction of the ellipsoidal meridian in the plane of the ellipsoidal horizon.

U : perpendicular to the N-E plane, pointing upwards.

The local-level frame is a right-handed system. This system is thus different from the local-geodetic system, which is a left-handed system because the sequence of the N-E axes interchanged. The local-level frame is defined with respect to the ellipsoid, and is therefore different from the local-astronomic frame, which is defined with respect to an equipotential surface, in most cases the geoid.

III- The World Geodetic System 1984 (WGS-84):

The WGS-84 as a geodetic reference system is defined as a reference ellipsoid with a known reference gravity potential. This frame is defined as (Sherrer,1985), (DMA,1991), and (Malys and Slater,1994):

origin : centre of mass of the Earth.

Z : pointing towards the Conventional Terrestrial Pole (CTP) for polar motion, as defined by the Bureau International de l'Heure (BIH) for the epoch 1984.0. It is the rotational axis of the WGS-84 frame.

X : is the intersection of the reference meridian plane and the equatorial plane defined by the CTP, where the reference meridian is the Zero Meridian (meridian of Greenwich) defined by the BIH for the epoch 1984.0.

Y : completes a right-handed system, and lies in the equatorial plane defined by the CTP.

The relation between antenna vectors in the local-level frame (r_l) and in the WGS-84 frame ($r_{WGS\text{-}8}$) can be given as:

$$r_{WGS\text{-}84} = T_U(\Lambda\text{-}180)\ T_E(\Phi\text{-}90)\ r_l \qquad (2.1)$$

Where:

$T_E(\Phi\text{-}90)$: the rotation matrix about the east axis of the local-level frame by the angle (Φ-90), where Φ is the geodetic latitude of the local-level frame origin,

$T_U(\Lambda\text{-}180)$: the rotation matrix about the vertical axis of the local-level frame by the angle (Λ-180), where Λ is the geodetic longitude of the local-level frame origin.

2.3 Parameterization of the Attitude

The attitude, i.e. the orientation of the body frame with respect to the local-level frame can be defined by three rotational angles, known as heading (azimuth), pitch and roll. In some references, they are given as yaw, pitch and roll. These parameters are widely used in navigation because they have a simple and clear physical interpretation. Figure 2.1 illustrates these parameters.

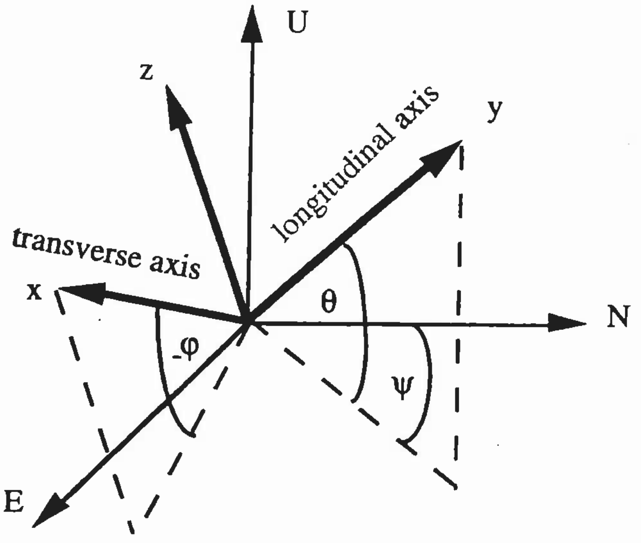

Fig. 2.1 Attitude parameters

From Figure 2.1, attitude parameters can be defined as follows:

heading (ψ) : the angle between the north axis of the geodetic local-level frame and the projection of the longitudinal axes (forward axis) of the body frame on the ellipsoidal horizon. It is positive in clockwise direction when viewed from the positive end of the vertical axis of the body frame.

yaw (η) : this angle has the same meaning and value as the azimuth angle, but differs in sign, i.e. it is positive in counter-clockwise direction.

pitch (θ) : the elevation angle of the longitudinal axis of the body frame from the ellipsoidal horizon. The positive rotational direction of this angle is counter-clockwise when seen from the positive end of the transverse axis of the body frame. Thus, the angle is positive above the horizon.

roll (φ) : the elevation of the transverse axis of the body frame from the ellipsoidal horizon. The positive direction of this angle is counter-clockwise when viewed from the positive end of the longitudinal axis of the body frame. Thus the angle is positive below the horizon (depression angle).

Parameterization of the attitude can also be done in other ways. Four of them, namely the Cayley axis/angle representation, the Euler symmetric parameter representation, the Gibbs vector representation, and the Euler angle representation are given in Appendix A following (Wertz, 1978). The attitude in these parameterization methods is represented by way of a coordinate transformation matrix, which transforms the body frame to a chosen reference coordinate system, (Goldstein,1980). Therefore, the transformation matrix is often called the attitude matrix. All attitude parameterization are related to the general attitude matrix. The attitude matrix is a proper real orthogonal matrix. Thus, its elements are not all independent, and theoretically only three parameters are needed to define the attitude matrix. However, a four parameters parameterization is often preferable to avoid singularities in parameter estimation.

Although Euler angles, determined from the attitude matrix, are often called heading, pitch and roll, they are not exactly the same as the attitude parameters defined above. The attitude matrix is obtained from the matrix product of three elementary matrices which describe successive rotations about the axes of the body frame. Thus, the Euler angles after each rotation refer to the new orientation of the body frame with respect to the local-level frame. Changes in heading, pitch, or roll angles are thus dependent on the sequence of rotation used. Therefore, Euler angles, determined from the attitude matrix, must be corrected to be compatible with heading, pitch and roll as defined above. A method for correcting Euler angles for the case of using the rotation sequence pitch-roll-heading will be given below. This sequence is given as it will be used in the field tests described in the remainder of the thesis. Similar corrections will be needed if other sequences are adopted.

Assuming that the chosen sequence of rotations is pitch-roll-heading. First, the z-y plane of the body frame is rotated about the x axis by the pitch angle (θ). In this case, the pitch angle of the Euler rotation angles is the same as the pitch angle defined above. However, the z axis is rotated and becomes z', as shown in Figure 2.2. This means that the next rotation angle, the Euler-roll, that will rotate the plane z'-x about the y axis, will be φ_2 instead of the original roll angle φ_1. For convenience, the angles φ_1 and φ_2 are shown above the N-U plane in Figure 2.2.

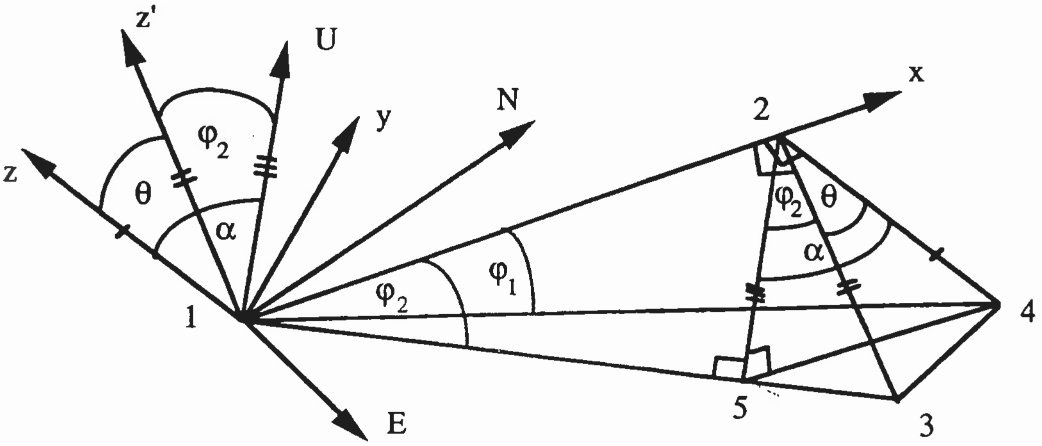

Fig. 2.2 Determination of the roll angle

Determination of the angle φ_1 from φ_2 can be performed by first obtaining φ_1 from :

$$\tan \varphi_1 = \frac{l_{24}}{l_{12}} , \tag{2.2}$$

where l_{12} is the length of the baseline 1-2 along the x axis of the body frame, and l_{24} is length of the line 2-4, which is parallel to the z axis and intersects with the ellipsoidal-horizon (the plane N-E) in point 4. After rotation by the angle θ, the plane z'-x becomes orthogonal to the N-E plane. Thus, the line 2-5 that is parallel to the U axis and intersects the N-E plane at point 5, will be orthogonal to the line 5-4 and 1-3, where 1-3 is the intersection of the plane z'-x with the N-E plane, and the line 2-3 is parallel to z'. The length 2-5 is determined from:

$$l_{25} = l_{12} \sin \varphi_2 \tag{2.3}$$

The line 2-4 can then be determined from the triangle 2-5-4 as follows:

$$l_{24} = \frac{l_{25}}{\cos \alpha} \tag{2.4}$$

The angle α can be determined from the spherical triangle z-z'-U, shown in Figure 2.3, using the cosine rule (or Napier's rule for right angled spherical triangles) as follows:

$$\cos \alpha = \cos \theta \ \cos \varphi_2 \tag{2.5}$$

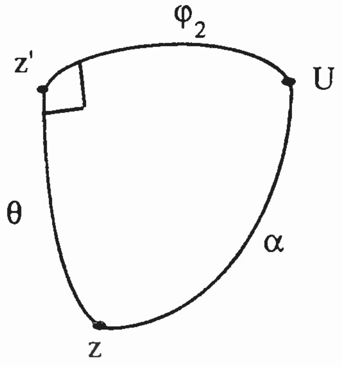

Fig. 2.3 Spherical triangle of rotations of the z axis of the body frame

Substitution into equation (2.3) and (2.4) gives:

$$l_{24} = l_{12} \frac{\tan \varphi_2}{\cos \theta} \tag{2.6}$$

Finally, using (2.2) gives the roll angle φ_1 in terms of the rotation angle φ_2, where:

$$\tan \varphi_1 = \frac{\tan \varphi_2}{\cos \theta} \tag{2.7}$$

After rotating the plane z'-x by the angle φ_2, the plane x-y is rotated by the heading angle (ψ). The heading angle determined from Euler rotations is the same as defined in this study. Thus, in the rotation sequence pitch-roll-heading using the Euler angle representation, only the roll angle will be different from the one estimated from the attitude matrix.

Equation (2.7) shows that the difference between Euler-angle (φ_2) and the roll angle (φ_1) is dependent on the magnitude of the pitch and roll angles. For small angles (less than three degrees) the difference between the two angles is less than 14 arcseconds. However, as the angles grow, the difference increases and reaches the arcminute level.

2.4 The Concept of Attitude Determination Using GPS Measurements

The attitude of a rigid body, such as a vehicle, ship or airplane, is the orientation of its body frame in space with respect to a well defined reference frame. By defining a body frame by a set of at least three non-collinear GPS antennas attached to the vehicle, attitude determination can be done by measuring the orientation of the antenna baseline vectors with respect to the reference frame.

Figure 2.4 shows the concept of attitude determination using GPS measurements. For simplicity, the baselines A-A’ and A-A” are assumed parallel to the longitudinal and transverse axes of the body frame of a moving vehicle. Two different instants are considered, between them the vehicle changes its position and orientation.

The principle of determining orientation of antenna baseline vectors from GPS measurements uses the satellites as reference points with known positions. By measuring the ranges between the antennas and the satellites, the relative positions between the antennas are determined in the WGS-84 frame. These relative positions are sufficient to determine the baselines orientation in the WGS-84 frame. To obtain the attitude in the local-level frame, the position of the origin of the local level frame is determined in the WGS-84 system. Antenna A can be selected as the origin of the local-level frame, where its coordinates can be determined using GPS measurements. The orientation of the local-level frame can then be obtained by using the transformation formula given in equation 2.1.

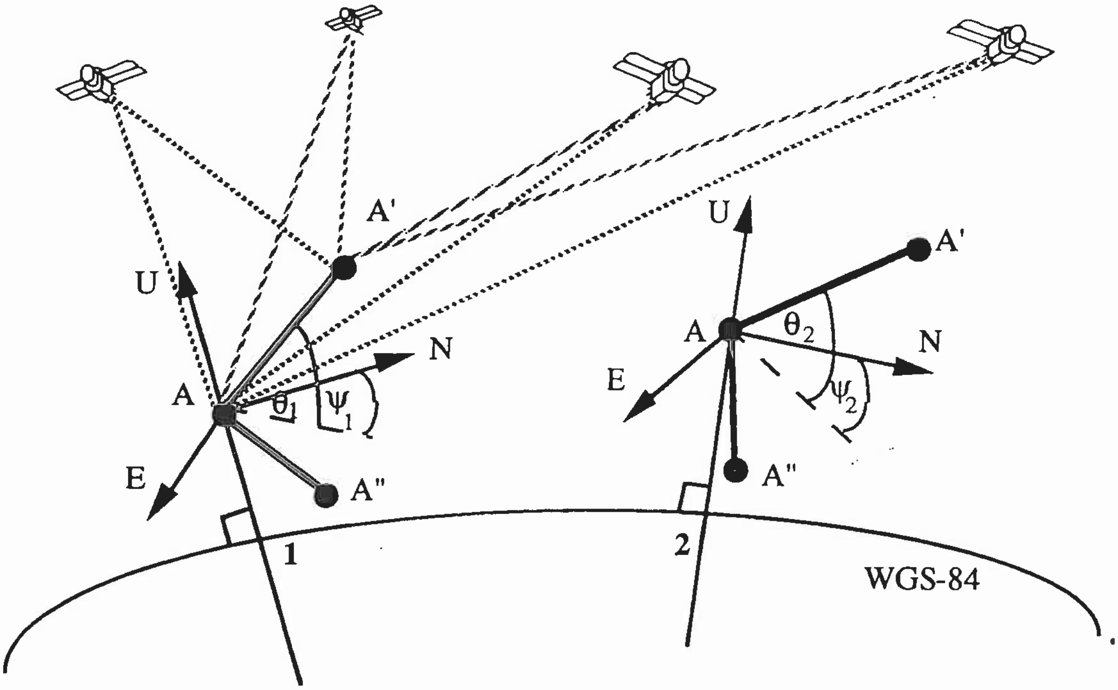

Fig. 2.4 The concept of determining the attitude of antenna baselines in the local-level frame using GPS measurements

After fixing the position and orientation of the local-level frame and the orientation of the antenna baselines in the WGS-84 frame, the baseline orientation with respect to the local-level frame can be determined. This is shown as heading ψ_1 and pitch θ_1 for the baseline A-A' at point 1. By determining the orientation of the baseline A-A", the roll can be defined in a similar fashion. This completes the 3D attitude determination at point 1. Similarly, the attitude of the vehicle at point 2 can be determined.

One should notice that, because of the change in curvature of the WGS-84 ellipsoid from one point to another, the orientation of the local-level frame changes with changes in the position of its origin. Thus, even if the antenna baseline triad (A-A', A-A") have the same orientation with respect to the WGS-84 frame at point 1 and 2, its orientation with respect to their local-level frames will change. Therefore, the attitude changes as a function of changes in baseline orientation as well as changes in the position of the antennas on the ellipsoid.

A GPS based attitude determination system is usually known as a multi-antenna system. It can either use a common receiver for all antennas or independent receivers. In the first case, the antennas are connected to the same oscillator. Thus, there will be one oscillator governing all GPS measurements, and therefore these measurements are correlated. In the second case, separate receivers and antennas are used. In this case, measurements from each antenna are governed by an independent oscillator; thus, measurements from different antennas will be uncorrelated. The use of one oscillator for all antennas theoretically cancels receiver time error, and thus phase single differences can be used instead of phase double differences. More details will be given in Chapters 3 and 7.

2.5 Realization of the Rigid Body Assumption

For determination of the attitude of a moving vehicle using GPS measurements, stability of the body frame is the main concern. Since no vehicle is completely rigid, the GPS antennas must be mounted at stable points that represent the main axes of the vehicle as well as possible. The antennas, as the points representing the moving vehicle and its body frame, should be rigidly mounted on the surface of the moving vehicle.

In practice, the body of large vehicles, ships or airplanes may experience changes due to torsion, vibration, bending, flexing or temperature changes. These changes may result in significant attitude errors. For instance, an error of 1 mm in relative positioning produces an orientation error of 1 arcminute for a baseline of 3 m in length. In attitude determination, the relative changes in antenna positions are more important than the changes at the individual antennas. Therefore, the effect of these errors on attitude determination is dependent on relative antenna positions.

Changes in the body of the vehicle due to the errors mentioned above are usually small in land vehicles and do not exceed a few millimetres. In airborne mode, antennas on the fuselage may have errors between 1 cm - 2 cm, mainly due to temperature changes (Lachapelle et al.,1994a). However, if they are placed on the wings, changes will be much larger and can approach the decimetre level (Corbett,1993). In relative mode, these large errors can be differenced out if a symmetric antenna configuration is used. In shipborne mode, changes are less consistent. Therefore, it is important to choose antenna locations on the surface of the moving vehicle which minimize the effect of non-rigidity of the body on attitude determination. Other considerations which govern the choice of antenna location, are baseline length, minimization of multipath, and clear reception of satellite signals (see Chapter 4).

Antenna mounting is another factor that must be considered carefully to ensure stability of the antennas. For instance, in shipborne mode, the antennas can usually not be mounted on the surface as in land vehicle and in airborne modes. When elevating the antennas above the surface, great care has to be given to the antenna supporting structure to minimize antenna vibrations.

Studying changes of the body due to temperature changes, torsion, vibration, bending and flexing in different environments can provide important information to assess attitude changes due to these errors. Sometimes, modeling of these errors is possible and their effect can be removed to some extent. For instance, (Cohen et al.,1994) and (Cannon et al.,1994) used wing flexing models to estimate changes in antenna positions on the wings to reduce this error.

2.6 Applications of the GPS Multi-Antenna Attitude Determination System

For GPS attitude determination system, the baselines used are short, typically between 2 and 30 metres; therefore, most of the orbital and atmospheric errors cancel. The error sources that affect system accuracy are multipath, phase noise, and antenna phase centre variation. Other factors affecting system accuracy are baseline length, satellite number and distribution, and antenna configuration, see Chapter 4 for more details on these factors. Using a baseline of 3 metres length, heading accuracies of 3-7 arcminutes, and pitch and roll accuracies of 5-8 arcminutes can be achieved, (El-Mowafy and Schwarz,1994a,b). Sub-arcminute accuracy can be achieved by using longer baselines (Lachapelle,1994b).

This level of accuracy is sufficient for a number of applications. Table 2.1 shows accuracy requirement of applications where the multi-antenna technology can be used, see (Wells et al.,1986) and (Schwarz et al.,1994). In general, the multi-antenna system is usable for applications that tolerate arcminute level accuracies.

Application	Attitude Accuracy
Airborne remote sensing for Cartographic mapping	10’ -20’
Airborne remote sensing for resource applications	20’ 30’
Hydrographic bathymetry	6’
Satellites in orbit	1°
Most low accuracy hydrographic navigation in open water	1°
Land vehicle navigation for most civilian and military applications	30’ - 1°
Airborne navigation (except during take off and in the final approach)	30’ - 1°

Table 2.1 Attitude accuracy requirement for some major applications

CHAPTER 3

GPS ATTITUDE DETERMINATION TECHNIQUES

This chapter presents different techniques that can be applied for attitude determination, using GPS measurements. These techniques are: indirect determination using the transformation matrix between the body frame and the local-level frame, determination from direct vector orientation in the local-level frame, and direct determination of attitude parameters from phase measurements. The chapter starts by describing GPS observation equations. Next, the detailed description of each technique including concept, development and implementation is given.

3.1 GPS Observables and the Observation Equations

GPS signals received at the measuring antennas are carrier waves defined on the L1 and L2 bands, C/A and P pseudo random noise codes, and the satellite message. GPS signals give two types of measurements, namely pseudorange measurements, estimated from the C/A or the P codes, and carrier phase measurements, derived from carrier waves of L1 or L2. Both measurements can be used to give the distance between the transmitting satellite and the receiving antenna. The pseudorange measurement is the measured signal transit time scaled by the speed of light. The transmission time is determined by correlating the incoming satellite pseudo random noise code (C/A or P codes) to an identical code generated by the receiver. It is then estimated as the time needed by the receiver's internal code-tracking loop to shift the receiver replica of the code to achieve maximum correlation with the code incoming from the satellite. Phase measurements are obtained by differencing between the phase of the received satellite carrier signal, measured at the receiver, and the phase of the receiver local oscillator, at the epoch of measurement (Leick,1990). By multiplying the total number of phase cycles by the known carrier wavelength, the satellite-to-receiver distance is determined. The major problem of using phase measurements is that the receivers are capable of measuring only a fraction of a cycle. Thus, there is an unknown number of whole cycles that cannot be measured when first locking on the received signal. This unknown number of cycles is called the phase ambiguity.

The wavelength of the C/A and P codes are approximately 293.3 and 29.3 metres, respectively. Those of the L1 and L2 carriers are approximately 0.190 and 0.244 (Milliken and Zoller,1980). With recent developments in receiver technology, the accuracy of measuring any GPS observables is better than 1/100 of the observable wavelength. Reliable attitude estimation requires the determination of antenna vectors at the millimetre level. Since the accuracy of the estimated vector components used for attitude determination is directly related to the accuracy of the measurements employed, carrier phase measurements are the only measurements that can be used for this purpose.

The carrier phase observation equation is given as:

$$-\phi = \rho + \delta\rho + c\,(\delta t - \delta T) + \lambda\, n - \delta_{ion} + \delta_{trop} + \varepsilon(\phi) \qquad (3.1)$$

see (Wells et al., 1986), where ϕ is the measured phase in metres, estimated as the measured phase in cycles multiplied by the carrier wavelength. ρ is the satellite-to-receiver range, $\delta\rho$ is the range correction due to orbital estimation errors, c is the speed of light in the vacuum, δt and δT are the satellite and receiver clock errors, respectively. λ is the carrier wavelength, n is the phase ambiguity, δ_{ion} and δ_{trop} are the ionospheric and tropospheric errors, and finally $\varepsilon(\phi)$ is the combined receiver and multipath noise. Figure 3.1 shows the carrier phase range error for the satellite A with respect to the baseline 1-2.

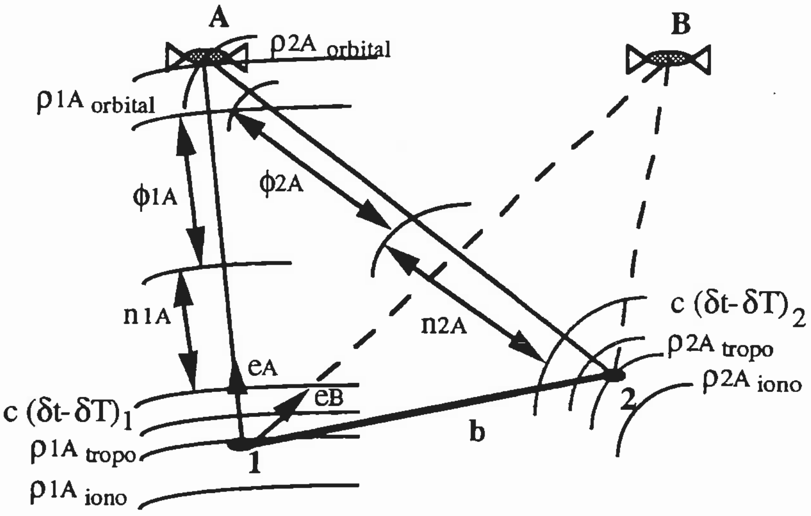

Fig. 3.1 Carrier phase measurements and range errors

3.1.1 Carrier Phase Single Differences

To eliminate some of the measurement errors, differencing techniques are usually employed. For instance, the difference of phase measurements at two antennas removes the satellite related errors (Wells et al.,1986). It is called between antenna phase single difference. Due to the short distances spacing the antennas in an attitude determination system, the orbital, tropospheric and the ionospheric errors cancel out. However, the noise term is increased by a factor of $\sqrt{2}$ because two measurements are used in the differencing process. The single difference observation equation, between the antennas 1 and 2, can be written as:

$$\Delta\phi = \vec{e} \cdot \vec{b} + c\,(\delta T_1 - \delta T_2) + (n_1 - n_2)\,\lambda + \Delta\varepsilon(\phi) \tag{3.2}$$

where $\vec{e}$ is the baseline-to-satellite unit vector, $\vec{b}$ is the antenna baseline vector, defined in the WGS-84 frame, $(\delta T_1 - \delta T_2)$ is the difference between receiver clock errors of the two antennas (1 and 2) channels, and $(n_1 - n_2)$ is the single difference ambiguity.

3.1.2 Estimation of the Receiver-to-Satellite Unit Vectors

To compute the receiver-to-satellite unit vectors, one can consider that GPS signals are transferred as carrier wave fronts, which are planes perpendicular to the direction of their transmission. The reason behind this assumption is that the distance between the satellites and the antennas baseline are very big compared to the baseline lengths, which are limited to few metres. As shown in Figure 3.2, the assumption made means that the two wave transmission lines between the satellite i and the antennas 1 and 2 (the rays w1 and w2 in the figure) are parallel and perpendicular to the plane **P**. The plane **P** is defined as the wave front plane. The ray w1 intersects with the plane **P** in the point 1'. Therefore, the distance 1-1' can be considered the same as the carrier phase single difference, expressed in metres, between the two antennas. Since the rays w1 and w2 are parallel, the antenna-to-satellite unit vectors along the two rays are assumed parallel. Therefore the unit vector included in the observation equation can be computed from coordinates at either ends of the baseline.

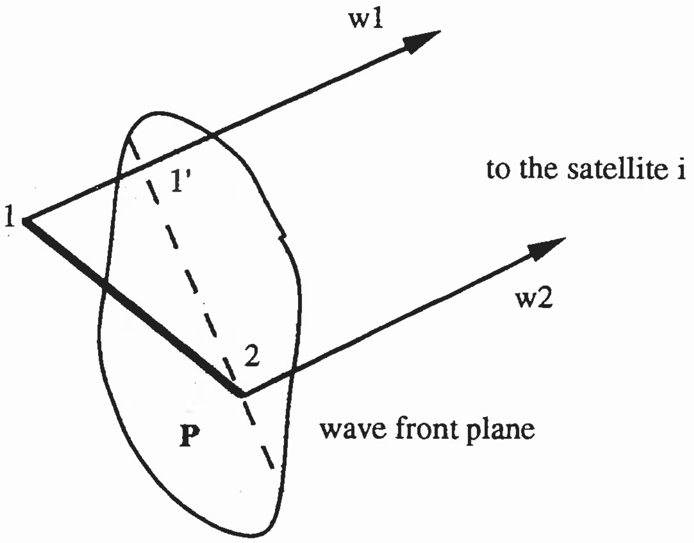

Fig. 3.2 Baseline-to-satellite vectors

Figure 3.3 illustrates the unit vector orientation in the WGS-84 frame. If the unit vector is computed from the coordinates of antenna number 1, i.e. $(X,Y,Z)_1$, and the satellite coordinates $(X,Y,Z)_s$, the unit vector components in the WGS-84 frame (e_X,e_Y,e_Z) can be determined as follows:

$$e_X = \cos \upsilon \;\; \sin \mu \tag{3.3}$$

$$e_Y = \cos \upsilon \;\; \cos \mu \tag{3.4}$$

$$e_Z = \sin \upsilon \tag{3.5}$$

where:

$$\upsilon = \tan^{-1} \frac{(Z_s - Z_1)}{\sqrt{(X_s - X_1)^2 + (Y_s - Y_1)^2}} \tag{3.6}$$

$$\mu = \tan^{-1} \frac{(X_s - X_1)}{(Y_s - Y_1)} \tag{3.7}$$

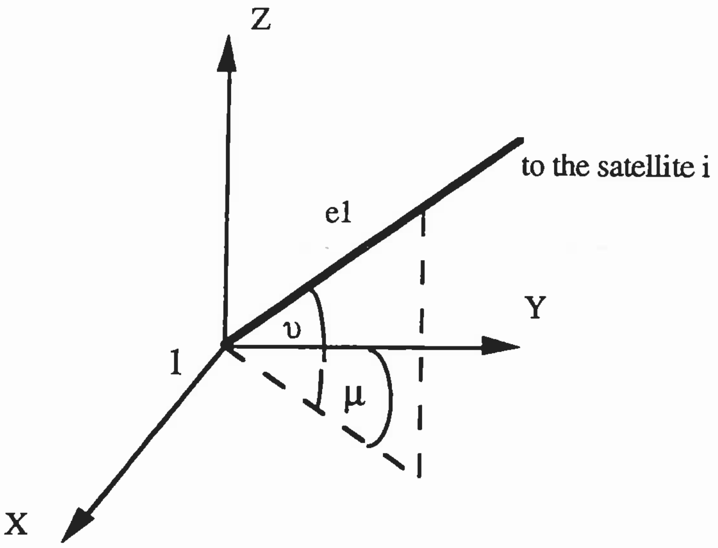

Fig. 3.3 Satellite unit vector components

3.1.3 Carrier Phase Double Differences

If the phase single difference of satellite A is differenced with that of satellite B, the result is known as the phase double difference (Wells et al.,1986). In double differencing, all receiver common errors cancel out; however, the noise is multiplied by a factor of 2 with respect to the original measurement, and a factor of $\sqrt{2}$ with respect to that of the single difference measurement. The double difference observation equation is given as:

$$\nabla\Delta\phi = \Delta\phi_A - \Delta\phi_B = (\bar{\mathbf{e}}_A - \bar{\mathbf{e}}_B) \cdot \bar{\mathbf{b}} + (\Delta n_A - \Delta n_B)\,\lambda + \nabla\Delta\varepsilon(\phi) \qquad (3.8)$$

where $\bar{\mathbf{e}}_A$ and $\bar{\mathbf{e}}_B$ are the unit vectors between the antenna baseline and the satellites A and B, respectively, computed at either one of the baseline antennas.

When using the differencing techniques, the satellite ionospheric errors are eliminated; therefore, there is no practical use of the L2 carrier phase for estimating the ionospheric correction. However, it can be used for faster ambiguity resolution. Since new techniques are available now for fast and reliable ambiguity resolution using only L1 carrier phase (El-Mowafy and Schwarz,1994a), the use of L2 measurements is, in general, not needed in attitude determination. Moreover, since the attitude determination system uses two or more antennas, which means using many channels for tracking L1 phase measurements, the number of channels needed will be doubled if measurements of L2 are used. This means very expensive hardware. Therefore, almost all multi-antenna systems use only measurements of the L1 carrier signals and track the C/A code only.

By eliminating orbital and atmospheric errors, the accuracy of using the carrier in single difference positioning mode is higher than using the double differencing technique. Even though, double differencing is usually preferred because it eliminates receiver time error. However, if a multi-antenna system is used, consisting of only one receiver connected to all antennas, the phase replica in each of the receiver channels is generated from only one replica carrier generator (common oscillator for all channels). Therefore, if phase observables, from the same satellite, are received by two channels, i.e. two antennas of the multi-antenna system, the common mode noise and time skew between the two channels will theoretically vanish. In this case, single differencing would have the same effect as double differencing in eliminating receiver related errors.

Although the noise after double differencing is $\sqrt{2}$ times larger than that after single differencing, double differencing is usually the preferred technique for attitude determination for the following reasons:

- It is not likely that single differencing will completely eliminate receiver clock error. Available commercial receivers still have a small time skew error left. Double differencing cancels such time error.

- Common-mode errors between antennas exist due to electrical path bias errors between channels. To eliminate this error, differencing between receiver channels is required.

If these problems are overcome, the use of single differencing will be preferable. With the rapid improvements in receiver technology, the potential to achieve this goal is there.

3.2 Attitude Determination Using the Transformation Matrix between the Body Frame and the Local-Level Frame

A widely used method for representing the attitude of a rigid body, caused by rotational motion, is by way of a coordinate transformation matrix, which transforms a coordinate system fixed in the rigid body to a chosen reference coordinate system (Goldstein,1980).

In this method, it is assumed that a well-defined body frame exists, such that the axes of the body frame coincide with the main axes (centre lines) of the rigid body. In this case, the attitude of the rigid body is the same as the orientation of the body frame with respect to the local-level frame.

3.2.1 Determination of the Transformation Matrix

If antenna vectors are known in both the body frame and the local-level frame, the transformation matrix is derived using the equation:

$$T_l^b = R_l \, R_b^{-1} \tag{3.9}$$

where:

T_l^b is the transformation matrix from the body frame to the local-level frame.

R_b and R_l are the matrices of antenna relative coordinates in the body and local-level frames, respectively.

It is assumed in equation (3.9) that the origins of the two frames coincide, and the scale factor is taken as unity. Otherwise, the general equation of the transformation of coordinates should be used. This equation can be written as follows:

$$R_l = s \; T_l^b \; R_b + r_o \tag{3.10}$$

see (Slama et al.,1980), where s is a scale factor and r_o is the shift vector between the origins of the body and the local level frames, expressed in the local-level frame. The transformation matrix is then determined from the equation:

$$T_l^b = (R_l - r_o) \; (1/s) \; R_b^{-1} \tag{3.11}$$

Using Euler angles for attitude parameterization, the transformation matrix can take 12 distinct forms. These forms differ according to the sequence of rotations about the body axes, see Appendix B. If the sequence of rotations is known, the three rotation angles can be determined by solving trigonometric functions of the elements of the transformation matrix (Ferguson et al., 1991a). For instance, if the rotation sequence is known to be about the axes y-x-z respectively, the transformation matrix takes the form:

$$T_l^b = \begin{bmatrix} s(\psi_E)s(\theta_E)s(\varphi_E)+c(\psi_E)c(\varphi_E) & c(\theta_E)s(\psi_E) & s(\psi_E)s(\theta_E)c(\varphi_E)-c(\psi_E)s(\varphi_E) \\ s(\varphi_E)s(\theta_E)c(\psi_E)-c(\varphi_E)s(\psi_E) & c(\theta_E)c(\psi_E) & c(\psi_E)s(\theta_E)c(\varphi_E)+s(\psi_E)s(\varphi_E) \\ s(\varphi_E)c(\theta_E) & -s(\theta_E) & c(\varphi_E)c(\theta_E) \end{bmatrix} \tag{3.12}$$

where s and c denote the sine and cosine, respectively. ψ_E is the Euler heading angle, θ_E is the Euler pitch angle and φ_E is the Euler roll angle. The three angles can be determined from the equations:

$$\psi_E = \tan^{-1}\frac{T_{12}}{T_{22}} \tag{3.13}$$

$$\theta_E = \sin^{-1}(T_{32}) \tag{3.14}$$

$$\varphi_E = \tan^{-1}\frac{T_{31}}{T_{33}} \tag{3.15}$$

Note that, these angles have to be corrected to obtain heading, pitch, and roll as defined in Section 2.3. The correct quadrants can be obtained from the proper signs of the elements of the attitude matrix. However, using equation (3.13) to (3.15) to determine Euler angles directly from the transformation matrix cannot be done unless the rotation sequence is known. Unfortunately, this cannot be realized in practice. Therefore, other approaches should be implemented instead of the direct approach. This will be shown in Section 3.2.4.

In this technique, antenna locations are of no importance. The only focus is on the ease of determining relative antenna positions in both the body and the local- level frames in addition to considering other factors such as multipath minimization and using long baselines, see Chapter 4.

Since the body frame is chosen to be fixed with respect to the rigid body, the relative positions of the antennas in the body frame, the matrix R_b, are considered fixed in the whole survey operation. Thus, it is determined once in a pre-survey mode. Due to the problem of antenna phase centre migration, it is preferable to determine the matrix R_b after a sufficient period of static initialization using GPS measurements. If the antennas move relative to each other due to deformations in the surface of the rigid body, the method will not work unless the new R_b is determined. In this case, the computed attitude will no longer represent the rigid body orientation. Instead, it will represent its orientation as well as changes resulting from the non-deterministic temporal variations of the rigid body. An example is the case when the antennas are mounted on airplane wings, and the wings experience some flexing. Such a problem can be avoided by installing the antennas at stable locations, chosen properly to well represent the rigid body, where the possibility of experiencing relative movements is minimal. The flexing error can also be determined using a suitable model, and encountered in the attitude estimation process to give the correct attitude, see (Cohen et al.,1994) and (Cannon et al.,1994).

3.2.2 Determination of Relative Antenna Coordinates in the Body Frame

Choosing the body frame axes to pass through some of the antennas simplifies the computations. For instance, if antennas number 1 and 2, shown in Figure 3.4, are mounted along or parallel to the longitudinal axis of a vehicle, the y axis of the body frame is chosen to run through these two antennas, pointing forward. In this case, the origin can be chosen at antenna 1. Since the x-y plane can be defined by three points, these points can be taken as phase centres of three antennas. The plane containing antennas 1, 2 and 3 can be chosen for this purpose. The x axis is then defined as the axis perpendicular to the y axis, in the plane 1-2-3, pointing to the right, which will be parallel to the transverse axis of the vehicle. The z axis is chosen pointing upwards, perpendicular to the x-y plane. In this scheme, the coordinate frame x-y-z is chosen to be a right-handed system, with its origin at antenna number 1. The same point can be chosen as the origin of the local-level system.

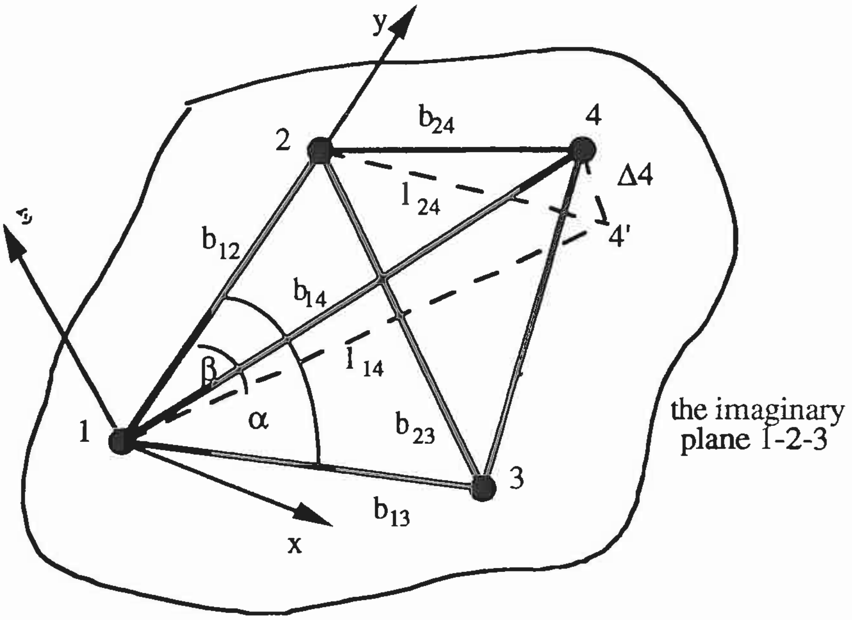

Fig. 3.4 Determining antenna coordinates in the body frame

From the description of the body coordinate frame given above, the components of the vector 1-2 in the body system, can be defined as $(0, b_{12}, 0)$, where b_{12} is the length of the baseline 1-2. Determination of the vector 1-3 body components can be done by estimating the angle (α) contained between the y axis (along the baseline 1-2) and the baseline 1-3. Since the slant distances between the antennas, shown in boldface in Figure 3.4, are usually accurately pre-measured, the angle α can be estimated as follows:

$$\alpha = \cos^{-1} \frac{[\,(b_{12})^2 + (b_{13})^2 - (b_{23})^2\,]}{2\, b_{12}\, b_{13}} \tag{3.16}$$

where b_{13} is the length of the baseline 1-3. The components of the baseline 1-3 in the body frame are then determined as ($b_{13} \sin \alpha$, $b_{13} \cos \alpha$, 0).

The three antennas 1, 2 and 3, with the two independent baselines 1-2 and 1-3, are sufficient to uniquely determine the 3D attitude of the rigid body. However, if measurements from redundant antennas are available, the redundant antennas introduce new baselines that increase solution reliability. To compute the components of the redundant baselines in the body frame, the following technique is adopted. First, let us assume, for simplicity, that only one redundant antenna exists, and as a result, a new baseline is formed between this antenna and antenna number 1. The equation of the plane containing this baseline and the baselines 1-2 and 1-3, can be given as:

$$\begin{vmatrix} dX & dY & dZ \\ dX_{12} & dY_{12} & dZ_{12} \\ dX_{13} & dY_{13} & dZ_{13} \end{vmatrix} = 0 \tag{3.17}$$

see (Wong, 1979). Where dX, dY, dZ, dX_{12}, dY_{12}, dZ_{12}, dX_{13}, dY_{13}, and dZ_{13} are the WGS-84 X, Y, and Z vector components of the redundant baseline and the baselines 1-2 and 1-3, respectively. Solving equation (3.17) gives:

$$A\ dX + B\ dY + C\ dZ = 0 \tag{3.18}$$

where:

$$A = dY_{12}\, dZ_{13} - dY_{13}\, dZ_{12} \tag{3.19}$$

$$B = dX_{12}\, dZ_{13} - dX_{13}\, dZ_{12} \tag{3.20}$$

$$C = dX_{12}\, dY_{13} - dX_{13}\, dY_{12} \tag{3.21}$$

If the redundant antenna does not lie in the plane 1-2-3, its orthogonal height above this plane (Δ) is estimated from (Wong, 1979):

$$\Delta = \frac{A\ dX + B\ dY + C\ dZ}{\sqrt{A^2 + B^2 + C^2}} \tag{3.22}$$

As an example, when antenna number 4 (shown in Figure 3.4) is used, a redundant baseline (1-4), is generated. The vertical component of the baseline 1-4 in the body frame is the same as the orthogonal height of antenna 4 above the plane 1-2-3. It is determined from equation (3.22) as follows:

$$\Delta 4 = \frac{A\ dX_{14} + B\ dY_{14} + C\ dZ_{14}}{\sqrt{A^2 + B^2 + C^2}} \tag{3.23}$$

where $dX_{14,}$ dY_{14}, and dZ_{14} are the WGS-84, X, Y, Z vector components of the baseline 1-4. Since the lengths of the baselines 1-4 and 2-4 are pre-measured, their projections on the plane 1-2-3 are estimated as follows:

$$l_{14} = \sqrt{b_{14}^2 - \Delta 4^2} \tag{3.24}$$

$$l_{24} = \sqrt{b_{24}^2 - \Delta 4^2} \tag{3.25}$$

where b_{14} and b_{24} are the spatial (slant) distances of the baselines 1-2 and 2-4, respectively, and l_{14} and l_{24} are their corresponding projections on the antenna plane 1-2-3. The angle β contained between the baseline 1-2 (y axis) and the projection of the baseline 1-4 on the platform plane can be computed as follows:

$$\beta = \cos^{-1} \frac{[\ (b_{12})2 + (l_{14})^2 - (l_{24})^2\ ]}{2\ b_{12}\ l_{24}} \tag{3.26}$$

The x-y components of the baseline 1-4 in the plane 1-2-3 (dx_{14}, dy_{14}) are then determined as:

$$dx_{14} = l_{14} \sin \beta \tag{3.27}$$

$$dy_{14} = l_{14} \cos \beta \tag{3.28}$$

Finally, the components of the vectors 1-2, 1-3 and 1-4 in the body frame are given in matrix form as follows:

$$R_b = \begin{bmatrix} 0 & b_{13}\sin(\alpha) & l_{14}\sin(\beta) \\ b_{12} & b_{13}\cos(\alpha) & l_{14}\cos(\beta) \\ 0 & 0 & \Delta 4 \end{bmatrix} \qquad (3.29)$$

If more than one redundant antenna exists, their redundant baselines will be dealt with in the same way as described for the baseline 1-4.

3.2.3 Determination of Relative Antenna Coordinates in the Local-Level Frame

Unlike the fixed matrix of antenna vector components in the body frame R_b, the matrix of relative antenna coordinates in the local-level frame R_l is variable and will change if the rigid body moves or changes its orientation. The matrix R_l is computed using GPS measurements in three steps. The first step is to determine antenna baseline vectors in the WGS-84 coordinate frame. Then, GPS measurements are used to define the coordinates of the origin of the local-level frame in the Cartesian WGS-84 system. This is usually taken as the antenna used as the body frame origin. Finally, the coordinates of the origin are transformed to geodetic coordinates, which are used to transform antenna vectors from the WGS-84 frame to the local-level frame. More detail is given in the following.

If antenna baselines are solved independently, i.e. each is determined in a separate adjustment process, the number of unknowns considered for each baseline is three, which are (dX, dY, dZ) in the WGS-84 frame. Therefore, the minimum number of phase double difference equations required is three, which means observations to four satellites. For simplicity, the observation equations given in this section will be written assuming that the ambiguities are correctly determined and subtracted from the phase measurements. All phase measurements are then given, corrected from ambiguity biases. For n satellites, the full structure of the observation equations, ignoring error terms, can be written as:

$$\begin{bmatrix} \Delta\phi_1 - \Delta\phi_2 \\ \Delta\phi_1 - \Delta\phi_3 \\ \cdot \\ \Delta\phi_1 - \Delta\phi_n \end{bmatrix} = \begin{bmatrix} (e_{X1}-e_{X2}) & (e_{Y1}-e_{Y2}) & (e_{Z1}-e_{Z2}) \\ (e_{X1}-e_{X3}) & (e_{Y1}-e_{Y3}) & (e_{Z1}-e_{Z3}) \\ \cdot & \cdot & \cdot \\ (e_{X1}-e_{Xn}) & (e_{Y1}-e_{Yn}) & (e_{Z1}-e_{Zn}) \end{bmatrix} \begin{bmatrix} b_X \\ b_Y \\ b_Z \end{bmatrix} \qquad (3.30)$$

where $\Delta\phi_i$ is the single difference carrier phase observation between the satellite i and the baseline after subtracting the resolved ambiguities, and $(e_X, e_Y, e_Z)_j$ are the receiver-to-satellite unit vector components with respect to the satellite j. The quantities b_X, b_Y, and b_Z are the antenna baseline vector components in the WGS-84 coordinate system; i.e. the relative antenna coordinates (dX, dY, dZ).

The satellite number 1 given in equation (3.30) is chosen as the reference satellite, where the double differences are taken as the differences of the single difference measurements of the remaining satellites with respect to that of the reference satellite. The choice of the reference satellite is usually governed by the criterion that the reference satellite should have the strongest signal-to-noise ratio. The choice of the satellite of highest elevation angle usually gives this result.

Due to using short distance baselines for attitude determination, the baseline lengths can be measured in a pre-survey mode with accuracies at the sub-millimetre to millimetre level. If antenna relative positions during the survey mission do not experience any changes, the baseline lengths can be considered fixed, i.e. of constant value. The constant baseline lengths can be used as constraints in the solution to increase solution reliability. The measured lengths can be used, in a different methodology, as additional measurements beside the GPS phase double differences. In this case, only two double difference phase measurements (three satellite observations) are sufficient to solve for the baseline components. The observation equations can then be written as:

$$\begin{bmatrix} \Delta\phi_1 - \Delta\phi_2 \\ \Delta\phi_1 - \Delta\phi_3 \\ \|b\|^2 \end{bmatrix} = \begin{bmatrix} (e_{X1}-e_{X2}) & (e_{Y1}-e_{Y2}) & (e_{Z1}-e_{Z2}) \\ (e_{X1}-e_{X3}) & (e_{Y1}-e_{Y3}) & (e_{Z1}-e_{Z3}) \\ b_X & b_Y & b_Z \end{bmatrix} \begin{bmatrix} b_X \\ b_Y \\ b_Z \end{bmatrix} \qquad (3.31)$$

where $\|b\|$ is the magnitude of the measured baseline length. In a symbolic form, equation (3.30) or (3.31) can be written as:

$$\nabla\Delta\phi = E \ \vec{\mathbf{b}} \qquad (3.32)$$

where $\vec{\mathbf{b}}$ is $(b_X, b_Y, b_Z)^T$, and E is the coefficient matrix of the differenced unit vectors. The direct solution for the baseline vector if only the minimum number of measurements is available will be:

$$\vec{\mathbf{b}} = E^{-1} \ \nabla\Delta\phi \qquad (3.33)$$

In the presence of redundant measurements, the use of an adjustment technique is necessary. This can be done either using the least-squares approach or Kalman filtering approach. After estimating the WGS-84 antenna baseline vector components, i.e. the vector $\vec{\mathbf{b}}$, they are transformed to the local-level frame.

In kinematic mode, antenna coordinates (Φ, Λ) are computed from epoch to epoch. If the multi-antenna system is used in stand-alone mode, the coordinates can only be computed by point positioning. If no initial ambiguity determination is available to use phase measurements, pseudoranges will be the only available type of measurements that can be used for the determination of antenna coordinates. In this case, if C/A code is used, and if selective availability is on, the accuracy of determining point coordinates will range between few metres to tens of metres.

If attitude results are not urgently needed in real time, and post-mission processing can be applied, the antenna position can be estimated in a classical relative mode using phase measurements. This can be done by performing relative positioning between two simultaneous data sets, one from a receiver occupying a known fixed station, and the other from the reference antenna of the multi-antenna system. In this scheme, accuracy of few centimetres can be achieved. The main problem in this scenario is the carrier phase ambiguity resolution. In full kinematic applications, like in the airborne or marine modes where the receivers have long separation distance, this type of relative ambiguities can only be resolved at the beginning and at the end of the mission when static initialization is available. Consequently, if cycle slips occur during the kinematic mission, such that phase lock for less than four satellites is being maintained, the whole ambiguity resolution process should be re-initialized once the number of visible satellites is again four or more. The only solution for this problem is to develop an efficient "on-the-fly" ambiguity resolution method capable of handling long baselines.

3.2.4 Attitude Determination Using a Least-Squares Approach

To avoid computation of the transformation matrix directly from equation (3.9), an adjustment technique is suggested. The adjustment procedure can be done in the form of the least-squares approach or Kalman filtering. In either case, the measurements are taken as the estimated baseline components in the local-level frame, and the unknowns are considered as the Euler angles, see also (Lu et al.,1993). In the adjustment approach, predicted (approximate) values of the unknowns are estimated, and corrections to these approximations are determined and added to them to give the correct values. The basic difference between using the equations (3.13) to (3.15) directly and using the adjustment approach is that in the latter Euler angles are treated as the unknowns that should have a unique value which best fits the measurements, regardless of the transformation model used. Thus, no ambiguity in the results is expected.

The observation equation used in this approach is:

$$\underset{3xn}{R_l} = \underset{3x3}{T_l^b}\ \underset{3xn}{R_b} \tag{3.34}$$

Where n is the number of antenna baselines used. The transformation matrix used can take any of the 12 possible forms given in appendix B. However, one should consider that the transformation matrix is sensitive to the rotation angles (Blais,1979). Therefore, the expected values of attitude angles governs the choice of the sequence of rotations. Usually, the order of rotation starts with the small rotation angles. In addition, to minimize errors in baselines projection, shorter baselines are rotated first. As an example, take the sequence y-x-z (roll, pitch, heading), which is suitable for land applications, as pitch and roll are usually small, and the longer baselines are mostly in the forward direction, the rotation is:

$$T_l^b = T_{y\text{-}x\text{-}z} = T_z(\psi_E)\, T_x(\theta_E)\, T_y(\varphi_E)$$

$$= \begin{bmatrix} s(\psi_E)s(\theta_E)s(\varphi_E)+c(\psi_E)c(\varphi_E) & c(\theta_E)s(\psi_E) & s(\psi_E)s(\theta_E)c(\varphi_E)-c(\psi_E)s(\varphi_E) \\ s(\varphi_E)s(\theta_E)c(\psi_E)-c(\varphi_E)s(\psi_E) & c(\theta_E)c(\psi_E) & c(\psi_E)s(\theta_E)c(\varphi_E)+s(\psi_E)s(\varphi_E) \\ s(\varphi_E)c(\theta_E) & -s(\theta_E) & c(\varphi_E)c(\theta_E) \end{bmatrix} \tag{3.35}$$

The observation equations can be written symbolically as:

$$l = f(\chi) \tag{3.36}$$

where l denotes the observation vector, and χ denotes the vector of unknowns $(\psi_E, \theta_E, \varphi_E)^T$. The linearized form of the observation equation is written as:

$$v = A\,\hat{\chi} + w \qquad (3.37)$$

and in differential form equation (3.37) will be:

$$v = A\,\widehat{\delta} + w \qquad (3.38)$$

where: $\hat{\chi}$ is the corrected unknown vector

$\widehat{\delta}$ is the vector of corrections to the unknowns

v denotes the vector of corrections of the observations,

A is the matrix of partial derivatives,

w is the misclosure vector, see (Vanicek and Krakiwsky,1982).

The misclosure vector is computed from the following equation:

$$w = l - f(\chi)|\chi_o \qquad (3.39)$$

where $f(\chi)|\chi_o$ is the right hand side of equation (3.36) computed from the approximate values of the unknowns. It is explicitly written as:

$$W = R_l - T_l^b|\chi_o\, R_b \qquad (3.40)$$

where $T_l^b|\chi_o$ is the transformation matrix computed from the approximate values of the unknowns.

The general form of the A matrix is given as:

$$A = \frac{\partial f(\chi, l)}{\partial \chi}\,|\chi_o \qquad (3.41)$$

and explicitly is written as:

$$A = \begin{bmatrix} \frac{\partial \Delta E}{\partial \psi_E} & \frac{\partial \Delta E}{\partial \theta_E} & \frac{\partial \Delta E}{\partial \varphi_E} \\ \frac{\partial \Delta N}{\partial \psi_E} & \frac{\partial \Delta N}{\partial \theta_E} & \frac{\partial \Delta N}{\partial \varphi_E} \\ \frac{\partial \Delta U}{\partial \psi_E} & \frac{\partial \Delta U}{\partial \theta_E} & \frac{\partial \Delta U}{\partial \varphi_E} \end{bmatrix} \qquad (3.42)$$

The elements of the A matrix are given as follows:

$$\frac{\partial \Delta E}{\partial \psi} = - \{ c(\varphi)\, b_x - s(\varphi)\, b_z \}\, s(\psi) + \{ s(\theta)\, s(\varphi)\, b_x + c(\theta)\, b_y + s(\theta)\, c(\varphi)\, b_z \}\, c(\psi)$$

$$\frac{\partial \Delta E}{\partial \theta} = - \{ s(\psi)\, b_y \}\, s(\theta) + \{ s(\psi)\, s(\varphi)\, b_x + s(\psi)\, c(\varphi)\, b_z \}\, c(\theta)$$

$$\frac{\partial \Delta E}{\partial \varphi} = - \{ c(\psi)\, b_x + s(\psi)\, s(\theta)\, b_z \}\, s(\varphi) + \{ s(\psi)\, s(\theta)\, b_x - c(\psi)\, b_z \}\, c(\varphi)$$

$$\frac{\partial \Delta N}{\partial \psi} = - \{ s(\theta)\, s(\varphi)\, b_x + c(\theta)\, b_y + s(\theta)\, c(\varphi)\, b_z \}\, s(\psi) + \{ s(\varphi)\, b_z - c(\varphi)\, b_x \}\, c(\psi)$$

$$\frac{\partial \Delta N}{\partial \theta} = - \{ c(\psi)\, b_y \}\, s(\theta) + \{ c(\psi)\, s(\varphi)\, b_x + c(\psi)\, c(\varphi)\, b_z \}\, c(\theta)$$

$$\frac{\partial \Delta N}{\partial \varphi} = - \{ c(\psi)\, s(\theta)\, b_z - s(\psi)\, b_x \}\, s(\varphi) + \{ c(\psi)\, s(\theta)\, b_x + s(\psi)\, b_z \}\, c(\varphi)$$

$$\frac{\partial \Delta U}{\partial \psi} = 0$$

$$\frac{\partial \Delta U}{\partial \theta} = - \{ s(\varphi)\, b_x + c(\varphi)\, b_z \}\, s(\theta) + \{ - b_y \}\, c(\theta)$$

$$\frac{\partial \Delta U}{\partial \varphi} = - \{ c(\theta)\, b_z \}\, s(\varphi) + \{ c(\theta)\, b_x \}\, c(\varphi) \qquad (3.43)$$

where ψ, θ and φ are the approximate values of Euler angles in heading, pitch and roll, respectively.

For simplicity, the observations can be assumed uncorrelated. Therefore, the variance-covariance matrix of the observations (CL) is taken as a diagonal matrix. On the other hand, if the correct covariance matrix is required, it can be estimated through a process of covariance propagation from the covariance matrix of the relative antenna coordinates in the WGS-84 frame. The unknown vector of corrections is then estimated from:

$$\widehat{\delta} = (A^T \ CL^{-1} \ A)^{-1} \ A^T \ CL^{-1} \ w \tag{3.44}$$

see (Vanicek and Krakiwsky,1982). Adding the corrections to the approximate values gives the corrected unknowns. This is formalized as:

$$\hat{\chi} = \chi_o + \widehat{\delta} \tag{3.45}$$

The attitude parameters, i.e. heading, pitch, and roll are then determined from Euler angles using a method similar to the one given in section 2.3, taking the sequence of rotation into account.

The variance-covariance matrix of Euler angles ($C\hat{\chi}$) are then estimated as:

$$C\hat{\chi} = C\widehat{\delta} = \sigma^2 (A^T \ CL^{-1} \ A)^{-1} \tag{3.46}$$

and the variance-covariance matrix of the attitude parameters is estimated by applying the covariance law. The *posteriori* variance (σ^2) in equation (3.46) is estimated from:

$$\sigma^2 = \frac{v^T \ CL^{-1} \ v}{df} \tag{3.47}$$

and df is the degrees of freedom.

3.3 Attitude Determination from Vector Orientation in the Local-Level Frame

The attitude of the rigid body can be directly found by estimating the orientation of the antenna vectors in the local-level frame. In this method, the antennas are placed on or parallel to the main axes of the rigid body (the longitudinal and transverse axes). Accordingly, if the relative positions in the local-level frame of at least two antenna phase centres are determined on each of the main axes, the axes orientation with respect to the local-level frame, and thus the attitude, can be determined. Since the attitude can be estimated from the orientation of two of the rigid body main axes, the minimum number of antenna vectors needed is two, i.e. three antennas.

3.3.1 Determination of Attitude Parameters

Figure 3.5 shows the basic antenna configuration used in this method. Antennas 1 and 2 are placed on the longitudinal axis, such that the baseline 1-2 represents the axis. The baseline 1-3, consisting of the antennas 1 and 3, is chosen in the direction orthogonal to the baseline 1-2, i.e. along the transverse axis. Attitude components, defined as the orientation of the longitudinal and the transverse axes with respect to local level frame, are then estimated using the equations:

$$\psi = \tan^{-1} \frac{\Delta E_{12}}{\Delta N_{12}} \tag{3.48}$$

$$\theta = \tan^{-1} \frac{\Delta U_{12}}{\sqrt{\Delta E_{12} + \Delta N_{12}}} \tag{3.49}$$

$$\varphi = \tan^{-1} \frac{- \Delta U_{13}}{\sqrt{\Delta E_{13} + \Delta N_{13}}} \tag{3.50}$$

where :

$$\Delta E_{12} = E_2 - E_1 \tag{3.51}$$

$$\Delta N_{12} = N_2 - N_1 \tag{3.52}$$

$$\Delta U_{12} = U_2 - U_1 \tag{3.53}$$

$$\Delta E_{13} = E_3 - E_1 \tag{3.54}$$

$$\Delta N_{13} = N_3 - N_1 \tag{3.55}$$

$$\Delta U_{13} = U_3 - U_1 \tag{3.56}$$

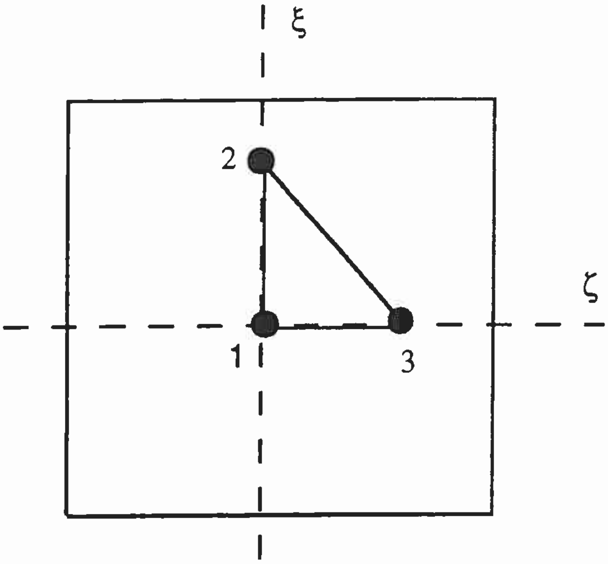

Fig. 3.5 An orthogonal multi-antenna configuration

In practice, however, it is usually possible to determine a line that coincides with or is parallel to the longitudinal axis, and hence, to place two antennas on that line to determine its direction. This direction is determined by two components, the heading and pitch. On the other hand, roll estimation requires placing another antenna such that it makes, in addition to one of the former two antennas, a line orthogonal to the longitudinal axis, i.e. the transverse axis. However, determining the location of the transverse axis or an axis parallel to it to place the third antenna on requires the use of accurate classical techniques. To avoid using this tedious procedure, a simple approach can be employed for roll determination, in which the third antenna can be placed anywhere on the plane containing the two main axes. Figure 3.6 shows a general antenna configuration that can be used in this approach. It is assumed that the line 1-2, passing through the phase centres of the antennas 1 and 2 is parallel to the platform longitudinal axis. The heading and pitch can then be directly estimated using equation (3.48) and (3.49), respectively.

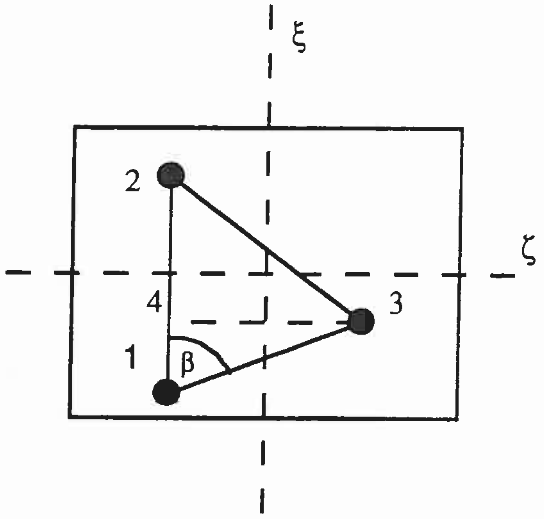

Fig. 3.6 General antenna configuration on the platform

Since the roll can only be estimated from an axis parallel to the transverse axis, a virtual axis (3-4) is assumed to meet this criterion. This axis is taken in the plane containing the antennas 1, 2 and 3. It runs through antenna number 3 and a virtual point on the axis 1-2, defined as point 4, such that it is orthogonal to the axis 1-2. The roll angle defined as the orientation of the transverse axis with respect to the local level frame can then be determined from the components of the axis 4-3 in the local-level frame.

3.3.2 Roll Determination in a General Antenna Configuration

In this approach, the in-plane baseline lengths are first computed, then the length ratios are used to estimate the components of the vector 4-3 from the determined vector components of the baselines 1-2 and 1-3. To estimate the length of the baselines 1-4, the angle β contained between the baselines 1-2 and 1-3, in the plane 1-2-3 is first computed. It can be obtained from the baseline vectors as follows:

$$\beta = \cos^{-1} \frac{\vec{b}_{13} \cdot \vec{b}_{12}}{\| b_{13} \| \| b_{12} \|} \tag{3.57}$$

The length 1-4 is then determined from:

$$b_{14} = b_{13} \cos \beta \tag{3.58}$$

where b_{13} is the length (magnitude) of the vector 1-3. Next, the components of the vector 1-4 are determined as follows:

$$\Delta E_{14} = \frac{b_{14}}{b_{12}} \Delta E_{12} \tag{3.59}$$

$$\Delta N_{14} = \frac{b_{14}}{b_{12}} \Delta N_{12} \tag{3.60}$$

$$\Delta U_{14} = \frac{b_{14}}{b_{12}} \Delta U_{12} \tag{3.61}$$

Knowing the components of the vectors 1-4 and 1-3, the vector components of the baseline 4-3 are estimated as:

$$\Delta E_{43} = \Delta E_{13} - \Delta E_{14} \tag{3.62}$$

$$\Delta N_{43} = \Delta N_{13} - \Delta N_{14} \tag{3.63}$$

$$\Delta U_{43} = \Delta U_{13} - \Delta U_{14} \tag{3.64}$$

Finally, the roll angle (φ) is estimated from the relation:

$$\varphi = \tan^{-1} \frac{-\Delta U_{43}}{\sqrt{\Delta E_{43} + \Delta N_{43}}} \qquad (3.65)$$

3.3.3 Singularity of the Solution and Attitude Recovery

In certain orientations of the rigid body a singularity of the solution occurs if the mathematical form presented here is used. However, this method has the advantage that the attitude can be interpreted easily, even in the presence of these singularities. For instance, when ΔN_{12} is zero, the heading cannot be computed using equation (3.48). In reality, this situation implies either of the following cases: if ΔE_{12} has a positive value, then the heading is 90 degrees, in contrast, if ΔE_{12} has a negative value, the heading will be 270 degrees.

A similar case is shown in pitch estimation using equation (3.49). If ΔE_{12} and ΔN_{12} become zero, the pitch cannot be directly estimated using this equation. However, the pitch can be interpreted intuitively from the sign of ΔU_{12}. If ΔU_{12} is positive, the pitch will be +90 degrees, and if it is negative the pitch will be -90 degrees. Since roll equation is similar to the equation of the pitch, interpretation of roll singularities can be performed in the same manner as what have been done for the pitch.

3.4 Direct Determination of Attitude Parameters from Phase Measurements

3.4.1 The Direct Observation Equations

Instead of determining the attitude from phase measurements in stages, it can be determined using one model. Equation (3.8), ignoring error terms, can be written as:

$$\nabla\Delta\phi - (\Delta n_A - \Delta n_B)\,\lambda = (\vec{e}_A - \vec{e}_B)\,.\,\vec{b} \qquad (3.66)$$

The receiver-to-satellite unit vectors are usually determined in the WGS-84 frame because satellite coordinates are given in this frame. Thus, equation (3.66) can be written in the same frame as:

$$\nabla\Delta\phi - (\Delta n_A - \Delta n_B)\,\lambda = (e_A - e_B)_X\,\Delta X + (e_A - e_B)_Y\,\Delta Y + (e_A - e_B)_Z\,\Delta Z \quad (3.67)$$

where ($\Delta X,\Delta Y,\Delta Z$) are the components of the baseline vector in the WGS-84 frame.

The baseline vector in the WGS-84 frame ($b_{WGS\text{-}84}$) can be determined from the baseline vector in the local-level frame (b_l) using equation (2.1). It is explicitly written as:

$$b_x = -\cos\Lambda\sin\Phi\,\Delta N - \sin\Lambda\,\Delta E + \cos\Lambda\cos\Phi\,\Delta U \quad (3.68)$$

$$b_y = -\sin\Lambda\sin\Phi\,\Delta N + \cos\Lambda\,\Delta E + \sin\Lambda\cos\Phi\,\Delta U \quad (3.69)$$

$$b_z = \cos\Phi\,\Delta N + \sin\Phi\,\Delta U \quad (3.70)$$

In the multi-antenna system, the baseline lengths can be pre-measured with sufficient accuracy. Therefore, for a single baseline, the baseline components in the local-level frame can be expressed in terms of the known baseline length (b) and the baseline heading (ψ) and pitch (θ), as Figure 3.7 shows, from the relations:

$$\Delta N = b\cos\theta\cos\psi \quad (3.71)$$

$$\Delta E = b\cos\theta\sin\psi \quad (3.72)$$

$$\Delta U = b\sin\theta \quad (3.73)$$

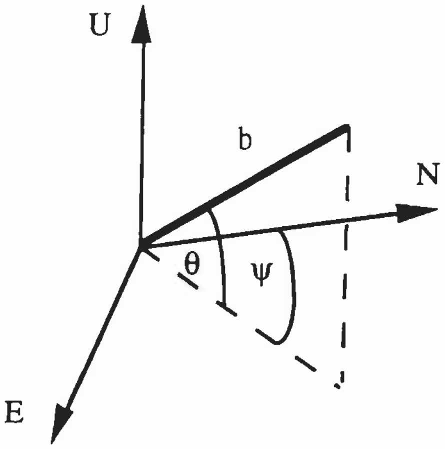

Fig. 3.7 Antenna baseline orientation in the local-level frame

Finally substituting equation (3.71) to (3.73) into (3.68) to (3.70) and these into (3.67) gives:

$$
\begin{aligned}
&\nabla\Delta\phi - (\Delta n_A - \Delta n_B)\,\lambda = \\
&(e_A - e_B)_X\ (-\cos\Lambda \sin\Phi\, b \cos\theta \cos\psi - \sin\Lambda\, b \cos\theta \sin\psi + \cos\Lambda \cos\Phi\, b \sin\theta) \\
&+ \\
&(e_A - e_B)_Y\ (-\sin\Lambda \sin\Phi\, b \cos\theta \cos\psi + \cos\Lambda\, b \cos\theta \sin\psi + \sin\Lambda \cos\Phi\, b \sin\theta) \\
&+ \\
&(e_A - e_B)_Z\ (\cos\Phi\, b \cos\theta \cos\psi + \sin\Phi\, b \sin\theta) \qquad (3.74)
\end{aligned}
$$

After determining the phase ambiguities ($\Delta n_A - \Delta n_B$), equation (3.74) describes the direct relation between the measured carrier phase and the unknown attitude parameters, heading and pitch, given the baseline length and the coordinates of the origin of the local-level frame. If another baseline exists which is perpendicular to the first one, the roll angle of the antenna triad consisting of the two baselines can be determined as the pitch of the second baseline. To satisfy the right hand convention defining the positive direction of attitude angles, the pitch angle of the second baseline should have a negative sign to give a proper roll representation. The second baseline should not necessarily be orthogonal to the first one. Its direction can be chosen arbitrarily, and a technique similar to that given in Section 3.3.2 can be applied to determine roll. This will be shown in the next section.

3.4.2 Determination of Attitude Parameters

The heading and pitch of the primary baseline can be determined from the observation equation (3.74) using the least-squares adjustment approach. The same procedure given in Section 3.2.4 can be applied here, where the vector of observations in this case will be the phase double difference measurements.

In this case, the design matrix A, for n phase double differences, is written as:

$$A = \begin{bmatrix} \frac{\partial \nabla\Delta\phi_1}{\partial \psi} & \frac{\partial \nabla\Delta\phi_1}{\partial \theta} \\ \cdot & \cdot \\ \cdot & \cdot \\ \frac{\partial \nabla\Delta\phi_n}{\partial \psi} & \frac{\partial \nabla\Delta\phi_n}{\partial \theta} \end{bmatrix} \qquad (3.75)$$

From equation (3.74), the elements of the A matrix are derived as:

$$\frac{\partial \nabla\Delta\phi}{\partial \psi} =$$

$$\begin{aligned} &(e_A - e_B)_X \ (\cos\Lambda \sin\Phi\, b \cos\theta_o \sin\psi_o - \sin\Lambda\, b \cos\theta_o \cos\psi_o) \\ &+ \\ &(e_A - e_B)_Y \ (\sin\Lambda \sin\Phi\, b \cos\theta_o \sin\psi_o + \cos\Lambda\, b \cos\theta_o \cos\psi_o) \\ &+ \\ &(e_A - e_B)_Z \ (-\cos\Phi\, b \cos\theta_o \sin\psi_o) \end{aligned} \qquad (3.76)$$

$$\frac{\partial \nabla\Delta\phi}{\partial \theta} =$$

$$\begin{aligned} &(e_A - e_B)_X \ (\cos\Lambda \sin\Phi\, b \sin\theta_o \cos\psi_o + \sin\Lambda\, b \sin\theta_o \sin\psi_o + \cos\Lambda \cos\Phi\, b \cos\theta_o) \\ &+ \\ &(e_A - e_B)_Y \ (\sin\Lambda \sin\Phi\, b \sin\theta_o \cos\psi_o - \cos\Lambda\, b \sin\theta_o \sin\psi_o + \sin\Lambda \cos\Phi\, b \cos\theta_o) \\ &+ \\ &(e_A - e_B)_Z \ (-\cos\Phi\, b \sin\theta_o \cos\psi_o + \sin\Phi\, b \cos\theta_o) \end{aligned} \qquad (3.77)$$

Where ψ_o and θ_o are the approximate values of heading and pitch, respectively.

For roll determination, the adjustment process can be augmented to include double difference observations of a second baseline, perpendicular to the first one. Only the pitch angle of the second baseline is of interest as it represents roll of the antenna triad, and the heading is treated as a nuisance parameter. As mentioned before, the sign of the pitch angle should be reversed to represent the actual roll.

However, choosing antenna triad of two orthogonal baselines, while not difficult to achieve in practice, sets some restrictions on antenna distribution. A simple technique using a more general configuration consisting of three antennas, as shown in Section 3.3, can be applied. In this configuration, two antennas define a baseline parallel to the main longitudinal axis of the vehicle, and the third antenna makes with one of the other antennas a baseline that can have any direction. The heading and pitch of the baseline 1-2 and 1-3 are determined directly from phase measurements as described in this section. Heading and pitch of the antenna triad are taken as that of the baseline 1-2. From the known baseline lengths, vector components of the baselines 1-2 and 1-3 can be determined in the local-level frame using equation (3.71) to (3.73). The spatial angle β is computed from these components. Finally, the process of roll determination proceeds as given in Section 3.3.2.

All methods discussed in this chapter have been implemented and will be compared. This comparison will be given in Chapter 5.

CHAPTER 4

FIRST ASSESSMENT OF FACTORS AFFECTING ATTITUDE DETERMINATION ACCURACY

In this chapter the main factors affecting accuracy of attitude determination from a multi-antenna system are discussed. These factors have been categorized into two groups. The first comprises errors in the GPS measurements. These errors are multipath, receiver noise and antenna phase centre variation. The second group addresses operational considerations. Factors such as baseline length, satellite number and geometry, and antenna configuration are investigated.

4.1 Measurement Errors

Due to the short lengths of the baselines used in attitude determination, the long-term systematic errors, such as orbital and atmospheric errors, cancel out in the carrier phase observation equation when a differencing technique is applied. The main errors left are: multipath, receiver noise (carrier tracking loop noise), and antenna phase centre variation. The magnitude and pattern of these errors are directly reflected in the obtainable attitude accuracy. In this section, the question of how measurement errors affect system accuracy is briefly discussed. This limited discussion should be helpful in understanding system behavior under operational conditions.

4.1.1 Multipath

Multipath is a phenomenon whereby a signal arrives at a receiver via multiple paths due to reflection and diffraction (Braasch, 1992). Multipath is a major error factor limiting accuracy of attitude determination. It generates distortions in phase measurements due to interference of the direct and reflected signals. Multipath effects can be classified into two categories, common mode multipath and differential multipath (Ferguson et al., 1991b). Common mode multipath happens when the antennas are very close. In this case, the reflected signals producing multipath virtually take the same path to the antennas, and the correlation between multipath effects at the antennas becomes strong enough such that measurement differencing eliminates most of multipath effects. As the antennas move further apart, the geometry between satellite, reflector and antenna becomes less similar, and multipath effects at different antennas become less correlated. This type of multipath is defined as differential mutlipath, which cannot be eliminated by differencing.

Due to multipath, the GPS carrier signal received at the antenna will consist of both the direct signal and the reflected ones. The total signal received, following Georgiadou and Kleusberg (1988), will be:

$$\phi = H_p \cos(\omega t + \eta) + H_p \sum_{i=1}^{M} \alpha_i \cos(\omega t + \eta - \eta_r^i) \tag{4.1}$$

where:

ϕ is the received carrier phase (cycles)

H_p is the pseudo random noise code amplitude (1, -1)

ω is the carrier frequency (cycle/sec)

α_i is the ratio of the reflected/direct signal voltages due to reflection from the surface i (multipath strength)

M is the number of reflectors

η is the carrier initial phase (radian)

η_r^i is the phase delay due to multipath (radian)

The phase delay is the angle between the direct signal and the reflected one. It can be shown as a vector plot, see Figure 4.1 (Qiu,1993). Using equation (4.1), the multipath error η_r can be approximated as (Qiu, 1993):

$$\eta_r = \frac{1}{2\pi} \sum_{i=1}^{M} \alpha_i \sin \eta_r^i \qquad \text{(cycles)} \qquad (4.2)$$

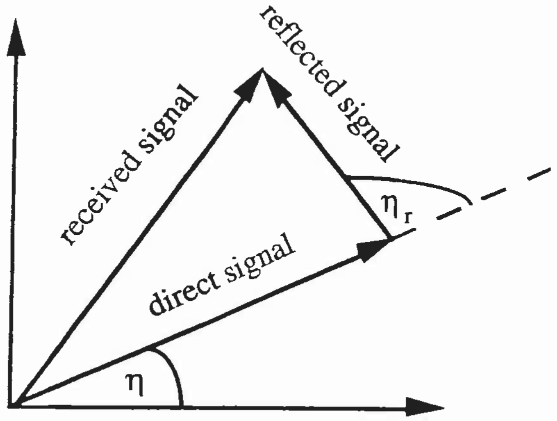

Fig. 4.1 Multipath effect on carrier phase

From equation (4.2), one can see that the multipath error is at a maximum when the reflected signal and the direct one are perpendicular. This means that the differential multipath error can reach up to 90 degrees (1/4 of the carrier wave length), i.e. approximately 4.7 cm using the L1 carrier wave (Lachapelle,1993). However, in typical applications, multipath usually does not exceed a few millimetres. This is still very harmful for attitude determination due to the short baselines used. In addition to accuracy degradation, multipath can produce loss of phase look. During motion of the receiver, rapid changes in the position of the reflector will occur. The result is randomization of the multipath effects. This may cause, in severe cases, the average phase of the received carrier signal to vary so rapidly that it may exceed the ability of the carrier tracking loop to track the phase (Pratt,1993).

The size of the reflecting objects that may generate multipath can be taken as the size of a circle whose radius is not less than the Fresnel zone radius (Braasch,1992). In optics, the first Fresnel zone is an ellipsoid about the line of sight consisting of all points whose combined path length to the receiver and transmitter is one-quarter wavelength longer than the line of sight distance. The same concept can be applied for GPS signal propagation. The Fresnel zone radius is the radius of the cross-section of the ellipsoid at a given point along the line of sight. Thus, the Fresnel zone radius is a function of wavelength and the receiver-reflector-transmitter separation (Braasch,1992). In practice, the Fresnel zone radius is small, even for receiver-reflector distances of more than few kilometres, small objects can produce multipath.

In vehicle mode applications, multipath may occur from signal reflections from the surrounding buildings, hills, vehicles, the ground and from the vehicle itself. In airborne applications the same sources affect the airplane during time of take-off and in the final approach. During flight, the smooth surfaces of the fuselage and the wings may cause multipath. In marine applications, the major sources of multipath reflections are the water and ship surface. Multipath may also result from signal diffraction introduced by the edges of the ground plane when used in ground or marine applications. Similarly, in airborne mode, the wings may cause signal diffraction which cause considerable multipath errors.

Since there is a variety of objects that can generate multipath, classification of different types of multipath is still a problem. Tranquilla and Carr (1991) distinguish three multipath classes for pseudorange measurements. They are:

- diffused forward scattering from a widely distributed areas, with a period of sub-minute to 2-3 minutes.
- Specular reflection from well-defined objects or reflective surfaces in the vicinity of the antenna. The period of fluctuations is of the order of 5-10 minutes.

- Very low frequency fluctuations, usually associated with reflection from the surface of the water. In this case, the fluctuation period ranges between 50 to 60 minutes.

Unfortunately, no corresponding studies for carrier phase measurements exist.

4.1.1.1 Characterization of Multipath

Multipath signals are characterized by their strength relative to the direct signals, polarization, time delay, and phase. Previous studies (Braasch,1992 and Van Nee,1991) have shown that the multipath error is:

- directly proportional to multipath strength,
- non-linearly dependent upon multipath time-delay,
- oscillates between positive and negative values depending upon the relative phase.

Multipath reflected signals have less power than the direct one because of free space loss, relative permitivity of the reflecting surface, value of the incident angle and change of polarization. In order to evaluate the attenuation due to signal reflection from a certain surface, all factors have to be investigated. The free space loss is the ratio of the received power to the transmitted power. It is a function of the difference between the distance traveled by the reflected signal and the direct one, where the reflected signal travels a longer distance. Because the satellite transmitter is approximately 20,000 km from the Earth, differences of path between the reflected signals and the direct one produce negligible loss of power (Van Nee,1991).

Studying the relative permitivity of the reflecting surfaces shows that surfaces of high permitivity produce strong multipath signals. Rodgers (1992) tested different types of surfaces and came to the conclusion that water is the strongest existing reflecting surface. On the other hand, GPS signals are emitted with right-hand circular polarization. Signal reflection from buildings result in a combination of right and left hand polarization. Metallic surfaces and water, on the other hand, change the polarization completely to the left hand direction (Pratt,1993). Due to the fact that GPS antennas attenuate signals with polarization different from the right-handed one, the time-delayed reflected signals causing multipath will have less strength (wave amplitude) compared to the direct signals.

The relative time delay caused by multipath is a function of the satellite-reflector separation and the satellite-reflector-receiver geometry. To clarify the geometry effect, it will be assumed for simplicity that the satellite, reflecting object and the antenna are all at the same height above ground. Also, as the satellites are at a distance of approximately 20,000 km from the Earth, plane wave propagation can be assumed. Thus, if the reflecting object lies in-between the satellite and the antenna, the minimum relative time delay is zero. If it is on the other side of the satellite-antenna line of sight, the minimum relative time delay is computed from double the separation distance between the reflector and the antenna. If the satellite is assumed above the reflector-antenna line, the minimum relative time delay will be reduced to the time of traveling the separation distance (Braasch,1992).

4.1.1.2 Software and Hardware Multipath Minimization Techniques

Multipath is a highly localized phenomenon. Its effects on the GPS carrier phase measurements are similar from day to day when the satellite-reflector-receiver geometry is repeated. The multipath induced carrier phase errors may have periods varying from less than a minute to several hours (Georgiadou and Kleusberg,1989). Multipath errors may show two superimposed forms. The first is a low frequency sinusoidal pattern which arises from motion of the satellite and/or the receiver with respect to the reflecting object. The second is noise like, of high frequency and arises from irregularities in the change of signal reflections and diffractions. For instance, in airborne mode, the wing tips can flex by

model of multipath interference which could be related to physical characteristics of the environment in which GPS signals propagate. He suggested the use of adaptive filtering to identify and model the key parameters of the largest amplitude multipath interference. Unfortunately, no details were given in his study.

Schwarz et al. (1993) have presented a mathematical method for multipath minimization. The method employed is a spectral technique, in which the direct and inverse FFT is used for multipath detection and removal. In this technique, multipath is modeled as a disturbance in the spectral domain. Multipath detection and removal using FFT consists of three major steps, described as follows:

I- The data are constructed in the frequency domain using FFT, then they are converted to the amplitude spectrum.

II- The multipath frequencies are determined, in a pre-defined window, and their amplitudes are reduced to the white noise level.

III- The data are reconstructed in the time domain by inverse FFT after multipath removal.

The method is mainly applicable in the static case. Results show that mitigation of the pseudorange and carrier phase multipath errors using the spectral technique was very successful. When the technique was applied for attitude determination using a multi-antenna system in static mode, the obtained accuracy was improved considerably (Schwarz et al.,1993).

Partial multipath rejection can be done by shaping the antenna gain pattern to have low gain at low elevations, such that the signals reflected from the ground, the water or the surface of the moving body (vehicle, ship or airplane) are significantly reduced. These reflecting sources have sufficient strength to cause measurable errors, especially with signals received from low elevation satellites. Multipath mitigation can also be achieved by setting a cut off angle for signal reception, such that the signal reflected from the mentioned amount of 15 cm for small airplanes (Corbett,1993). As a result, the wings may cause diffraction which reveals itself in the form of rapidly oscillating peaks and nulls in the pattern. Also flexing and bending of the wings will cause the phase and the magnitude of the multipath to oscillate, producing randomization of the multipath, which will then have noise like behavior. In the kinematic land or marine modes, the antenna pattern moves as the vehicle or the ship moves and flexes, multipath therefore arrives at peaks or nulls in the pattern in an almost random fashion.

Long-term averaging minimizes the low frequency errors, while filtering minimizes the noise-like errors. In static mode the low frequency error part is dominant. Therefore, current solutions to the problem in static mode take advantage of the correlation of multipath over short periods of time, and assume that multipath errors have a zero mean. By averaging the residuals, multipath errors can therefore be minimized. However, in kinematic mode, this is not the case as rapid changes in the reflections may occur. For this reason the signal level can be considered as Gausian distributed (Van Nee,1991). Braasch and Van Grass (1991) discusses the use of a complementary Kalman filter to minimize multipath effects on pseudoranges in kinematic mode. The main assumption made is that multipath errors will follow a random behavior. Complementary Kalman filtering uses the code measurements to "centre" the integrated carrier phase. For more details refer to (Hwang and Brown, 1989). It has been suggested to apply a similar technique for minimization of multipath errors in phase measurements. This technique has been applied successfully in airborne mode, even though a small bias remains in this case (Braasch and Van Grass, 1991).

Pratt (1993) argued that simple filtering does not remove contamination by multipath interference, as filtering using conventional linear techniques may remove the troublesome delay variation with time but leave systematic errors. Pratt has tried to provide a simple are dependent on the type of multipath considered. The author is not aware of a unified technique or hardware solution that works well in all situations.

4.1.1.3 Effect of Multipath on Attitude Determination

Attitude determination using a multi-antenna system can be considered as a special application of GPS relative positioning, where short baselines are used. Thus, even small multipath errors could be very damaging to system accuracy by introducing large orientation errors. For example, if multipath noise results in 5 mm of relative positioning error for a baseline of 3 metres in length, a 5.7 arcminute error in the orientation of the baseline is produced. However, there is a trade-off between baseline length and multipath errors. Short baselines experience relatively small multipath errors, as the common multipath is largely eliminated, whereas longer baselines experience large multipath errors as the relative multipath dominates. The effect of multipath errors on the orientation error is therefore dependent on two factors, multipath magnitude and baseline length.

Multipath errors do not only degrade system accuracy, but also limit a desirable feature of system performance, the instantaneous ambiguity resolution. In a variety of applications, real-time attitude determination is needed. To achieve this goal instantaneous ambiguity resolution is required. High multipath noise bounds this requirement. For instance, when applying a least squares search approach, a search is conducted for the correct set of ambiguities among different candidates in a preset window, see Chapter 7 for more details. The choice of the correct ambiguity set is based on finding the set that gives minimum variance of all phase measurements. In the presence of high multipath noise, the variance of more than one candidate set of ambiguities will be so close, that it is hard to identify which is the correct one. As a consequence, instantaneous ambiguity resolution will be hard to achieve, and further measurements will be needed.

sources and the lower satellites are rejected. For airborne users, this may not be desirable due to significant changes in the relative geometry that may occur during a short period. In this case, using a cut-off angle, may mask off useful satellites (Corbett,1993).

The use of ground planes to reject the reflected signals coming from below is a popular method for multipath minimization, even though, Tranquilla and Colpitts (1988) have mentioned that the use of large flat ground planes, while providing some pattern shaping control, is generally not advised when phase performance is most important because they may cause signal diffraction. In addition, they act as a "ground" or a reference for the voltage induced in the antenna by the incident GPS signal field. Knight and Hatch (1990) came to a similar conclusion, stating that in applications where the antennas experience continuous large tilts, e.g. in the shipborne mode, large ground planes cannot be used as an effective means for multipath reduction. On the other hand, Braasch (1992) has mentioned that by mounting RF absorbing material between the ground plane and the antenna, the resulting pattern looks more like the desired free-space pattern.

Antenna design can also contribute to multipath minimization. As mentioned above, multipath signals, due to reflections, have polarizations different from the right-hand polarization of the direct signals. For instance, the water, which is the least desirable multipath reflector, changes the polarization completely from the right-hand to the left-hand. In principle, the reflected signals can be rejected by polarization discrimination in antenna design, see (Rodgers,1992) and (Rodgers and Gardner,1993). However, useful results cannot be achieved unless the antennas are perfectly polarized.

Finally, it is worthwhile to mention that all presented techniques have only been applied in post-mission processing, no attempt has been made for real-time multipath resolution. In addition, results shown for hardware or software solutions are not always conclusive and

$$S/N = \frac{10^{-16}}{k\ T_E\ B_W} \qquad (4.4)$$

where k is Boltzmann's constant (1.3806×10^{-23} JK^{-1}) and T_E is the effective noise temperature in Kelvins. The equation of C/N_o can be written as follows:

$$\begin{aligned} C/N_o &= S/N \times B_w && \text{Hz} \\ &= 10 \log_{10} (S/N \times B_w) && \text{dB-Hz} \qquad (4.5) \end{aligned}$$

The definition of C/N_o yields a carrier-to-noise ratio independent of the bandwidth, see (Braasch and Van Grass,1991). From equation (4.3), using a 16 Hz bandwidth and C/N_o equals to 40 dB-Hz, the rms tracking noise would be approximately 1.2 mm.

The antenna gain pattern also has a direct effect on the estimated value of the carrier-to-noise ratio, which can be seen from (Jurgens et al., 1992):

$$C/N_o = FD \cdot G_A \cdot 1/N_F \qquad (4.6)$$

where:

FD : the flux density in W/M^2 (GPS signal power).

G_A : antenna gain as a function of elevation and azimuth angle.

N_F : receiver noise figure.

Equation (4.6) shows that higher antenna gains increase system performance by increasing the carrier-to-noise ratio, and accordingly lowering receiver error. Antenna gain changes according to antenna design. In most GPS antennas, the gain is small for low elevation angles; hence, measurements of low elevation angle satellites are noisier. The receiver noise figure is a constant that varies from 2 to 5 dB between different receivers.

Minimization of multipath effects is not only important in kinematic mode, but also in static mode. When using the system in kinematic mode some *a priori* static measurements are required. These measurements are used to determine the antenna baseline components and lengths. If these measurements are taken in a high multipath environment, the accuracy obtained will be poor. High accuracy estimation of the baselines is needed for different reasons. For example, in the transformation matrix approach between the pre-determined baseline components, expressed in the body frame, and the baseline components in the local-level frame, accuracy of attitude determination is highly dependent on the accuracy of the pre-determined baseline components. The known baseline lengths can also be used as constraints in the solution. These constraints play a two-fold role, they increase the redundancy of the solution, and can be used to solve for the attitude with fewer satellites, i.e. when the number of the observed satellites drops below four. In addition, the known baseline lengths accelerates ambiguity determination, and provides a viable cycle slip detection method. More details are given in Chapters 7 and 8.

4.1.2 Receiver noise (Carrier Tracking Loop)

4.1.2.1 Equation of Receiver Noise

Receiver noise is another error which affects attitude determination accuracy. The rms tracking error for a coherent carrier tracking loop with a small IF bandwidth can be given as:

$$\sigma = \frac{\lambda}{2\pi} \sqrt{\frac{B_w}{C/N_o}} \qquad (4.3)$$

see (Spilker,1977), where λ is the wavelength of the carrier phase in metres, B_w is the carrier tracking loop bandwidth, and C/N_o is the carrier-to-noise ratio of the GPS signal. The C/N_o is the signal-to-noise ratio (S/N) in a one Hertz bandwidth. The signal-to-noise ratio, defined as the total signal power divided by the noise, can be calculated from:

rate. Second, the bandwidth should be small enough to achieve small probability of cycle slip occurrence (Braasch,1992).

4.1.3 Antenna Phase Centre Variation

Due to the high accuracy required for attitude determination using carrier phase measurements, antenna phase centre variation is an error factor that should be taken into consideration. The antenna phase centre is the reference point in the antenna at which the signal is received. The location of the phase centre for a particular received signal is dependent on the direction of the signal. For GPS antennas, a mean phase centre is usually given by the manufacturer. This mean phase centre is computed in a calibration process. The location of the mean phase centre is thus a function of antenna type and design.

In field applications, however, the antennas receive signals coming from different directions. The signals are then received at different "actual" phase centres. The difference between the mean of the actual phase centres, which changes with satellite directions (azimuth and elevation), and the given nominal mean phase centre is defined as antenna phase centre variation (Lachapelle,1993). This variation is of the order of a fraction of a millimetre to a few millimetres depending on satellite geometry and antenna design.

Since a differencing technique is usually employed when GPS measurements are used in attitude determination, repeatability of phase centre variation between the antennas is more important in practice than stability of the phase centre (Sims,1989). In this case, the variations will be minimized in the differencing process. The repeatability among antennas can be reinforced by orienting the antennas the same way, and by using the same type of antennas. In the latter case, tight manufacturing quality control is required (Hwang,1990). Among the different types of available GPS antennas, the microstrip patch antennas are

4.1.2.2 Tuning of the Carrier Phase Bandwidth

The carrier tracking loop bandwidth (B_w) given in equation (4.3) incorporates the dynamic environment into the error analysis. The tracking loop should be tuned to accommodate changes in the satellite and receiver motions. Satellite motion is very well behaved. Thus, a tightly tuned tracking loop will find no problem in handling this motion. User motion, on the other hand, can vary considerably according to the application considered. Thus, user dynamics should be taken into account in the loop design.

If the receiver is known to be stationary, very narrow loop bandwidths can be used to produce phase measurements with very little noise. If the dynamics expected vary in a wide range, achieving an optimized performance for all situations with a specified moderate bandwidth becomes a difficult task. In this case, lower dynamics will have noisier measurements, while higher dynamics will encounter low-frequency errors due to lags arising from the tracking loop filter (Hwang,1990). Most modern digital GPS receivers can adjust the tracking loop bandwidth according to the dynamics measured. The tracking loop bandwidth is typically 20 Hz for use with dynamic movements up to 4G, (Jurgens et al, 1992). The magnitude of receiver noise in static applications can be less than 0.5 mm (Hwang,1990), depending on receiver models used. In kinematic applications, this value typically increases to 2-5 mm for low to high dynamic situations.

In some cases, rapid changes in receiver dynamics may cause the average phase of the received carrier signal to vary so rapidly that it may exceed the ability of the carrier tracking loop to track the phase. Therefore, the choice of the carrier tracking loop bandwidth for dynamic applications is usually driven by two considerations. First, the bandwidth should be large enough to avoid loss-of-lock during motion, and to allow for a high data renewal error is minimized. It is also apparent that the orientation error is inversely proportional to the baseline length in a linear way. This is not strictly true for two reasons. First, as the baseline grows, differential multipath becomes more uncorrelated and phase differencing can no longer cancel multipath errors (Ferguson et al., 1991b). Since multipath is a major error source in attitude determination, attitude accuracy degrades with the increase in multipath. The second reason depends on the rigidity of the surface carrying the antennas. For instance, when they are mounted on a ship or airplane, flexing and bending of the ship or airplane body will become more likely as the antenna baseline increases. The error in differential positioning due to flexing or bending will directly result in an attitude estimation error.

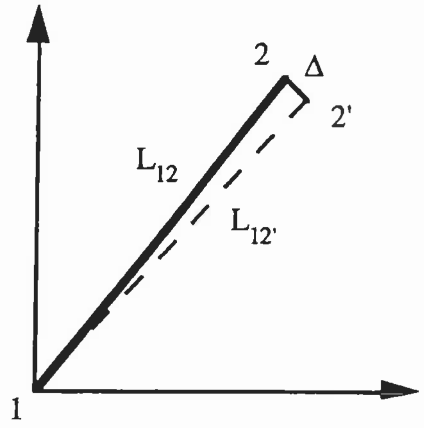

Fig. 4.2 Orientation error and baseline length

The effect of these two factors can be clearly seen when comparing results reported in (El-Mowafy and Schwarz, 1994a) and (Lachapelle et al., 1994b). In the former study, an rms of 3 arcminutes in heading is achieved with a baseline of 2.975m, using a ground vehicle in kinematic mode. The second study was performed on board of a ship and an rms of 3 arcminutes in heading is reported when using a baseline of 42.7 m. Test conditions are not the same for both studies, because larger multipath errors are likely in the marine test due to the existence of water as a reflecting surface. Even with this caution, it is clear, believed to be the best. They have minimum physical and electrical variations. In addition, they offer small size, low weight and cost and relative ease of installation (Balanis,1982).

Overall, from the discussion given in Section 4.1, one can see that in the static case multipath is the dominant error source, while phase noise and antenna phase centre variation have the smallest contribution in the error budget. Therefore, attitude determination accuracy in the static case is dependent on the multipath environment and the software or hardware multipath minimization solution. In the kinematic case, multipath is minimized due to its randomization. Filtering techniques along with hardware methods can reduce the remaining multipath effects. However, phase noise is increased with the increase in vibrations and dynamics, and usually represents the major error source in the kinematic mode. With the antenna phase centre variation, relative positioning errors in kinematic mode can easily reach 1 cm.

4.2 Operational Factors

In addition to measurement errors, the accuracy of attitude determination is also affected by operational factors such as baseline length used, satellite number and geometry, and antenna configuration. These factors are discussed in the following.

4.2.1 Baseline Length

For the problem of attitude determination, accuracy is dependent on baseline length, i.e. larger antenna baselines yield more accurate results. This can be easily explained from Figure 4.2. For the baseline 1-2, an orientation error of the size Δ/L_{12} is generated from an error (Δ) in the relative position of the two baseline end points, where L_{12} is the baseline length. It is apparent from this relation that as the baseline length increases, the orientation

No. of satellites	PDOP	AZDOP	El-DOP	Heading rms (deg)	Pitch rms (deg)
6	2	1.6	2.6	0.0516	0.0955
5	4	2.1	2.9	0.0668	0.1084
4	7	2.9	3.9	0.0817	0.1552

Table 4.1 Attitude determination accuracy using different numbers of satellites

Satellite geometry also has a profound impact on the achievable accuracy. Satellite geometry is defined by two factors, distribution of the satellites in the horizon, and their observation angles. In principle, positioning with GPS is a resection problem, where antenna positions are determined from the known satellite positions using range measurements. It is well known that in resection problems the positions of the known stations, the satellites in this case, affect position estimation of the unknown points, the antennas. In the relative mode, and when using phase double differences, the effect of satellite distribution is still significant. Attitude determination, as it is estimated from the relative positions of the antennas, is thus significantly affected by satellite distribution. Consequently, better attitude accuracy is expected if the satellites are well distributed over the sky.

The impact of the satellite observation angle can be interpreted in terms of changes in phase single difference measurements. As Figure 4.3 shows, the observed phase single difference, neglecting error terms, can be written as:

$$\Delta\phi = b\cos(\theta) \tag{4.7}$$

where b is the baseline length, and θ is the baseline-to-satellite observation angle. Equation (4.7) shows that when the observation angle approaches 90 degrees, the slope of the cosine however, that the accuracy achieved is not linearly dependent on baseline length. The difference is mainly attributed to the increase in differential multipath and surface flexing.

4.2.2 Satellite Number and Geometry

The minimum requirement for three-dimensional positioning with GPS are measurements from four satellites, any three of which must not lie in a plane containing the antenna. In addition, as mentioned before, if the antennas are mounted on a rigid body, such that the distance between the antennas remain constant as the body is rotated, then the known antenna spacing can be used as additional measurement, or as a constraint (Knight and Hatch,1990). In this case, only three satellite measurement are sufficient for attitude estimation.

Number and distribution of the observed satellites affect solution accuracy. Satellite numbers affect measurement redundancy. An additional satellite observation increases the phase double difference degrees of freedom by one. Table 4.1 shows the effect of increasing the number of satellites on attitude accuracy. An Aschtech Three-Dimensional Direction Finding (3DF) receiver was used, where the maximum number of satellites that can be tracked are six. The accuracy is represented by the rms (root mean square error). The data used are 532 epochs of a kinematic run, where the antennas are mounted on top of a van. Only the heading and pitch are estimated in this test, see Chapter 8 for more details about test conditions. The number of satellites observed for the considered period was originally six. After estimating the rms values using the full satellite constellation, one satellite is omitted and the rms are re-estimated. Next, measurements of another satellite are removed, such that only four satellites were used, and the rms are re-computed one more time. As Table 4.1 shows, attitude accuracy degrades with the decrease in the number of satellites observed and their geometry, and vice versa.

Different figures of merit have been introduce to characterize the effect of satellite geometry. For instance, HDOP, VDOP and PDOP, which stand for Horizontal, Vertical and Position Dilution Of Precision (Wells et al.,1986), are among the most widely used to evaluate "goodness" of satellite constellations. They represent respectively the horizontal and vertical position uncertainty, and a combination of both, due to a specific satellite constellation. Taking for instance PDOP, as the three-dimensional measure of DOP, small values usually indicate better satellite geometry than large PDOP values. Brown and Evans (1990) and Jurgens et al. (1991) discuss the capability of the PDOP in rating the goodness of satellite geometry and introduce other figures of merit, such as the AZDOP and El-DOP. AZDOP denotes AZimuth Dilution Of Precision, and El-DOP is the Elvation Dilution Of Precision. The lower the AZDOP, the better azimuth determination will be. Similarly, the lower the El-DOP, the more accurate pitch and roll can be estimated, this is clearly shown before in Table 4.1. AZDOP and El-DOP are given as:

$$\text{AZDOP} = \sqrt{\cos^2(\psi)\, \sigma^2{}_N + \sin^2(\psi)\, \sigma^2{}_E} \tag{4.8}$$

$$\text{El-DOP} = \sigma_U \tag{4.9}$$

where (σ_N, σ_E, σ_U) are the uncertainty in the baseline components in the N, E, U directions in the local-level frame, and ψ is the azimuth (heading) of the antenna baseline.

In attitude determination, the use of figures of merit is not just convenient for rating the goodness of a given satellite distribution, but also for another important task, namely satellite selection. Satellite selection is often needed for two reasons. The first one is related to phase ambiguity resolution. If a search approach is used, a widely used method is to choose a primary group of four satellites, that can uniquely determine the baseline, to test specific ambiguity candidates and thus find the correct ambiguity set. The four satellites of the angle θ, illustrated in Figure 4.4, becomes nearly one, which means that small changes in the observation angle will lead to small changes in the observed phase single difference. In contrast, when θ approaches zero, small changes in the observation angle will correspond to large single difference phase changes, which result in large angular uncertainty in attitude determination. Therefore, the closer the satellites are to being lined up with the axis of measurement, the less accurate the attitude can be determined (Jurgens et al.,1991). In addition, low elevation satellites can induce a high level of multipath and cause frequent cycle-slips.

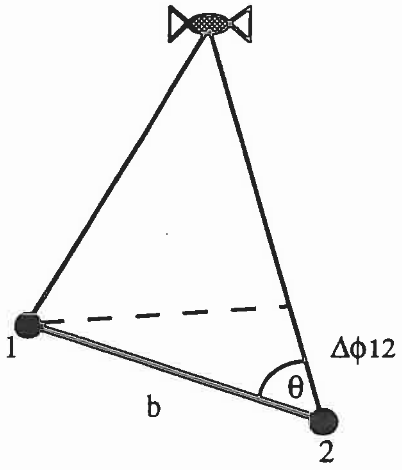

Fig. 4.3 Phase single difference

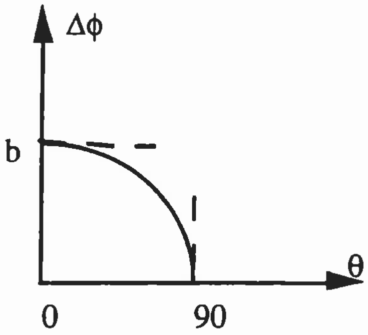

Fig. 4.4 Changes in the observation angle and the measured phase single difference

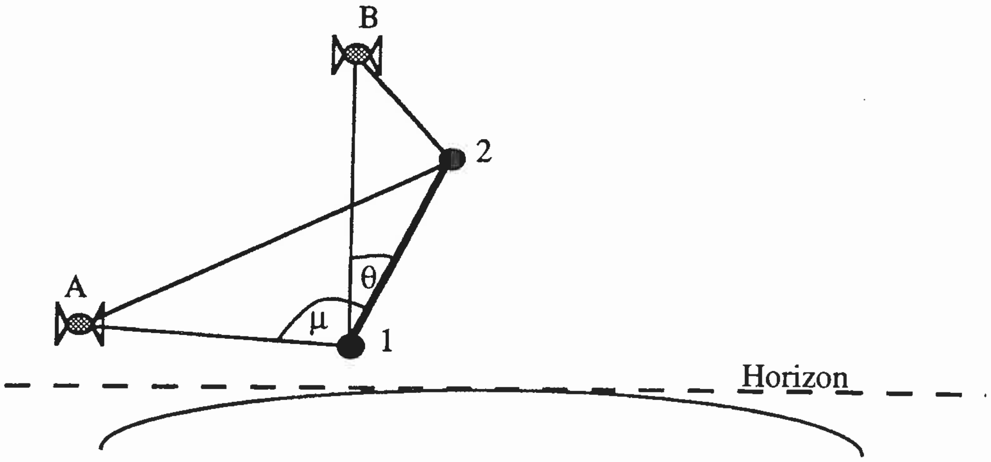

Fig. 4.5 Changes in baseline-to-satellite observation angle with changes in baseline-to-satellite geometry

Another problem related to the use of the figures of merit in satellite selection is the long time needed in reaching a decision about the best satellite constellation that can be used. Because an iterative process is needed to test different permutations, this process becomes more time-consuming as the number of available satellites increases. An alternative approach is to use empirical methods that take the reference satellite as the higher one and choose the remaining satellites according to their distribution and elevation angles. The best choice is achieved when they are well distributed over the horizon, taking the actual baseline-to-satellite observation angle into consideration.

Finally, when using AZDOP and El-DOP, the optimum set of satellites that gives lowest AZDOP is not necessarily the one that gives lowest El-DOP, i.e. it may not be the optimum set for roll or pitch estimation. As a result of this contradictory situation the user should specify for which attitude parameter highest achievable accuracy is required, and accordingly use the satellite group that satisfies this requirement.

should have a good geometry to determine the correct ambiguities. More details about this technique will be given in Chapter 7. The second reason is an operational rather than a technical one. If a commercial multi-antenna system is used, consisting of one receiver, connected to all antennas, there is often a limit on the number of satellites that can be tracked with each antenna. Usually, only six channels are dedicated to each antenna (Ashtech 3DF and Trimble TANS Vector). This means that the maximum number of satellites that the multi-antenna system can track is six. If more than six satellites are available, those which contribute least to geometrical strength should be neglected.

The use of AZDOP, El-DOP, and PDOP is somewhat problematic when used in satellite selection. These figures of merit always assume that satellites which are low above the horizon are worse than those higher above. This is true in differential GPS with long distances. In that case, the baseline-to-satellite observation angle is dominantly affected by the elevation angle of the satellite. In attitude determination, the picture can be different. The baseline length is usually short, and small changes in the differential heights between the antennas vary the baseline vector orientation considerably. Thus, the baseline-to-satellite observation angle becomes dependent on the orientation of the baseline as well as the satellite elevation and direction. An example of aircraft take-off and landing is shown in Figure 4.5 in two dimensional approximation. Although the satellite B has a higher elevation than satellite A, satellite A has a larger baseline-to-satellite observation angle than satellite B (μ versus θ). In this case, the DOP figures of merit would neglect satellite A in favor of satellite B. This would not be an optimal choice.

accuracy. Second the signal-to-noise ratio (S/N) increases, where the signal-to-noise ratio is defined as the ratio of the measured differenced phase to multipath and phase noise.

The increase in S/N can be explained as follows. In attitude determination, the baseline lengths are usually short and limited to few metres. As a result, differenced phase measurements typically have values in the sub-centimetre to metres range, depending on the geometry of the antenna vectors and the satellites. In the presence of errors like multipath and phase noise, which are at a level of a few millimetres to a few centimetres, small phase differenced measurements become very noisy and affect attitude accuracy in a negative way. Thus, the signal-to-noise ratio is an important factor for attitude accuracy that should be taken into consideration. Elevating one of the baseline antennas creates a synthetic antenna differential height, which increases the value of the measured differenced phase, which, in turn, increases the signal-to-noise ratio. This can be seen when comparing Figure 4.7a to Figure 4.7b, where $\Delta\phi$ is the single difference phase measurement and $\delta\Delta\phi$ is the resulting error. Figure 4.7b, with a significant difference in antenna heights, clearly shows a better signal-to-noise ratio. Although this is true in most cases, it will not always work because the signal-to-noise ratio is dependent on the relative geometry between antenna vectors and the satellites.

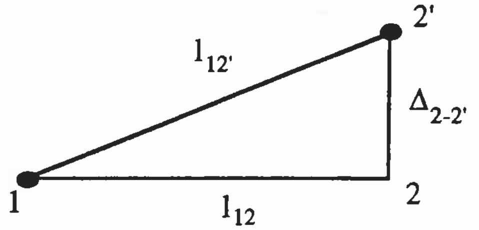

Fig. 4.6 Increasing the baseline length due to elevating one of the baseline antennas

4.2.3 Antenna Configuration

Recall that the number of antennas required for 3D attitude determination is three or more. The main condition for achieving the 3D representation is that not all antennas are collinear. Factors such as attitude determination method used, multipath minimization, choosing long baselines and best possible reception of satellite signals are of major concern when choosing antenna location.

While the last three factors given above are environment dependent, some restrictions apply on antenna locations according to attitude determination method used. Three methods of attitude determination are given in Chapter 3, among which, the use of the transformation matrix for determination of attitude parameters is the most flexible one with respect to antenna configuration. Therefore, when discussing antenna configuration, this method is considered.

When using the transformation matrix approach, antenna locations can be chosen arbitrarily; hence, some antenna configurations may be more advantageous than others. Therefore, the main objective in studying antenna configurations is to find the one that gives highest attitude determination accuracy.

4.2.3.1 Choosing Antenna Locations with Significant Height Differences

Locating the antennas such that they have significant height differences enhances attitude estimation accuracy. For instance, when considering the baseline 1-2 located on the surface of a vehicle, shown in Figure 4.6, putting one antenna at point 1 and elevating a second one to position 2' with height $\Delta_{2-2'}$ above point 2 has two advantages. First, the baseline length increases ($l_{12'}$ versus l_{12}), which in turn improves attitude determination also possible applications. All of these factors are environment dependent. The discussion of optimal antenna configurations from mathematical point of view, given in this section, should be seen with this restriction in mind.

In Chapter 3, when determining attitude parameters from the attitude matrix using the least squares approach, the covariance matrix of the unknowns is determined from:

$$C_{\hat{\chi}} = \sigma^2 (A^T P A)^{-1} \tag{4.11}$$

The optimal antenna configuration can be found when the covariance matrix of the unknowns reduces to an optimal criterion matrix. The criterion matrix is an artificial variance-covariance matrix that can be selected to satisfy certain quality and optimality criteria of antenna configuration. For an optimal criterion matrix, all eigenvalues of the covariance matrix of the unknowns must be equal (Grafarend and Frenando,1985). In this case, the optimal solution of the problem, defined as the E-solution in statistics, transforms the error hyper-ellipsoid (confidence ellipsoid) of the unknowns into a hyper-sphere. The maximum standard deviation of the unknowns is thus minimized. As a result, the effect of measurement errors on the solution is also minimized.

To find the antenna configuration that gives the optimal criterion matrix, one should analyze elements of the covariance matrix $C_{\hat{\chi}}$. From equation (4.11), it is clear that antenna configuration affects only the coefficient matrix A. To analyze this effect, an example of an antenna network consisting of the three baselines AB, AC, and AD is considered. The observation equations for the baseline AB take the form:

$$\begin{aligned}
\Delta E_{AB} &= T_{11}\,\Delta x_{AB} + T_{12}\,\Delta y_{AB} + T_{13}\,\Delta z_{AB} \\
\Delta N_{AB} &= T_{21}\,\Delta x_{AB} + T_{22}\,\Delta y_{AB} + T_{23}\,\Delta z_{AB} \\
\Delta U_{AB} &= T_{31}\,\Delta x_{AB} + T_{32}\,\Delta y_{AB} + T_{33}\,\Delta z_{AB}
\end{aligned} \tag{4.12}$$

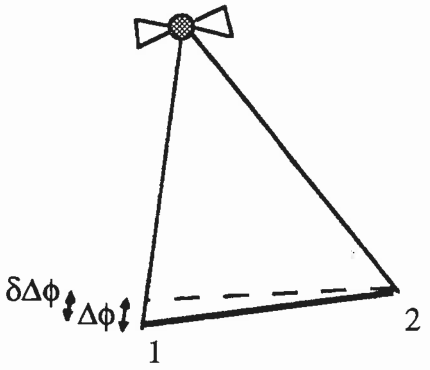

Fig. 4.7a Small S/N ratio with low antenna

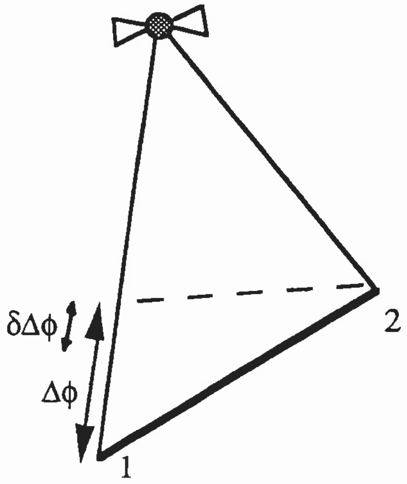

Fig. 4.7b High S/N ratio with high antenna

When elevating any of the antennas above the surface of the vehicle, the three antennas define a plane that is different from the one defined by the vehicle surface. In this case, the orientation of the vehicle's surface can be computed from that of the antenna plane using a transformation process. The transformation equation can be written as:

$$T_V = T_V^A \, T_A \qquad (4.10)$$

where T_A is the attitude matrix of the antenna plane, and T_V is the attitude matrix of the vehicle surface. T_V^A is the transformation matrix between the two planes, which is computed beforehand from known T_A and T_V matrices, usually determined in static mode.

4.2.3.2 Optimal Antenna Configuration

As mentioned before, studying optimality of the antenna configuration must consider the fact that choosing antenna locations is dependent on other considerations such as minimization of multipath effects, increasing baseline length, best satellite visibility and

Using the baselines AC and AD, the partial derivatives matrix takes the form:

$$A = \underset{9x9}{\begin{bmatrix} b^T{}_{AB} & 0 & 0 \\ 0 & b^T{}_{AB} & 0 \\ 0 & 0 & b^T{}_{AB} \\ & & \\ b^T{}_{AC} & 0 & 0 \\ 0 & b^T{}_{AC} & 0 \\ 0 & 0 & b^T{}_{AC} \\ & & \\ b^T{}_{AD} & 0 & 0 \\ 0 & b^T{}_{AD} & 0 \\ 0 & 0 & b^T{}_{AD} \end{bmatrix}} \underset{9x3}{\begin{bmatrix} c_1 & d_1 & f_1 \\ c_2 & d_2 & f_2 \\ c_3 & d_3 & f_3 \\ & & \\ g_1 & k_1 & l_1 \\ g_2 & k_2 & l_2 \\ g_3 & k_3 & l_3 \\ & & \\ m_1 & n_1 & p_1 \\ m_2 & n_2 & p_2 \\ m_3 & n_3 & p_3 \end{bmatrix}} \qquad (4.16)$$

This equation can be written as:

$$A = R\,C \qquad (4.17)$$

where:

$$R = \begin{bmatrix} b^T{}_{AB} & 0 & 0 \\ 0 & b^T{}_{AB} & 0 \\ 0 & 0 & b^T{}_{AB} \\ & & \\ b^T{}_{AC} & 0 & 0 \\ 0 & b^T{}_{AC} & 0 \\ 0 & 0 & b^T{}_{AC} \\ & & \\ b^T{}_{AD} & 0 & 0 \\ 0 & b^T{}_{AD} & 0 \\ 0 & 0 & b^T{}_{AD} \end{bmatrix} \quad \text{and } C = \begin{bmatrix} c_1 & d_1 & f_1 \\ c_2 & d_2 & f_2 \\ c_3 & d_3 & f_3 \\ & & \\ g_1 & k_1 & l_1 \\ g_2 & k_2 & l_2 \\ g_3 & k_3 & l_3 \\ & & \\ m_1 & n_1 & p_1 \\ m_2 & n_2 & p_2 \\ m_3 & n_3 & p_3 \end{bmatrix} \qquad (4.18)$$

The covariance matrix of the unknowns is then given as:

$$C\hat{\chi} = \sigma^2 \left((R\,C)^T P\, (R\,C) \right)^{-1} \qquad (4.19)$$

Assuming that the measurements have a diagonal covariance matrix for simplicity, i.e. P=I, equation (4.19) can be written as:

$$C\hat{\chi} = \sigma^2\, C^{-1}\, (R^T R)^{-1}\, (C^T)^{-1} \qquad (4.20)$$

where (ΔE_{AB}, ΔN_{AB}, ΔU_{AB}) are the baseline components in the local-level frame and (Δx_{AB}, Δy_{AB}, Δz_{AB}) are the corresponding baseline vector components in the selected body frame. T_{ij} is the element in the i row and j column of the transformation matrix T. The A matrix is then given as:

$$A = \underset{3x9}{\begin{bmatrix} c_1 & c_2 & c_3 & d_1 & d_2 & d_3 & f_1 & f_2 & f_3 \\ g_1 & g_2 & g_3 & k_1 & k_2 & k_3 & l_1 & l_2 & l_3 \\ m_1 & m_2 & m_3 & n_1 & n_2 & n_3 & p_1 & p_2 & p_3 \end{bmatrix}} \underset{9x3}{\begin{bmatrix} b_{AB} & 0 & 0 \\ 0 & b_{AB} & 0 \\ 0 & 0 & b_{AB} \end{bmatrix}} \qquad (4.13)$$

or:

$$A = \underset{3x9}{\begin{bmatrix} b^T_{AB} & 0 & 0 \\ 0 & b^T_{AB} & 0 \\ 0 & 0 & b^T_{AB} \end{bmatrix}} \underset{9x3}{\begin{bmatrix} c_1 & d_1 & f_1 \\ c_2 & d_2 & f_2 \\ c_3 & d_3 & f_3 \\ g_1 & k_1 & l_1 \\ g_2 & k_2 & l_2 \\ g_3 & k_3 & l_3 \\ m_1 & n_1 & p_1 \\ m_2 & n_2 & p_2 \\ m_3 & n_3 & p_3 \end{bmatrix}} \qquad (4.14)$$

where $b_{AB} = \begin{bmatrix} \Delta X_{AB} \\ \Delta Y_{AB} \\ \Delta Z_{AB} \end{bmatrix}$

and

$$c_1 = \frac{\partial T_{11}}{\partial \psi} \quad c_2 = \frac{\partial T_{12}}{\partial \psi} \quad c_3 = \frac{\partial T_{13}}{\partial \psi}$$

$$d_1 = \frac{\partial T_{11}}{\partial \theta} \quad d_2 = \frac{\partial T_{12}}{\partial \theta} \quad d_3 = \frac{\partial T_{13}}{\partial \theta}$$

$$f_1 = \frac{\partial T_{11}}{\partial \varphi} \quad f_2 = \frac{\partial T_{12}}{\partial \varphi} \quad f_3 = \frac{\partial T_{13}}{\partial \varphi} \qquad (4.15)$$

Similarly, the parameters [$g_{1,2,3}$, $k_{1,2,3}$, $l_{1,2,3}$] and [$m_{1,2,3}$, $n_{1,2,3}$, $p_{1,2,3}$] are the partial derivatives of the second and third rows of the transformation matrix with respect to the attitude parameters (ψ, θ, φ), respectively.

The optimal configuration is therefore baseline dependent, which agrees with the conclusion given in Section 4.2.1.

Rather than choosing an upright orthogonal triad as shown in Figure 4.8a, the antenna configuration can be chosen as an inverted orthogonal triad, shown in Figure 4.8b, where the reference antenna (antenna A) is located at the origin. This choice will give reasonable differential heights for all baselines as recommended in the previous section. Similar optimal antenna configurations are recommended in (Cohen et al., 1992) and (Comp,1993) which arrived at these conclusions in somewhat different manner.

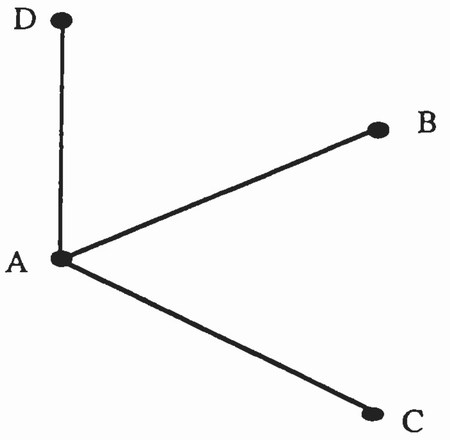

Fig. 4.8a Upright orthogonal antenna triad

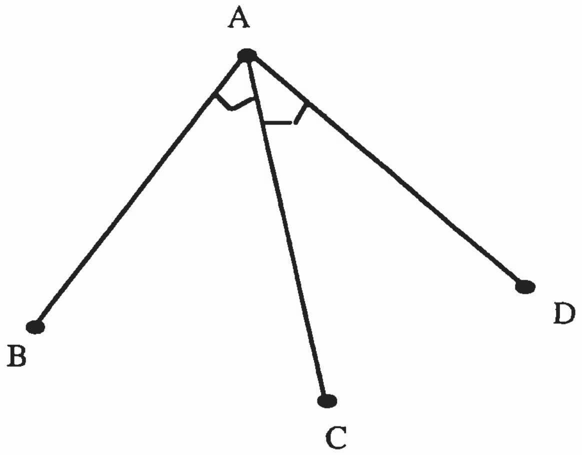

Fig. 4.8b Inverted orthogonal antenna triad (optimal)

Since the choice of antenna locations is application dependent, one has to consider optimal configurations in light of the intended applications. In shipborne application, the orthogonal antenna triad can, in principle, be used. Factors such as baseline length, multipath minimization and satellite visibility should also be carefully considered. In airborne mode, it is not likely that such orthogonal antenna triad would be acceptable. To investigate the gain (or loss) in accuracy when using the suggested antenna configuration, a simple test was performed.

In equation (4.20), the partial derivatives are computed using specific values of the unknowns; consequently, the matrices C and C^T can be dropped from consideration as they will be independent of antenna configuration. Since the objective is to find the optimal antenna configuration in the body frame, optimization of the covariance matrix of the unknowns reduces to optimizing the covariance matrix $(R^T R)^{-1}$. This matrix is the cross-covariance matrix of the antenna components in the body frame, which can be given as:

$$R^T R = \begin{bmatrix} J & 0 & 0 \\ 0 & J & 0 \\ 0 & 0 & J \end{bmatrix} \tag{4.21}$$

where:

$$J = \begin{bmatrix} \Sigma\Delta X^2 & \Sigma\Delta X\Delta Y & \Sigma\Delta X\Delta Z \\ \Sigma\Delta Y\Delta X & \Sigma\Delta Y^2 & \Sigma\Delta Y\Delta Z \\ \Sigma\Delta Z\Delta X & \Sigma\Delta Z\Delta Y & \Sigma\Delta Z^2 \end{bmatrix} \tag{4.22}$$

taking into consideration the baseline sequence given in matrix R in equation (4.18).

If the baselines are orthogonal, such that each baseline samples one axis of the 3D body frame, their cross-covariances become zero. In addition, if the baselines are chosen of equal lengths, the matrix $(R^T R)$ becomes:

$$(R^T R) = a\ I \tag{4.23}$$

where a is the square of the unified baseline length, and I is the unit matrix. The covariance matrix $(R^T R)^{-1}$ with this antenna configuration will indeed have equal eigenvalues, and optimality of the criterion matrix is thus reached. The covariance matrix of the unknowns is then given as:

$$C\hat{\chi} = \frac{1}{a}\ \sigma^2\ C^{-1}\ (C^T)^{-1} = \frac{1}{a}\ \sigma^2\ (C^T C)^{-1} \tag{4.24}$$

In the first test, antenna number 1 was the reference antenna, such that the baselines used in attitude determination were 1-2, 1-3, and 1-4. The attitude of the plane (A), defined by the antennas 1-2-4, is determined in this test. In the second test, antenna number 3 was the reference antenna, and the baselines used were 3-2, 3-4, and 3-5. Antenna number 5 was elevated above the plane 3-2-4 by 0.23m. In this test, the attitude of the plane (B), defined by the three antennas 3-2-4, is determined. Antenna number 3, 2 and 4 used the same data of the first test, while antenna number 5 used a data set taken simultaneously. Thus, phase measurements have the same number of satellites and the same satellite geometry in both tests.

After computing the attitude of the plane A using the optimal configuration, it was transformed to that of the plane B using a transformation process. Where:

$$T_B = T_B^A \, T_A \tag{4.25}$$

where T_A, T_B are the attitude matrices of the planes A and B, respectively, and T_B^A is the transformation matrix, computed from the average values. The attitude determined from the plane A after transformation is thus compatible to that of the plane B.

Attitude results of the two tested configurations were very close. The mean values, as determined by the optimal antenna configuration, were 310.74, -0.075, and 0.534 degrees for heading, pitch and roll, respectively. Table 4.2 shows, in its second and third columns, the rms (in degrees) of the attitude parameters as computed by the two configurations independently. Their variance ratio is shown in the last column. The variance ratio was tested using Fisher test. Considering the number of epochs, the Fisher ratio is taken to be 1.06. Results of Fisher test are not consistent. While the accuracy of pitch and roll improved using the optimal antenna configuration, the accuracy of heading estimation was degraded. Although differences are statistically significant, practically the obtained

4.2.3.3 Testing the Optimal Antenna Configuration

To assess the performance of the optimal antenna configuration, a test was performed on top of the Engineering Building of The University of Calgary. The multi-antenna system used is the Ashtech 3DF system, which consists of one receiver connected to four antennas. Static data of 3698 epochs was collected, with PDOPs between 3 and 4, AZDOP between 1.2 to 2.2, and El-DOPs between 0.9 to 2.7. The antenna configuration used is illustrated in Figure 4.9. From the geometry of the figure, the baselines 1-2, 1-3 and 1-4 are orthogonal and of equal length.

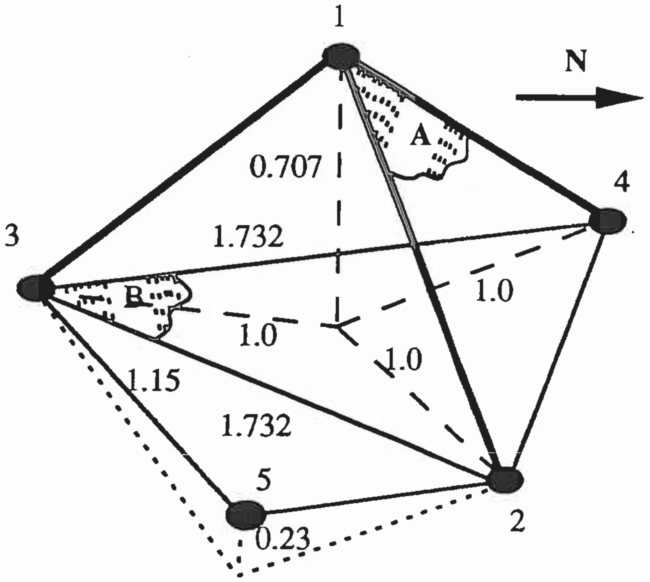

Fig. 4.9 Test configuration of optimal antenna distribution
(units are metres)

To give a reliable assessment of the tested antenna configuration, a head-to-head comparison was made between this configuration and a more general one. The second configuration used the antennas 3, 2, 4 and 5. The fifth antenna was operated by an Ashtech Z-XII receiver. The output data of each test configuration was processed independently.

CHAPTER 5

COMPARISON BETWEEN DIFFERENT ATTITUDE DETERMINATION TECHNIQUES

Three methods for attitude determination have been discussed in Chapter 3, using either the transformation matrix between the body frame and the local-level frame, or the vector orientation in the local-level frame, or the direct approach using phase observations. Each technique has its pros and cons, which clearly affect decision making about which one to use in a certain application. In this chapter a comparison between these techniques is made. The chapter starts by giving a conceptual comparison that shows capabilities and differences between different approaches. Then a practical comparison is performed using a van, where all techniques are applied independently using the same data set. Results are compared and analyzed to assess the performance of these techniques.

5.1 Conceptual Comparison

In this section a comparison between different techniques for attitude determination is given. This comparison is directed towards showing the capabilities of each technique under possible operational conditions.

Attitude determination from the direct approach and from vector orientation in the local-level frame has the advantage that it does not need an initialization period. In attitude determination from the transformation matrix, a sufficient static initialization is needed to compute the components of the baselines in the body frame.

accuracies of the two attitude sets are very close. These results have to be taken with some caution because only one test was performed. An earlier study by (Comp,1993) with a similar optimal antenna configuration showed that all attitude parameters improved. Further testing is required, including applications in kinematic mode to decide whether or not the antenna configuration has a significant effect.

Attitude parameter	Optimal configuration 1-2-3-4 (rms)	General configuration 3-4-2-5 (rms)	Variance ratio
Heading	0.088	0.063	1.951
Pitch	0.078	0.095	1.483
Roll	0.106	0.111	1.097

Table 4.2 Comparing optimal and standard antenna configurations

lie on the longitudinal main axis of the vehicle, or, their baseline should be parallel to this axis. If they are not, a transformation approach will be needed to determine the attitude of the vehicle from the attitude of the antenna triad. In this case, the situation will be similar to the method of attitude determination from the transformation matrix.

If more than three antennas are available for attitude determination, i.e. if redundant antennas and baselines exist, using a transformation matrix is superior, especially when the antenna have differential heights in the body frame. The redundant baselines are treated as additional measurements and, therefore, need no special treatment. This increases solution reliability with a small increase in the size of the matrices. On the other hand, in attitude estimation using the direct approach or the vector orientation method in the local-level frame, heading, pitch and roll are computed from specific vectors, and additional vectors cannot be included in the same solution equations. The redundant antennas can be used without the need for a transformation process if they lie in the same plane of the three primary antennas. In this case, the easiest way to benefit from the additional antennas is an arrangement parallel to the primary baselines. Thus, attitude parameters can be computed from more than one baseline, and the results can be averaged to give more reliable attitude values. However, this arrangement is difficult to achieve in practice when high accuracy is required.

The additional antennas can also be used when placed anywhere in the same plane of the primary antennas. This is shown in Figure 5.1, where, for example, one additional antenna (antenna number 4) is used. In this case, heading and pitch can be obtained from the baseline 1-2 and the virtual baseline 4-4", and the roll is estimated from the components of the virtual baselines 3-3' and 4-4', which can be determined as described in Section 3.3.2. Attitude results can thus be averaged to give more reliable solution. However , this is an approximate procedure, since the additional antennas cannot, in general, be assumed

Attitude determination from the direct approach is the most straightforward method, relating phase measurements directly to attitude parameters in one step. Therefore, computations are limited to one adjustment process. In the vector orientation approach, an adjustment process is first needed to determine antenna baseline vectors in the WGS-84 frame from phase measurements, then baseline vectors are transformed to the local-level frame. Finally, attitude parameters are determined from the derived vectors in the local-level frame. The computations in the last two steps are simple, and this technique is very compatible to the first approach. In the transformation matrix approach, an additional adjustment process is needed to compute attitude parameters after determining baseline vectors in the local-level frame. The computations are therefore more involved than for the other approaches.

In terms of computation time, the direct approach is the fastest, followed by the vector orientation method and the transformation matrix approach. However, the difference in computation time is limited to a few milliseconds, using for instance a 486 DX computer with 50 MHz clock. Therefore, all three methods are applicable for real-time attitude determination.

When using only two antennas to determine the direction (heading and pitch) of a line, only the direct approach and the method of vector orientation can be used. The method of attitude determination using the transformation matrix cannot be applied since it works only for two-dimensional or 3D transformations, but not for lines.

The transformation matrix approach is more flexible with respect to antenna configuration. The antennas can be placed anywhere on the surface of the vehicle and at any height without changing the general procedure of the technique. In the direct approach and in the method of vector orientation in the local-level frame, at least two antennas must has shown that they have the potential of resolving attitude at the level of .05 to 0.1 degrees if multipath is largely eliminated, see for instance (Brown and Evans,1990) and (Brown and Ward,1990). Results from dynamic tests are not so consistent and seem to be poorer, in general, see for instance (Kruczynski et al,1989), or (Brown and Evans,1990). Therefore, the use of an inertial system with an accuracy better than 0.05 degree is sufficient for comparison purposes.

In the proposed tests, the attitude will be computed three separate times, using each time one of the three methods of attitude determination. The same data set will be used in each time. Differences between the three methods will be compared and analyzed. Next, attitude results will also be differenced from the inertial system output to show the accuracy of each method.

5.2.2 Test Design and Description

The hardware selected for the use in these tests consisted of an Ashtech's Three-Dimensional Direction Finding (3DF) system and a Litton LTN 90/100 strapdown inertial system. The first system will be referred to as the 3DF, the second system as the INS. The two systems were mounted on a truck in both test modes.

Ashtech's 3DF multi-antenna system consists of a 24-channel receiver arranged in four banks of six channels, each with a separate RF section (Ashtech,1991). The first bank, designated as the primary bank, is used to compute position and velocity. The other three banks, denoted as secondary banks, are used to determine the attitude along with the primary one. Thus, the translation component of the system motion is determined by the primary bank, while the rotational component is determined from the differences between as laying on the same plane defined by the three primary antennas due to the problem of antenna phase centre variation, and as the antenna plane is a virtual plane not a physical one.

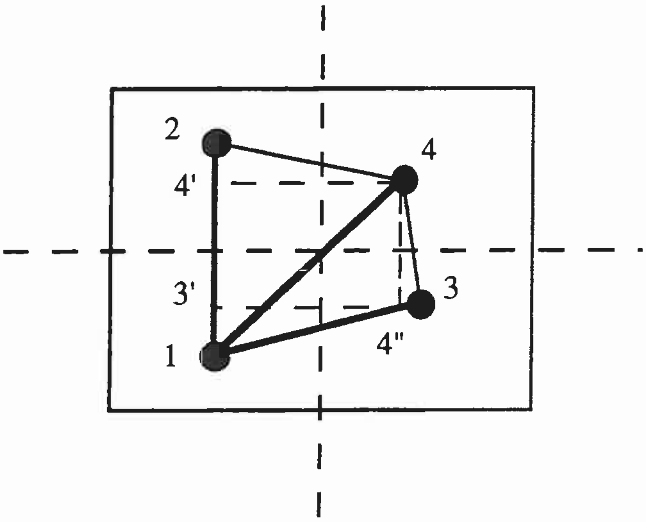

Fig. 5.1 The use of redundant antennas for attitude determination

5.2 Practical Comparison Based on Field Testing

In principle, attitude parameters estimated from either of the given methods should not differ significantly. In order to investigate this principle from a practical point of view and to analyze any differences that may occur, field tests have been performed. Since kinematic applications are the main interest, tests have been done in kinematic mode. Static testing has been performed to provide the basis for the kinematic case.

5.2.1 Test Methodology

To compare attitude results of the three attitude determination methods, a reference for comparison should first be established. The best candidate for an attitude reference in kinematic mode is an inertial system. Testing of GPS multi-antenna systems in static mode

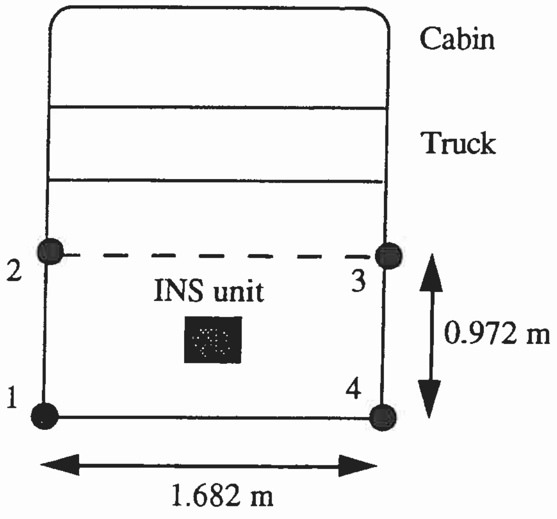

Fig 5.3 Mounting of INS and 3DF in test vehicle

The tests were conducted on a well-surveyed test traverse close to Calgary with an east-west leg of approximately 5 km and a north-south leg of about 4.5 km, see Figure 5.4. The selection of the test course was guided by two considerations. First, the area had few objects that would create multipath. Second, the geometry of the test course allowed a simple first check on the performance of each system. In order to get a reference trajectory of high precision, zero velocity updates for the INS were applied every four to five minutes.

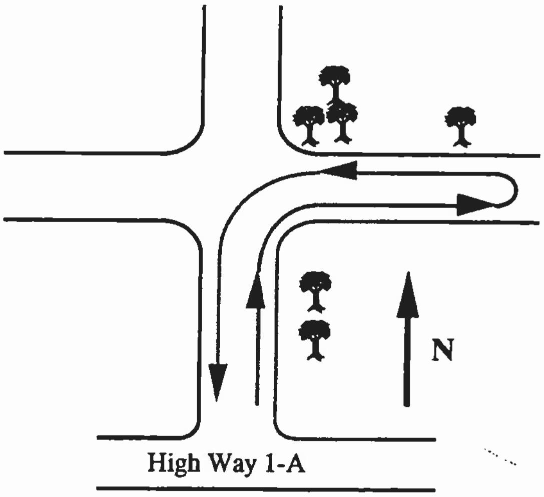

Fig 5.4 Test traverse

secondary and primary banks. The rotations are obviously referenced to the GPS coordinate system. The external output rate of the system raw data is 1 Hz.

The specific INS used here has an output rate of 64 Hz in terms of roll and pitch, and 32 Hz for heading. The high data rate is a major advantage in these tests because the INS-derived attitude will reflect details in the rotational motion which are not visible in the 1 Hz data rate of the 3DF-derived attitude. The accuracy of the derived rotation angles is better than 0.02 degrees/hour (Schwarz et al., 1992).

The sequence of tests performed starts with a static test followed by a kinematic test. In both static and kinematic tests, the antennas sit on heavy square tubes, directly attached to the steel frame of the truck. The square tubes are braced by round steel tubes to avoid movement of individual antennas. The INS is bolted to the loading surface and its centre is the {x,y}-centre of the four antennas. Figure 5.2 shows the test vehicle with the two systems mounted on deck, and Figure 5.3 shows the distances between the antenna centres. Differential rotations between the two systems are still possible because vibrations may affect one system differently than the other. Although no detailed vibration tests have been done, it is estimated that differential rotation between the two systems is less than 0.05 degrees.

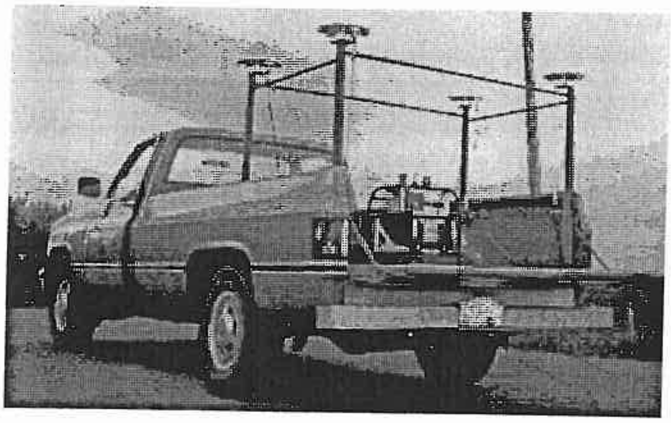

Fig 5.2 Test vehicle with INS and 3DF

The static and the kinematic tests took about 15 and 20 minutes, respectively. They were performed on July 12, 1992. During the tests, 5 satellites were available and the PDOP was between 2 and 4, the AZDOP was between 0.8 and 1.6, and El-DOP was between 0.9 and 2.6 . The maximum recorded acceleration during the test was 1.85 m/s^2, while the maximum velocity was 60 km/h, with 54 km/h as the average. The static run was preceded by a stationary period during which the inertial system was aligned, and the 3DF was initialized, as required by the transformation method. The kinematic run gives about 1200 data points for comparison. Thus, the results are significant from a statistical point of view.

Antenna number 3 was not used for the method of vector orientation in the local-level frame, or the direct approach using phase observations, since it cannot be assumed laying on the same plane defined by the three main antennas, number 1, 2 and 4, shown in Figure 5.3. Therefore, attitude results of the three techniques were processed using measurements from only the three main antennas (1, 2 and 4).

5.2.3 Considerations for the Comparison of the 3DF and INS

To achieve a meaningful comparison of the two time series of attitude data, the following points had to be considered in the test design:

- the two data streams have to be synchronized to an accuracy of 1 millisecond,
- the attitude results compared should refer to the same frame.

Time tagging of the INS and the 3DF is needed at a level of about one millisecond because maximum angular rates are about 20 degrees per second in this environment. One millisecond will therefore guarantee an accuracy of 0.02 degree if the maximum angular rate is not occurring for more than one second. This is usually a reasonable assumption.

Ashtech receivers and the Litton LTN 90/100 system had been synchronized to this level by referencing them to computer time by a system of well-defined GPS PPS interrupts.

Since the attitude results of the INS and the 3DF refer to different frames, that may not be parallel in space, it is required to relate the two attitude outputs to a unified frame, such that a head-to-head comparison becomes feasible. The 3DF and INS have two body frames and two local-level frames, where the origins of the local-level frames are taken at the origins of their corresponding body frames. Since, the position difference between the origins of the two local-level frames is usually small, it is safe to assume that the two local-level frames are parallel. In this case, an equivalent to the attitude matrix of the 3DF frame (T_l^{3df}) can be computed from the attitude matrix of the INS frame (T_l^{ins}) using the equation:

$$T_l^{3df} = T_l^{ins} \, (T_{3df}^{ins})^{-1} \tag{5.1}$$

where T_{3df}^{ins} is the transformation matrix between the inertial frame and the antenna frame. The matrix T_{3df}^{ins} can be computed from equation (5.1) using initial accurate values of the matrices T_l^{3df} and T_l^{ins}, pre-determined from a reliable length of measurements. This transformation matrix will be constant as long as the antenna system and the inertial system do not move with respect to each other.

If the transformation matrices are parameterized by Euler angles, equation (5.1) is then used to transform attitude components, measured in the inertial frame, to values representing the attitude of the 3DF frame. These attitude values are directly comparable to attitude components measured by the multi-antenna system.

5.2.4 Analysis of Results

Figure 5.5a and 5.5b show roll results in the static test as determined by the 3DF and INS, respectively. The roll is chosen as an example to show the behaviour of the two systems. Complete attitude results of the two systems are given in Appendix C. The 3DF data were processed using the vector orientation method. The results of different approaches were so close, that differences did not show at the scale given here. Therefore, all 3DF attitude results shown in the following figures will be for the vector orientation method. Figures 5.6 to 5.8 depict the static heading, pitch, and roll differences between the 3DF and INS outputs. The figures show clearly the presence of multipath in the 3DF results.

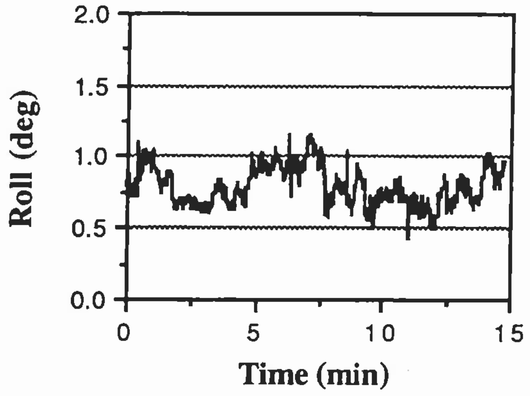

Fig 5.5a Static 3DF roll

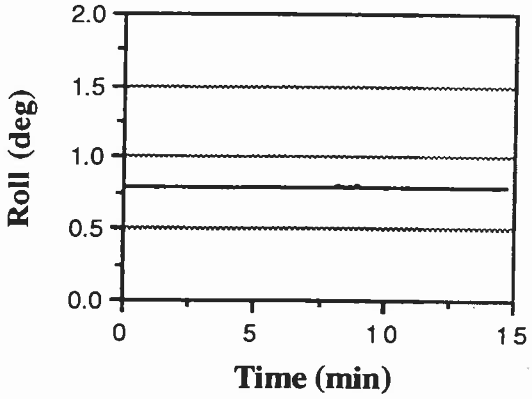

Fig 5.5b Static INS roll

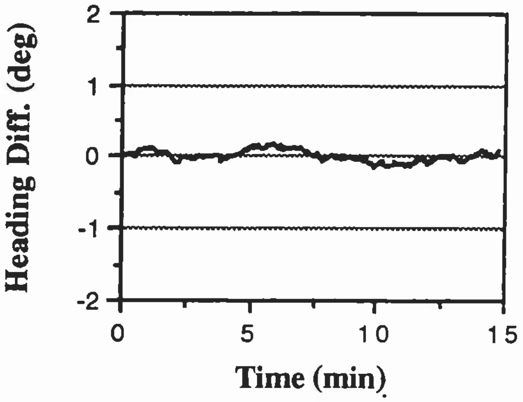

Fig 5.6 Static heading difference

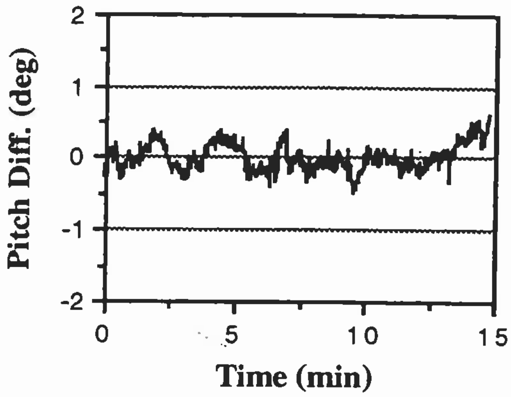

Fig 5.7 Static pitch difference

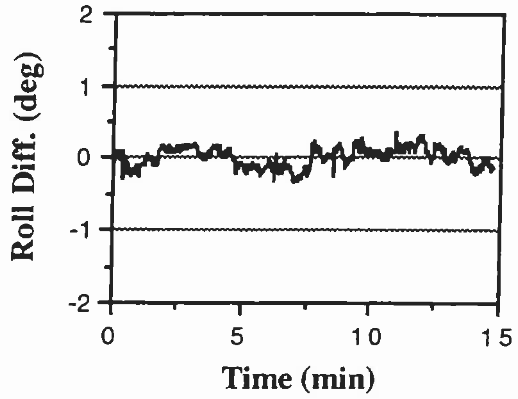

Fig 5.8 Static roll difference

Figure 5.9a and 5.9b show the kinematic roll results of the 3DF and the INS, and Figure 5.10 to 5.12 show the difference of the system outputs in heading, pitch, and roll, respectively in the kinematic case, see Appendix C for complete attitude results. The sequence of figures given here is the same as for the static test. The smaller amplitude in heading is very typical and is due to the fact that the height component does not enter into the computation. The larger amplitude for pitch as compared to roll is due to the shorter baseline length used in pitch computation.

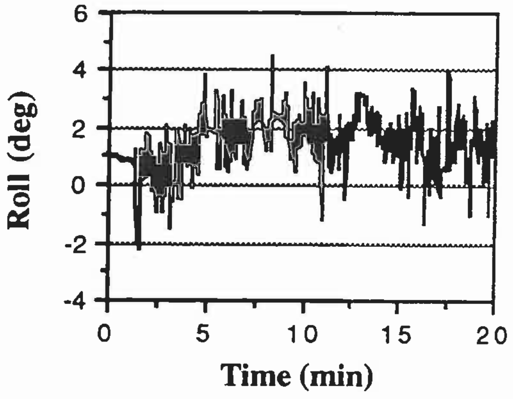

Fig 5.9a Kinematic 3DF roll

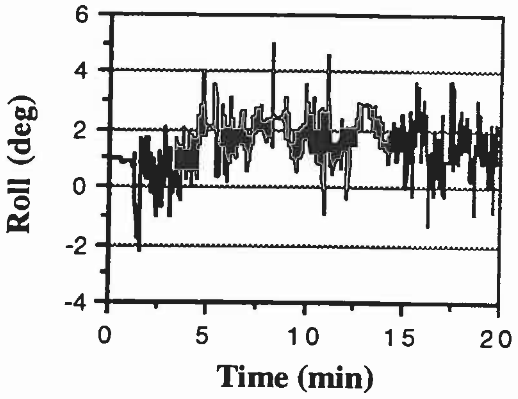

Fig 5.9b Kinematic INS roll

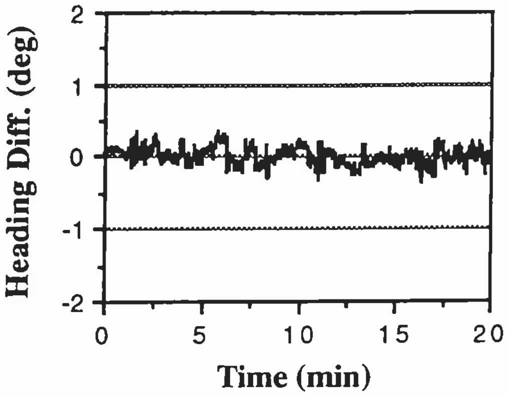

Fig 5.10 Kinematic heading difference

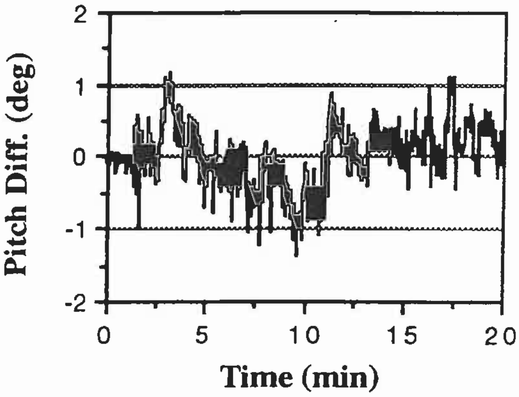

Fig 5.11 Kinematic pitch difference

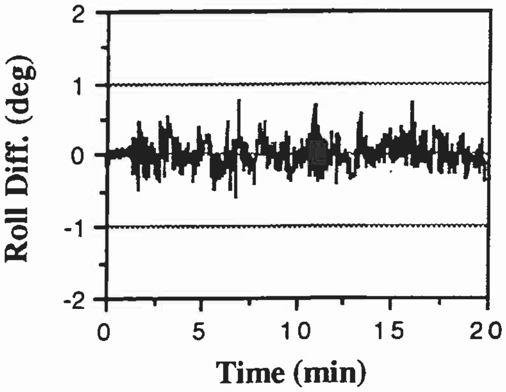

Fig 5.12 Kinematic roll difference

When comparing performance of the three attitude determination techniques, results show that the direct approach and the vector orientation method are compatible in terms of attitude determination accuracy. This is evident from Figures 5.13a to 5.13c, which give the differences in heading, pitch and roll between the outputs of the two techniques. As depicted, the differences are insignificant compared to the accuracy of the 3DF system shown in previous figures. The differences can be attributed to the expected computational differences when applying different mathematical models.

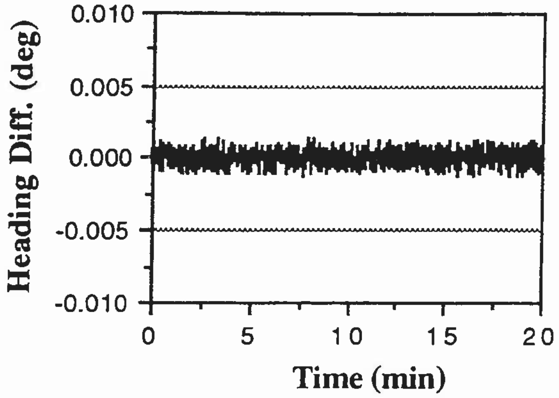

Fig. 5.13a Kinematic heading difference

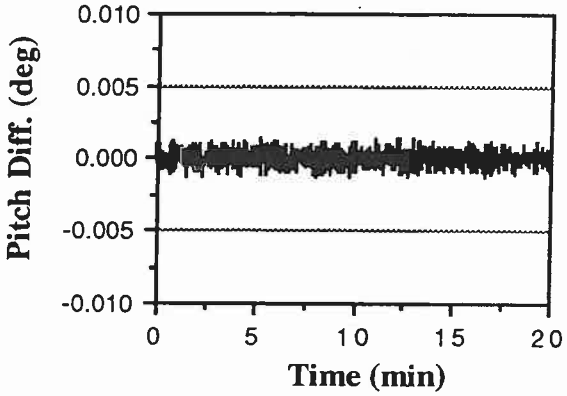

Fig. 5.13b Kinematic pitch difference

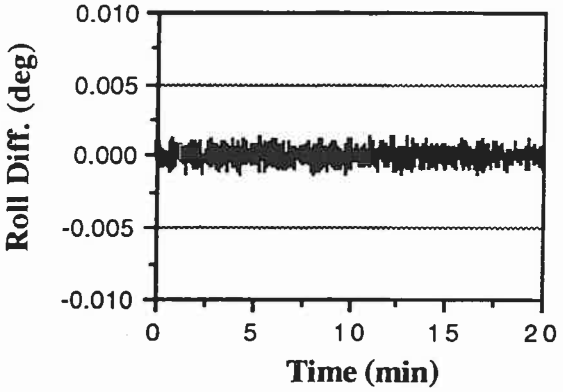

Fig. 5.13c Kinematic roll difference

Fig. 5.13 Attitude differences between the direct approach and the vector orientation approach

When determining the attitude from the transformation matrix approach, one has to consider that the transformation matrix is sensitive to large values of rotation angles, and insensitive to smaller angles (Blais,1979). This governs the choice of the sequence of rotations. For instance, in land environment, as for this test, roll and pitch usually have small changes, while heading may have large changes. Therefore, in principle, the body frame should first be rotated by the leveling angles (roll and pitch), then by heading. As mentioned in Chapter 3, to minimize errors in baselines projection when rotating the body frame to the local-level frame, short baselines should be rotated first. For the test under consideration, the baselines in the longitudinal direction are shorter than in the transverse direction. Therefore it appears that the rotation sequence x-y-z (or pitch, roll, heading) is the most appropriate for test conditions.

Comparing the attitude solution of the transformation matrix approach and the vector orientation method shows larger differences than in the previous case. The differences are shown in Figure 5.14a to 5.14c. These differences can be attributed to the non-linearity between attitude parameters in the transformation matrix and baseline vectors in the body frame and the local-level frame. The differences did not exceed, in general, one arc-minute for roll and pitch, and 1.5 arc-minute for heading. Some small spikes with values up to 5 arc-minutes are shown in the heading difference figure. They occurred when the truck had changes in heading of 90 degrees. The heading values are shown in Appendix C. These spikes in heading differences can be explained as follows. In the adjustment approach, the approximate heading values are estimated by way of linear extrapolation. Therefore, when heading changes by 90 degrees, the approximate values are completely out. The approximate values affect the final results, especially in this case where the attitude is determined from data of a single epoch and the number of measurements used is limited. It appears then, that the vector orientation method and the direct method are more stable than the transformation matrix approach.

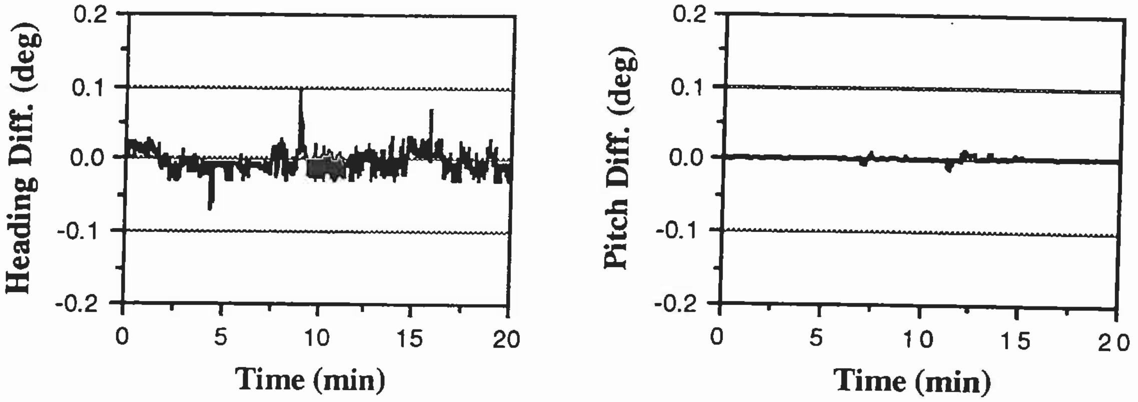

Fig. 5.14a Kinematic heading difference

Fig. 5.14b Kinematic pitch difference

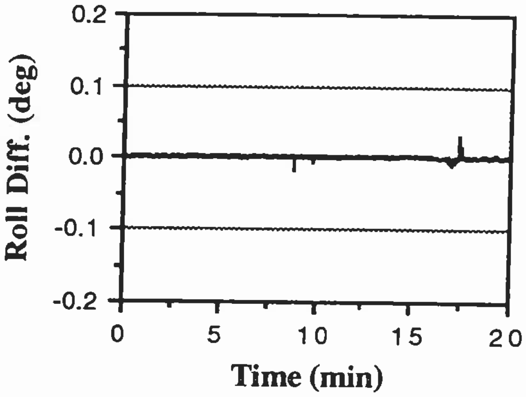

Fig. 5.14c Kinematic roll difference

Fig. 5.14 Attitude differences between the transformation matrix approach and the vector orientation approach

Table 5.1 shows the rms values of the difference in attitude parameters between the 3DF system and the inertial system. The rms values for the direct approach and the vector orientation approach are almost the same. Therefore, only two rms values are given for each parameter. The first represents the difference between the INS attitude and the attitude of the 3DF estimated by using the transformation method, while the second shows the difference with respect to the vector orientation technique, which is equivalent to the direct approach.

Attitude parameter	Static		Kinematic	
	Transformation Matrix	Vector orientation	Transformation Matrix	Vector orientation
Heading	0.079	0.076	0.128	0.108
Pitch	0.187	0.188	0.389	0.399
Roll	0.145	0.141	0.230	0.221

Table 5.1 rms of (INS-3DF) differences using different attitude determination techniques (deg)

To test the significance of the difference between the accuracy obtained from different methods, the variances where compared using the F-test. The test statistic is of the following form:

$$\frac{\sigma^2{}_2}{\sigma^2{}_1} \geq F_{df,\alpha} \qquad (5.2)$$

see (Comrey et al.,1989), where $\sigma^2{}_2$ is the larger variance, $\sigma^2{}_1$ is the smaller variance, and $F_{df,\alpha}$ is the Fisher ratio for the degrees of freedom df and significance level α. The Fisher ratio is determined from the Fisher table as 1.1, considering the number of epochs used in testing, and taking α as equal to 5%. Results of the comparison between the variances are given in Table 5.2 which shows that all differences in attitude determination are statistically insignificant, except for the case of kinematic heading. The reason for this has been described before. It should be emphasized that the results given here are conclusive for this test condition and the chosen order of rotations in the transformation matrix. In other situations, such as in airborne mode, roll and pitch may have large values, especially during take-off, landing or turns. Other rotation sequences may therefore become advantageous. Statistical significance of results may be different from the one shown in this comparison.

Attitude parameter	Static	Kinematic
Heading	1.080	1.405
Pitch	1.011	1.052
Roll	1.058	1.083

Table 5.2 Variance ratio of attitude differences using different attitude determination techniques

CHAPTER 6

ESTIMATION PROCEDURES AND THE NETWORK APPROACH

Determination of attitude from the transformation matrix between the body frame and the local-level frame or from direct vector orientation in the local-level frame requires estimation of the antenna baseline vectors in the local-level frame. These vectors are originally derived in the WGS-84 frame and then transformed to the local-level frame. Therefore, the accuracy of estimating attitude is directly proportional to the accuracy of determining antenna baseline vectors in the WGS-84 frame. In Section 3.2.3, vector determination in the WGS-84 frame using GPS phase measurements has been presented. In this approach, baselines are determined independently, i.e. the baselines are solved one by one. Consequently, if m antennas are used for attitude determination, there will be m-1 independent single baseline solutions.

In attitude determination, however, the baselines can be determined more accurately if all baselines are considered in one estimation process, i.e. in a network adjustment. There are two reasons for increasing the accuracy:

1- The antenna baseline lengths are short (typically in the range of 1 to 30 metres), and if the antennas are located properly on the rigid body, such that they do not experience significant relative movements, the geometry of the antenna configuration can be accurately determined. The elements of the determined geometry can be taken as the baseline lengths and the in-plane angles. The geometric elements either can be taken as constraints in the network solution, or they can be taken as additional measurements along with the GPS phase measurements. One should notice that the use of the in-plane angles is only possible in the network solution, as the baseline by baseline solution cannot benefit from such information.

2- In network adjustment, the correlation between the baselines are taken into account. This correlation is completely ignored if the baseline by baseline solution is implemented.

If the attitude is determined using m antennas, where measurements of n satellites are collected at each antenna, there will be (m-1)x(n-1) independent phase double difference measurements. In network adjustment, as mentioned above, the measured antenna baseline lengths and the in-plane angles increase number of measurements available. The number of baselines that can be identified in this case is m (m-1)/2, only (m-1) of them are independent. For the (m-1) independent baselines, there are 3(m-1) unknowns, where each independent baseline can be defined by the component set (ΔX, ΔY, ΔZ) in the WGS-84 frame. If the total number of measurements exceeds the number of unknowns, an over-determined solution using, either a least-squares approach or Kalman filtering can be used.

This chapter presents the method of solving the multi-antenna baselines as a small network. The constrained least-squares adjustment approach is given as an example. Details about the observation and constraint equations and the design matrices are given. Finally, a theoretical and practical comparison between solving the baselines one by one and as a network concludes the chapter.

6.1 GPS Carrier Phase Observation Equations in the Network Adjustment Approach

As mentioned in Section 3.3, the minimum number of antennas required for a unique 3D attitude determination is three, which gives two independent baselines. Therefore the network adjustment process will be given for this case of three antennas. Keeping in mind that the effect of adding redundant antennas will simply mean increasing the number of measurements, unknowns, and constraints. In other words, the redundant antennas and baselines do not need any special treatment.

If the three antennas A, B and C are used for attitude determination, as shown in Figure 6.1, the observation equations of the independent baselines AB and AC take the form:

$$\begin{bmatrix} \nabla\Delta\phi^{AB}{}_{n-1x1} \\ \nabla\Delta\phi^{AC}{}_{n-1x1} \end{bmatrix} = \begin{bmatrix} E^{AB}{}_{n-1x3} & 0 \\ 0 & E^{AC}{}_{n-1x3} \end{bmatrix} \begin{bmatrix} \bar{b}^{AB}{}_{1x3} \\ \bar{b}^{AC}{}_{1x3} \end{bmatrix} \tag{6.1}$$

where all phase measurements are used corrected from ambiguity biases after determining their values, and assuming that both baselines have the same number of measurements, which is n-1.

The baseline BC is treated here as a nuisance baseline, and no measurements are assigned to it. The reason behind this assumption is explained in the following. In GPS positioning, the measurements are all taken at the antennas, with no identification of the baselines realized. The virtual baselines are created and the measurements are assigned to them when formulating the differencing equations of the measurements taken at the ends of the sought baselines. Consequently, when the differenced phase measurements are corrected from phase ambiguity and other systematic errors, in a closed loop antenna traverse, one baseline should have dependent measurements, which can be calculated from measurements that are considered for other baselines. Similarly, in the example given, the double difference phase measurements of the baseline BC can be derived from the relation:

$$\nabla\Delta\phi_{BC} = \nabla\Delta\phi_{AC} - \nabla\Delta\phi_{AB} \tag{6.2}$$

As the measurement $\nabla\Delta\phi_{BC}$ is dependent, it cannot be used in the observation equations.

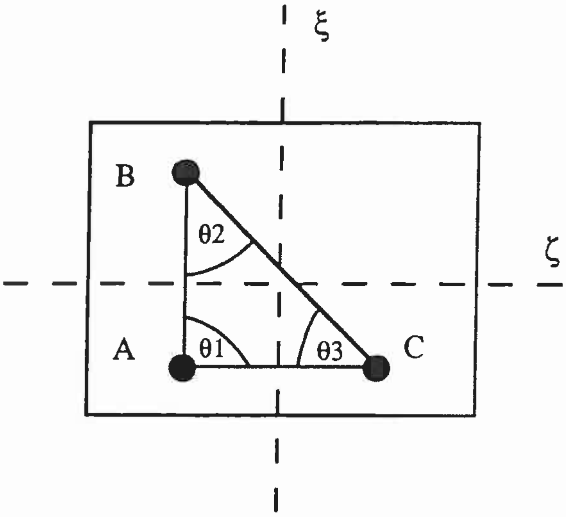

Fig. 6.1 Antennas configuration as a small network

6.2 The Constraint Equations

The network adjustment process is applicable when the antennas do not experience relative movements. If the known lengths of the baselines and angles are taken as constants, the small network formed between the antennas will have constraints of three categories, namely distances, angles and closure. For the example shown in Figure 6.1, the constraints can be identified as:

1- three constant spatial lengths (b_{AB}, b_{AC} and b_{CB}).

2- three constant in-plane angles ($\theta 1$, $\theta 2$ and $\theta 3$).

3- three closure constraints, namely are;

$$\Sigma b_X = \Sigma b_Y = \Sigma b_Z = 0$$

The constraint equations can be written in the general model $f_2(\chi) = 0$ explicitly as follows:

i- Length constraints:

$$b_{AB} - \sqrt{\Delta X^2{}_{AB} + \Delta Y^2{}_{AB} + \Delta Z^2{}_{AB}} = 0 \qquad (6.3)$$

$$b_{AC} - \sqrt{\Delta X^2_{AC} + \Delta Y^2_{AC} + \Delta Z^2_{AC}} = 0 \qquad (6.4)$$

$$b_{BC} - \sqrt{\Delta X^2_{BC} + \Delta Y^2_{BC} + \Delta Z^2_{BC}} = 0 \qquad (6.5)$$

where $(\Delta X, \Delta Y, \Delta Z)_{ij}$ are the components of the baseline ij along the principal axes (X, Y, Z) of the WGS 84 frame, and b_{AB}, b_{AC}, and b_{BC} are the lengths of the baselines AB, AC, and BC, respectively.

ii- In-plane angle constraints:

If the baseline vector components of two baselines, for instance b1 and b2, are known, the spatial angle (θ) contained between the two baselines can be determined from the equation:

$$\theta = \cos^{-1} \frac{\bar{\mathbf{b1}} \cdot \bar{\mathbf{b2}}}{\|b1\| \, \|b2\|} \qquad (6.6)$$

Where $\bar{\mathbf{b1}}$ and $\bar{\mathbf{b2}}$ are the baseline vectors, and $\|b1\|$ and $\|b2\|$ are their corresponding magnitudes. Similarly, the equations of the three angle constraints of the small network can be written as:

$$\theta_1 - \cos^{-1} \frac{\Delta X_{AB} \; \Delta X_{AC} + \Delta Y_{AB} \, \Delta Y_{AC} + \Delta Z_{AB} \; \Delta Z_{AC}}{b_{AB} \;\; b_{AC}} = 0 \qquad (6.7)$$

$$\theta_2 - \cos^{-1} \frac{\Delta X_{BA} \; \Delta X_{BC} + \Delta Y_{BA} \, \Delta Y_{BC} + \Delta Z_{BA} \; \Delta Z_{BC}}{b_{BA} \;\; b_{BC}} = 0 \qquad (6.8)$$

$$\theta_3 - \cos^{-1} \frac{\Delta X_{CA} \; \Delta X_{CB} + \Delta Y_{CA} \, \Delta Y_{CB} + \Delta Z_{CA} \; \Delta Z_{CB}}{b_{CA} \;\; b_{CB}} = 0 \qquad (6.9)$$

In this limited example, the baseline BC cannot be computed independently using phase measurements. Therefore, during the adjustment process its components in the WGS-84 system will simply be estimated as the difference between the components of the baselines AB and BC. As a result, the closure constraints cannot be used in the adjustment process since the basic assumption to apply this type of constraints is that all baseline components used should be independent. However, the length and angle constraints are all still valid since the constraints themselves, i.e. the values of the lengths and angles, are measured independently.

Under these conditions, equation (6.5), (6.8) and (6.9) can be re-written as:

$$b_{BC} - \sqrt{(\Delta X_{AB} - \Delta X_{AC})^2 + (\Delta Y_{AB} - \Delta Y_{AC})^2 + (\Delta Z_{AB} - \Delta Z_{AC})^2} = 0 \qquad (6.10)$$

$$\theta_2 - \cos^{-1} \frac{\Delta X_{BA} (\Delta X_{AC} - \Delta X_{AB}) + \Delta Y_{BA} (\Delta Y_{AC} - \Delta Y_{AB}) + \Delta Z_{BA} (\Delta Z_{AC} - \Delta Z_{AB})}{b_{BA}\, b_{BC}} = 0 \qquad (6.11)$$

$$\theta_3 - \cos^{-1} \frac{\Delta X_{CA} (\Delta X_{AB} - \Delta X_{AC}) + \Delta Y_{CA} (\Delta Y_{AB} - \Delta Y_{AC}) + \Delta Z_{CA} (\Delta Z_{AB} - \Delta Z_{AC})}{b_{CA}\, b_{CB}} = 0 \qquad (6.12)$$

6.3 The Constrained Least-Squares Approach

In Section 3.2.4, a summary of the least-squares approach was given for attitude determination using GPS phase measurements. In network adjustment, the same basic least-squares approach can be applied. However, in this case, the unknowns are the baseline vectors in the WGS-84 frame. Naturally, as the unknowns and the observation equations differ between the two cases, the structure of the design matrices also differ. The design matrices under consideration are: the observation partial derivatives matrix (A) and the observation misclosure vector (w). On the other hand, due to using some constraints in the network adjustment procedure, an additional process reflecting the effect of the constraints on the solution should be included.

The observation model used for phase double difference measurements in the least-squares approach is given as :

$$l = f_1(\chi)$$

Starting from approximate values of the baseline components (χ_o), the unknown vector of corrections (δ_1) is determined from:

$$\delta_1 = (A^T \cdot CL^{-1} A)^{-1} A^T CL^{-1} w_1 \qquad (6.13)$$

In network adjustment, the constraints model can be assumed as (Mikhail and Ackermann, 1977):

$$f_2(\chi) = 0 \qquad (6.14)$$

For the constraint equations given, there are two additional design matrices, which are: the constraint partial derivative matrix (D), and the constraint misclosure vector (w_2). The two design matrices are written as:

$$D = \frac{\partial f_2(\chi)}{\partial \chi} \,|\, \chi_o \qquad (6.15)$$

$$w_2 = f_2(\chi) | \chi_o \qquad (6.16)$$

Taking N as ($A^T CL^{-1} A$), the final vector of corrections ($\hat{\delta}$) can be determined as:

$$\hat{\delta} = \delta_1 - N^{-1} D^T (D N^{-1} D^T)^{-1} (w_2 + D \delta_1) \qquad (6.17)$$

see (Vanicek and Krakiwsky, 1982). Adding the corrections to the approximate values of the unknowns gives the corrected unknowns $\hat{\chi}$, where:

$$\hat{\chi} = \chi_o + \widehat{\delta} \qquad (6.18)$$

The variance-covariance matrix of the baseline components ($C\hat{\chi}$) is derived from:

$$C\hat{\chi} = C\widehat{\delta} = \sigma^2 \left(N^{-1} - N^{-1} D^T \left(D \; N^{-1} D^T \right)^{-1} D \, N^{-1} \right) \qquad (6.19)$$

where σ^2 is the *posteriori* variance of the unknowns.

6.4 The weight Matrix

GPS phase measurements without differencing are uncorrelated. In addition, since there is no prior information about the accuracy of individual phase measurements, the variance of all phase measurements has been assumed equal. Obviously, the derived single and double difference phase measurements are correlated through the differencing process. For instance, if phase measurements of n satellites are available for the baseline ij, the double differences are computed as (Hofmann-Wellenhof et al.,1992):

$$\begin{bmatrix} \Delta\phi_1^{ij} - \Delta\phi_2^{ij} \\ \Delta\phi_1^{ij} - \Delta\phi_3^{ij} \\ . \\ \Delta\phi_1^{ij} - \Delta\phi_{n-1}^{ij} \end{bmatrix} = [\, G \mid K \,] \; (\phi_1^i, \phi_2^i, \ldots, \phi_n^i \mid \phi_1^j, \phi_2^j, \ldots \phi_n^j)^T \qquad (6.20)$$

where :

$$G = \begin{bmatrix} 1 & -1 & 0 & . & 0 \\ 1 & 0 & -1 & . & 0 \\ . & . & . & . & . \\ 1 & 0 & 0 & . & -1 \end{bmatrix}_{n-1xn} \qquad (6.21)$$

and

$$K = \begin{bmatrix} -1 & 1 & 0 & . & 0 \\ -1 & 0 & 1 & . & 0 \\ . & . & . & . & . \\ -1 & 0 & 0 & . & 1 \end{bmatrix}_{n-1xn} \qquad (6.22)$$

Similarly, when solving for the antenna triad as a small network, the phase double difference measurements of the baselines AB and AC can be written as:

$$\begin{bmatrix} \Delta\phi_1{}^{AB} - \Delta\phi_2{}^{AB} \\ \Delta\phi_1{}^{AB} - \Delta\phi_3{}^{AB} \\ \cdot \\ \Delta\phi_1{}^{AB} - \Delta\phi_{n-1}{}^{AB} \\ \text{-----------} \\ \Delta\phi_1{}^{AC} - \Delta\phi_2{}^{AC} \\ \Delta\phi_1{}^{AC} - \Delta\phi_3{}^{AC} \\ \cdot \\ \Delta\phi_1{}^{AC} - \Delta\phi_{n-1}{}^{AC} \end{bmatrix} =$$

$$\begin{bmatrix} G & K & 0 \\ G & 0 & K \end{bmatrix} (\phi_1{}^A, \phi_2{}^A, ..., \phi_n{}^A \mid \phi_1{}^B, \phi_2{}^B, ...\phi_n{}^B \mid \phi_1{}^C, \phi_2{}^C, ...\phi_n{}^C)^T \qquad (6.23)$$

Assuming that the common variance of the single phase measurements is σ^2, the covariance matrix of the phase measurements is then estimated as $(\sigma^2 I)$, where I is the unity matrix. Taking:

$$Q = \begin{bmatrix} G & K & 0 \\ G & 0 & K \end{bmatrix} \qquad (6.24)$$

and applying the covariance law, the covariance matrix of the double difference phase measurements used in network adjustment can then be derived as:

$$\begin{aligned} CL &= Q\ (\sigma^2 I)\ Q^T \\ &= \sigma^2 Q\ Q^T \end{aligned} \qquad (6.25)$$

The weight matrix of the double difference measurements can simply be taken as the inverse of the covariance matrix multiplied by *apriori* variance.

Computation of the matrix CL is a straightforward process. Both the correlation between the double difference phase measurements and the correlation between the baselines are easily determined. During the different observation epochs, changes in the computation of the matrix CL is limited to changes in matrix size, which varies with the number of satellites observed for each baseline. Some algorithms assume, for simplicity, a unit weight matrix, ignoring the correlation between the measurements and the correlation between the baselines. Both approaches will be tested to show their difference in performance.

6.5 Design Matrices

The misclosure matrices (w_1 and w_2) are computed in a straightforward manner using the approximate unknowns. The elements of the partial derivative matrix of the double difference phase observation equations are determined as:

$$\frac{\partial \nabla\Delta\phi}{\partial \Delta X} = [\, e_{Xi} - e_{Xj} \,] \qquad (6.26)$$

$$\frac{\partial \nabla\Delta\phi}{\partial \Delta Y} = [\, e_{Yi} - e_{Yj} \,] \qquad (6.27)$$

$$\frac{\partial \nabla\Delta\phi}{\partial \Delta Z} = [\, e_{Zi} - e_{Zj} \,] \qquad (6.28)$$

where i and j are the satellites used in the observation equation.

The elements of the partial derivative matrix (D) for the distant constraints, are given as:

$$\frac{\partial b}{\partial \Delta X} = \frac{\Delta X}{b} \qquad (6.29)$$

$$\frac{\partial b}{\partial \Delta Y} = \frac{\Delta Y}{b} \qquad (6.30)$$

$$\frac{\partial b}{\partial \Delta Z} = \frac{\Delta Z}{b} \qquad (6.31)$$

As mentioned before, the in-plane angle θ contained between two baselines, for instance, the baselines 1 and 2, gives the angular constraint:

$$\theta - \cos^{-1}\frac{\Delta X1\ \Delta X2 + \Delta Y1\ \Delta Y2 + \Delta Z1\ \Delta Z2}{b1\ \ b2} = 0 \qquad (6.32)$$

taking

$$k = \frac{\Delta X1\ \Delta X2 + \Delta Y1\ \Delta Y2 + \Delta Z1\ \Delta Z2}{b1\ \ b2} \qquad (6.33)$$

The elements of the design matrix A for the angular constraint (θ) can be formulated as:

$$\frac{\partial\ \theta}{\partial \Delta X1} = \frac{-1}{\sqrt{1-k^2}}\ [\ \frac{\Delta X2}{b1\ b2} - \frac{\Delta X1\ (\Delta X1\ \Delta X2 + \Delta Y1\ \Delta Y2 + \Delta Z1\ \Delta Z2)}{b1^3\ \ b2}\ ] \qquad (6.34)$$

$$\frac{\partial\ \theta}{\partial \Delta Y1} = \frac{-1}{\sqrt{1-k^2}}\ [\ \frac{\Delta Y2}{b1\ b2} - \frac{\Delta Y1\ (\Delta X1\ \Delta X2 + \Delta Y1\ \Delta Y2 + \Delta Z1\ \Delta Z2)}{b1^3\ \ b2}\ ] \qquad (6.35)$$

$$\frac{\partial\ \theta}{\partial \Delta Z1} = \frac{-1}{\sqrt{1-k^2}}\ [\ \frac{\Delta Z2}{b1\ b2} - \frac{\Delta Z1\ (\Delta X1\ \Delta X2 + \Delta Y1\ \Delta Y2 + \Delta Z1\ \Delta Z2)}{b1^3\ \ b2}\ ] \qquad (6.36)$$

$$\frac{\partial\ \theta}{\partial \Delta X2} = \frac{-1}{\sqrt{1-k^2}}\ [\ \frac{\Delta X1}{b2\ b1} - \frac{\Delta X2\ (\Delta X2\ \Delta X1 + \Delta Y2\ \Delta Y1 + \Delta Z2\ \Delta Z1)}{b2^3\ \ b1}\ ] \qquad (6.37)$$

$$\frac{\partial\ \theta}{\partial \Delta Y2} = \frac{-1}{\sqrt{1-k^2}}\ [\ \frac{\Delta Y1}{b2\ b1} - \frac{\Delta Y2\ (\Delta X2\ \Delta X1 + \Delta Y2\ \Delta Y1 + \Delta Z2\ \Delta Z1)}{b2^3\ \ b1}\ ] \qquad (6.38)$$

$$\frac{\partial\ \theta}{\partial \Delta Z2} = \frac{-1}{\sqrt{1-k^2}}\ [\ \frac{\Delta Z1}{b2\ b1} - \frac{\Delta Z2\ (\Delta X2\ \Delta X1 + \Delta Y2\ \Delta Y1 + \Delta Z2\ \Delta Z1)}{b2^3\ \ b1}\ ] \qquad (6.39)$$

Equation (6.34) to (6.39) can be applied for the three constant angles θ1, θ2, and θ3 considered in the given network example. Note that, proper signs of the vector components should be taken into consideration when substituting into these equations.

6.6 General Remarks

When solving the multi-antenna baselines as a small network, some points are worth mentioning, such as:

- in attitude determination, the observation equations are linear. This is due to treating the receiver position as known information after it has been determined for the reference antenna of the network. The distance and angular constraint equations, on the other hand, are non-linear. Therefore, a few iterations are required to overcome the non-linearity problem.

- the maximum and minimum standard deviations can be easily determined from the covariance matrix of the relative antenna coordinates in the WGS-84 frame. For instance, taking the sub-matrix (2x2) representing the horizontal uncertainty of one of the vectors, the maximum and minimum standard deviations are expressed as the square roots of the maximum and minimum eigenvalues of this matrix. These standard deviations define the semi-major and semi-minor axes of the error ellipse. Their values can be directly determined from Richardus (1966):

$$\sigma_{max.} = \sqrt{\frac{1}{2}(\sigma_{\Delta X}{}^2 + \sigma_{\Delta Y}{}^2) + \sqrt{\frac{1}{4}(\sigma_{\Delta X}{}^2 - \sigma_{\Delta Y}{}^2)^2 + \sigma^2_{\Delta X \Delta Y}}} \qquad (6.40)$$

$$\sigma_{min.} = \sqrt{\frac{1}{2}(\sigma_{\Delta X}{}^2 + \sigma_{\Delta Y}{}^2) - \sqrt{\frac{1}{4}(\sigma_{\Delta X}{}^2 - \sigma_{\Delta Y}{}^2)^2 + \sigma^2_{\Delta X \Delta Y}}} \qquad (6.41)$$

The orientation of the semi-major axis (α) is obtained as:

$$(\alpha) = \frac{1}{2}\tan^{-1}\frac{2\,\sigma_{\Delta X \Delta Y}}{(\sigma_{\Delta X}{}^2 - \sigma_{\Delta Y}{}^2)} \qquad (6.42)$$

These standard deviations are calculated based on a 39.4% probability level. Other error ellipses with higher confidence region can be obtained by magnifying the eigenvalues by a constant taken from Fisher distribution tables.

6.7 Comparison between Solving the Multi-Antenna System Baseline-by-Baseline and as a Small Network

6.7.1 Conceptual Comparison

There are two methods that can be used for solving the multi-antenna baselines, namely the baseline-by-baseline approach or the network approach. The advantages and disadvantages of the two methods are summarized in the following.

- the degrees of freedom increase considerably when network adjustment is applied. Thus, the final solution will usually be more reliable. For instance, for the small network given in this chapter, the total number of constraints is six. Thus, for n phase double differences, the total number of observation and constraint equations will be (2n+6), assuming that both the baselines AB and AC have the same number of phase double difference measurements. Since the total number of independent unknowns are six, the total degrees of freedom will be $2n + 6 - 6 = 2n$.

In comparison to the baseline by baseline solution, the degree of freedom for each of the baselines is $n + 1 - 3$, where the baseline length is taken as a constraint. For both independent baselines AB and AC, the degree of freedom is $2 (n + 1 - 3) = 2n - 4$.

The degrees of freedom is thus increased by 4 using the network approach. For a real-time solution, when the number of measurements available is limited, such an increase in the degrees of freedom should improve results significantly.

- The correlation is not modeled correctly for the single baseline solution because correlation between baselines are neglected. This is not the case for the network solution.

- The computations are much simpler when using the baseline-by-baseline method. This is the single most important advantage of the baseline-by-baseline solution.

- Computation time needed using the baseline-by-baseline method is much less than that needed by the network solution. However, since the number of baselines is limited, the difference in computation time between the two methods is only a few milli-seconds for a 486 Dx computer with 50 MHz clock rate.

- Cycle slips are more easily detected and repaired in the network approach, see Beck et al., 1989.

- The use of constraints, which enhance the accuracy of the network adjustment and make it more elegant, is restricted to applications in which the antennas do not experience relative motion.

6.7.2 Practical Comparison Based on Field Testing

As shown before, the network solution is more rigorous than the baseline-by-baseline solution. However, no direct comparisons exist which would state the difference in accuracy between the two methods based on field data, and whether or not the accuracy gained worth applying the network adjustment technique.

This section covers these questions by analyzing results of field tests, where both methods have been applied. The field tests include three static tests and a kinematic one. Two of the static tests were performed with antennas mounted on tripods, while the third one and the kinematic tests were performed using a van. The tests have different antenna geometry (except for the third static and the kinematic tests which have the same antenna geometry), such that the investigation is not restricted to a special antenna configuration.

6.7.2.1 Test Methodology

Improvement of accuracy gained through using the network adjustment comes from two factors, namely the use of geometric information (the constraints), and the inclusion of baseline correlation. The change in accuracy due to each factor will be shown independently. Therefore, the multi-antenna baselines have been estimated in the WGS-84 using three separate approaches, namely:

1- baseline-by-baseline solution,
2- network solution with unit weight matrix,
3- network solution with correct weight matrix.

In each case, attitude parameters were determined following the approach described in Section 3.2.4. To illustrate differences in accuracy between the three solutions, the root mean square error (rms) is chosen as the accuracy figure. Comparing the rms of the first case with that of the second will show accuracy gain due to the use of geometric constraints. Comparing the rms results of the second and the third case will show change in accuracy due to proper consideration of correlations, i.e. the use of a fully populated weight matrix. Finally, comparing results of the first and the third case will show the full potential of the network solution.

6.7.2.2 Static Testing on the Roof of the Engineering Building, U of C

In the first segment of tests, two static tests have been performed. The tests were performed on top of the Engineering building at the University of Calgary. The antennas were mounted on tripods, which gave flexibility in choosing antenna locations and baseline lengths. The test configurations are shown in Figures 6.2 and 6.3. Due to the presence of surrounding buildings, the test site is considered as a high multipath environment.

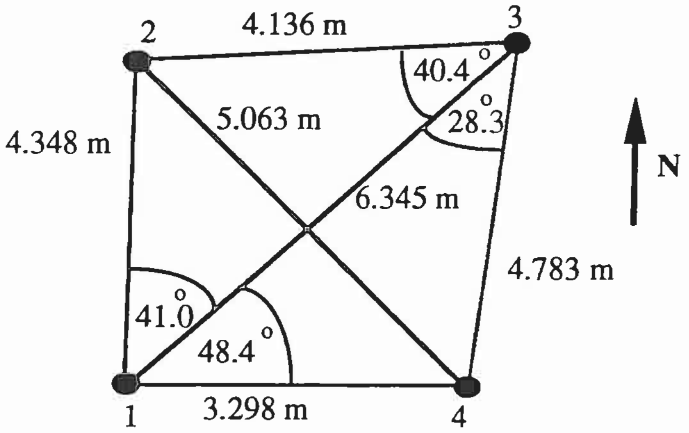
2
4.136 m
3
40.4°
28.3°
5.063 m
4.348 m
6.345 m
4.783 m
N
41.0°
48.4°
1
3.298 m
4

Fig. 6.2 First test configuration

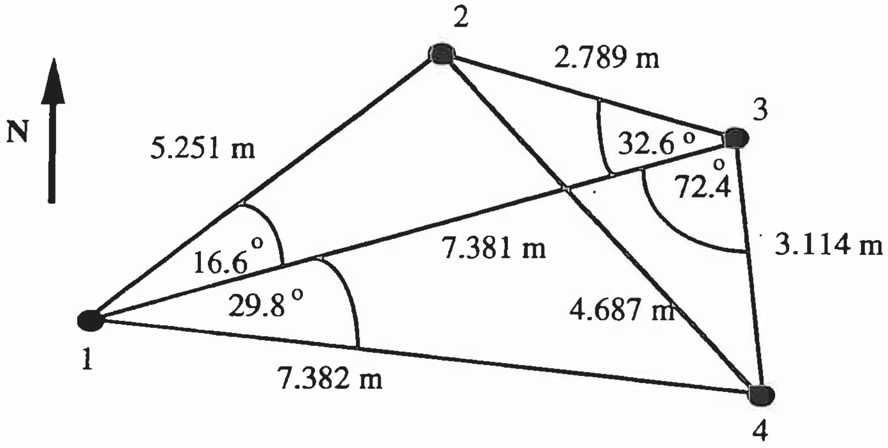
2
2.789 m
3
N
5.251 m
32.6°
72.4°
3.114 m
16.6°
7.381 m
29.8°
4.687 m
1
7.382 m
4

Fig. 6.3 Second test configuration

For each of the antenna configurations shown in Figure 6.2 and 6.3, there are six baselines and six internal angles that can be accurately determined. There are also three independent unknown baselines, namely 1-2, 1-3 and 1-4. Assuming that for each baseline, n phase double difference measurements are available, the degrees of freedom for the network solution will be:

$$3\,n + 6 + 6 - 3(3) = 3\,n + 3$$

while for the baseline-by-baseline solution the overall number of degrees of freedom is:

$$3\,n + 3 - 3(3) = 3\,n - 6$$

which means an increase by 9 degrees of freedom for the network adjustment approach.

The first test has 2145 epochs of measurements, with a data interval of one second, while the second test has 2161 epochs with the same data rate. The number of satellites observed ranged from four to six, which gave PDOP between 2.1 to 6.0, AZDOP between 1.0 to 3.5, and El-DOP between 0.9 to 4.3. Attitude parameters were computed at each epoch. The heading, pitch and roll outputs were referenced to mean values computed from the whole data set using the rigorous network approach. The data is long enough to consider the means as "close to the true". The estimated rms using each of the tested methods are shown in Table 6.1 for the first test, and in Table 6.2 for the second test. The rms values are given in degrees.

Attitude component	Baseline by baseline solution **case 1**	Network adjustment using unit weight **case 2**	Network adjustment using full weight **case 3**
Heading	0.0275	0.0288	0.0283
Pitch	0.0590	0.0412	0.0446
Roll	0.0642	0.0354	0.0452

Table 6.1 rms values (deg) for attitude parameters using different methods for the multi-antenna baseline estimation (**test 1**)

Attitude component	Baseline by baseline solution **case 1**	Network adjustment using unit weight **case 2**	Network adjustment using full weight **case3**
Heading	0.0354	0.0265	0.0312
Pitch	0.0441	0.0351	0.0339
Roll	0.0613	0.0463	0.0422

Table 6.2 rms values (deg) for attitude parameters using different methods for the multi-antenna baseline estimation (**test 2**)

To test the significance of the difference between accuracy obtained from different methods, the variances where compared using the F-test. Considering the number of epochs used in testing, the Fisher ratio is determined from Fisher table as 1.08, taking α equals to 5%. Results of comparison between the variances are shown in Table 6.3.

When comparing test results, it is clear that, in general, applying the network solution gives better results than applying the baseline-by-baseline solution. Only the accuracy of the heading in the first test shows slight degradation. Otherwise, the accuracy improvement is significant from the statistical point of view. However, the accuracy changes due to including the correct correlation give mixed results. In the first table, the heading accuracy does not change significantly when the fully populated weight matrix is used, while accuracies for pitch and roll are degraded. In the second test, the opposite happens, the heading degrades when utilizing the full weight matrix, while the accuracy of pitch and roll improves, although the improvement in pitch is not statistically significant. In general, the changes are small and not significant from the practical point of view.

Attitude parameter	First test			Second test		
	case 1 : case 2	case 1 : case 3	case 2 : case 3	case 1 : case 2	case 1 : case 3	case 2 : case 3
Heading	1.097	1.059	1.036	1.784	1.287	1.386
Pitch	2.051	1.750	1.178	1.578	1.692	1.072
Roll	3.289	2.017	1.630	1.753	2.110	1.203

Table 6.3 Variance ratio between different methods in roof tests

6.7.2.3 Static and Kinematic Van Tests

The second segment of testing was performed on data of static and kinematic tests similar to the ones given in the previous chapter. Five to six satellites were used in this case. Since four antennas with three main baselines are used in this case, the degrees of freedom was (3 n - 6) using the baseline-by-baseline solution and (3 n + 3) using the network adjustment approach. The same test methodology was applied as in the first test. The inertial system is used as the reference system in this test segment. Attitude outputs of the multi-antenna system were compared to those of the inertial system to show the behaviour and accuracy of the first one. Table 6.4 and 6.5 show the rms values of the static and kinematic tests, respectively. The F-test was used to test the significance of the differences between the accuracy obtained from different methods as shown in the previous section. Results are given in table 6.6. The Fisher ratio for the static test is 1.112, where df was 908, and α is taken 5%. For the kinematic case, using the same significance level and 1212 degrees of freedom, the Fisher ratio is taken as 1.1.

Attitude component	Baseline by baseline solution case 1	Network adjustment using unit weight case 2	Network adjustment using full weight case 3
Heading	0.0672	0.0641	0.0648
Pitch	0.1361	0.1157	0.1160
Roll	0.1141	0.1033	0.0922

Table 6.4 rms values (deg) for attitude parameters using different methods for the multi-antenna baseline estimation

(static van test)

Attitude component	Baseline by baseline solution case 1	Network adjustment using unit weight case 2	Network adjustment using full weight case 3
Heading	0.0958	0.0888	0.0813
Pitch	0.3262	0.2932	0.2726
Roll	0.1947	0.1734	0.1443

Table 6.5 rms values (deg) for attitude parameters using different methods for the multi-antenna baseline estimation

(kinematic van test)

Table 6.4 shows that the network method gives better results than the baseline-by-baseline solution in the static test. However, only pitch and roll results were statistically significant.

Attitude parameter	Static test			Kinematic test		
	case 1 : case 2	case 1 : case 3	case 2 : case 3	case 1 : case 2	case 1 : case 3	case 2 : case 3
Heading	1.099	1.075	1.022	1.164	1.389	1.193
Pitch	1.384	1.377	1.005	1.238	1.432	1.157
Roll	1.220	1.531	1.255	1.261	1.8205	1.444

Table 6.6 Variance ratio between different methods in van tests

When comparing results for uncorrelated and correlated weight measurement matrices, results are again not conclusive. The rms for heading and pitch using a unit weight matrix are smaller than those estimated utilizing the fully populated measurement weight matrix. For roll, it is the other way round. However, one should notice that the differences between the rms values are marginal and it was statistically significant only for roll. The kinematic results, given in table 6.5, depict clearly that the use of the network adjustment with a full weight measurement matrix gives the best results in all attitude parameters, and from the statistical point of view the differences were significant. Although small vibration of the antenna frame occurred during the kinematic test, under the experienced mild dynamics, this vibration was not a limiting factor to applying the network approach.

The limited study presented here confirms the theoretical considerations and shows that the use of a network solution in general improves attitude estimation as compared to a baseline-by-baseline approach. The additional computational time needed to apply the network approach is few milliseconds for each epoch. The network approach can therefore be used in real-time.

CHAPTER 7

AMBIGUITY RESOLUTION TECHNIQUES

In order to determine the attitude of a moving vehicle from carrier phase measurements, phase ambiguities must be resolved. They are the unknown whole carrier cycles not measured by the receiver. Different techniques have been developed to estimate phase ambiguities in Differential GPS positioning (DGPS). When attitude determination using GPS became feasible in the late 1980's, ambiguity resolution techniques have been modified to accommodate the conditions and requirements of attitude determination.

Since attitude determination is mainly needed in kinematic applications, instantaneous ambiguity resolution becomes the key element in achieving a reliable solution. Therefore, the chapter is focused on instantaneous ambiguity resolution techniques. First, a brief overview of existing techniques is given. Next, two efficient approaches are described. Both techniques use a search approach in finding the correct ambiguities. The first identifies the correct ambiguities according to a statistical criterion. The second uses a physical condition, requiring that the correct ambiguity set should give an antenna geometry close to the known one. Different factors and algorithms that can enhance computation speed and reliability of the solution are also discussed.

7.1 Existing Methods of Ambiguity Resolution

In DGPS, resolving the carrier phase ambiguities is possible by collecting and analyzing measurements within an initialization period during which significant movement of the satellites is desirable. The methods used in DGPS, which are also applicable to attitude determination, vary in concept. Most are based on finding an initial set of ambiguity values, determined from an initial solution of the antenna baseline, and assuming that the correct values lie in a preset range determined by the estimated accuracy of the initial baseline solution. Different sets of ambiguity solutions are then tested to find the correct one satisfying a specific criterion.

The criterion usually used to determined the correct ambiguity set is that it gives minimum errors in all measurements. Examples of the different techniques available are the ambiguity function method, where the maximum ambiguity function is required, see (Remondi,1984), (Remondi,1990), (Mader,1990) and (Erickson,1992a), and least-squares search approach, where ambiguity combination giving the smallest variance usually is selected as the correct one, see (Hatch,1989), (Lachapelle et al.,1992b), (Teunissen,1994), and (Jonge and Tiberius,1994). Others use Kalman filtering instead of least squares, for instance, (Landau and Euler,1992), and (Sauermann et al.,1993).

Instead of waiting for the satellites to have significant changes in geometry, controlled rotations of the antenna baselines can be used to resolve the ambiguities. In this case, the ambiguities are determined without performing any search. The baselines are first determined, and the ambiguities are then identified, for more details refer to (Brown and Ward,1990), and (Cohen and Parkinson,1992).

Fundamental differences between DGPS positioning and attitude determination exist, which should be considered when either modifying DGPS ambiguity resolution techniques or developing new ones for the case of attitude determination. They are summarized as follows:

- in DGPS, usually one station (antenna) has a fixed known position, while the other is unknown. The unknown parameters are the coordinates of the second antenna. In attitude determination both stations are unknown, and the parameters to be solved are only the baseline vector components.

- most of the traditional DGPS applications only consider one baseline at a time, some use multiple baselines, like the Wide Area Differential GPS (WADGPS). In 3D attitude determination, multiple baselines are always simultaneously considered.
- in attitude determination, the baselines are short; thus, atmospheric errors cancel out when differencing the measurements.
- in attitude determination the antennas are usually fixed on the same surface (platform); hence, baseline lengths can be measured accurately and used as additional measurements or constraints as long as the antennas do not experience relative translation motion. In addition, the spatial geometry of the antenna configuration should be the same under all conditions.
- attitude determination is mostly required in kinematic applications; thus, large changes in the dynamics of the motion can occur.

In kinematic applications, real-time output is usually required. The main problem facing real-time attitude determination is the instantaneous resolution of the carrier phase ambiguities. This is due to the fact that in kinematic applications, operations cannot be delayed for a period of static initialization or re-initialization after a loss of lock. Even in post-mission processing of airborne or ship borne data, the data collected between two loss-of-lock periods may be useless, if the phase has been lost twice (Goad and Yang,1994). If loss-of-lock occurs more frequently, all data in between the first and the last one cannot be recovered, simply because an extended time period for re-initialization of ambiguities is not available. The only way to recover all data and handle such situations is instantaneous ambiguity resolution.

Realizing that real-time ambiguity resolution is the key-element for making attitude determination achievable in almost all situations, the thesis puts great emphasis on developing techniques for instantaneous ambiguity resolution. The adopted methods use an epoch-by-epoch determination approach. The search technique is implemented because it has proven to be the most successful in DGPS, and because its main alternative, solving the ambiguities by controlled motion of the baselines, is not suitable, when re-initialization of ambiguities is required during operation. Forcing the airplane, ship or ground vehicle to go through a pattern of direction changes after loss of lock, is usually not possible, while on route.

In general, ambiguity search techniques follow four basic steps (Blomenhofer et al. 1993):

- initial estimation of the baseline vector,
- estimation of initial ambiguity values determined from the initial baseline solution,
- setting a search range for the ambiguities based on the accuracy of the initial estimation,
- testing all ambiguity combinations in the search range to determine the best one based on a specific criterion.

What makes the techniques described in this study different from the ones used in DGPS is the details in each of these steps. They will be described in the following sections.

7.2 Initial Estimation of the Carrier Phase Ambiguity

The first step in the least-squares search approach is the estimation of the initial values of the ambiguities. The search can then be conducted around the initial ambiguities within the range of their estimated accuracy. Since in the multi-antenna system the antennas are closely enough spaced, the tropospheric, ionospheric and orbital errors can be considered as virtually the same for all antennas, and are therefore eliminated in the differencing process. Assuming a combined receiver and multipath noise of less than a full cycle, which is usually the case, and neglecting other error terms, the single difference ambiguity can be determined from the equation:

$$\Delta n = n_2 - n_1 = \text{integer} \ \{ (\phi_2 - \Delta\phi_{12}) - \phi_1 \} \qquad (7.1)$$

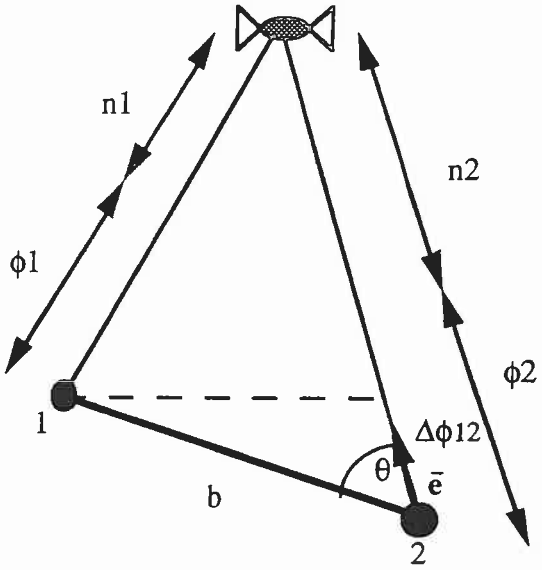

Fig. 7.1 Phase measurements and ambiguities

As shown in Figure 7.1, ϕ_1 and ϕ_2 are the phases measured at antennas 1 and 2, respectively, n1 and n2 are the corresponding ambiguities, and $\Delta\phi_{12}$ is the phase single difference between the two antennas.

To estimate the initial ambiguity values, first the antenna vector components are approximately determined. Then, the part of the phase single difference related to the baseline vector is estimated as follows:

$$\Delta\phi_{12} = \bar{\mathbf{e}} \cdot \bar{\mathbf{b}}_o + \text{errors less than one cycle} \qquad (7.2)$$

where $\bar{\mathbf{b}}_o$ is the approximate estimate of the vector, and $\bar{\mathbf{e}}$ is the receiver-to-satellite unit vector. After estimating the approximate phase single difference using equation (7.2), the estimated value is substituted into equation (7.1) to generate the initial single difference ambiguity Δn_o. The initial double difference ambiguity between satellites A and B is then estimated from the differencing relation:

$$\nabla\Delta\, n_o^{AB} = \Delta n_o^{A} - \Delta n_o^{B} \qquad (7.3)$$

7.3 Initial Estimation of the Antenna Baseline

Equations (7.2) and (7.1) show that the accuracy of the initial phase ambiguities is directly related to the accuracy of the initial baseline. As mentioned before this accuracy sets the search range for the ambiguities. Thus, the more accurate the initial baselines can be determined, the smaller the search range will be; and consequently, the smaller the number of combinations to be searched. As the number of candidate ambiguity sets decreases, ambiguity resolution becomes increasingly faster. In DGPS, the code information (pseudorange measurements) is the main source for the initial estimation of antenna positions because the code does not need any ambiguity determination (Frei et al.,1993). To increase accuracy, phase smoothing of the pseudoranges is usually applied, for more details refer to (Sauermann et al.,1993).

The use of the phase smoothing technique for the initial estimation of the baselines in attitude determination is not suitable for two reasons. First, a long observation period is needed to achieve a reliable solution. Second, the accuracy of the phase smoothed pseudoranges is still poor, especially in the presence of Selective Availability. The search region will therefore be very large.

The use of redundant information can improve initial baseline estimation and accelerate ambiguity searching. This information can be obtained from an external sensor, from redundant antennas, or by using the known baseline lengths and geometry of the antenna configuration.

Cannon et al., (1992) used the heading of a dead-reckoning system to confine the search range to ambiguity combinations that approximate this heading in the accuracy range of the external system. On the other hand, the number and distribution of antennas play a vital role in accelerating the ambiguity resolution process. The minimum number of antennas required to estimate the direction of a line in space (heading and pitch) is two. If a 3D attitude is needed, a third antenna is required to estimate roll by determining the direction of another vector orthogonal to the first one. Instead of using the minimum number of antennas, additional antennas can be added to speed up ambiguity resolution. The benefit of placing three collinear antennas along the target line when determining heading in a static environment has been discussed in (Hatch,1989), (Jurgens et al., 1991 and 1992). Two of the antennas are placed within a distance of less than one cycle, so that their short baseline can be estimated without ambiguity resolution, see Jurgens et al. (1991) for details. The heading of the two farthest antennas is then roughly estimated from the heading of the two closely spaced antennas. This heading is used to limit the region within which a least-squares approach is conducted to find the correct ambiguities.

The use of redundant antennas to accelerate ambiguity resolution will be studied in the following, keeping in mind that kinematic applications, and hence, real-time attitude determination, are of major interest. Extensions of the previous work will be presented and applied to kinematic situations. This includes enhancing the initial baseline estimation, streamlining the computational technique to reduce processing time, and developing new algorithms for robust ambiguity identification. Two major search approaches are used.

First, the method of least squares is utilized. Second, a new technique is presented where the known geometry of the antenna configuration is used to set the criterion for the correct solution.

7.4 Using Redundant Antennas for Reliable Initial Vector Estimation

If redundant antennas are placed within a short distance from one or both of the baseline antennas, such that all antennas are collinear, the closely spaced antennas can be used to estimate the main one. Initial estimation of the short baseline is not a cumbersome process as their ambiguities can be easily determined. Thus, using the length ratio between the short baseline and the longer one, initial estimation of the main baseline becomes readily possible.

Four basic configurations have been briefly discussed in here (El-Mowafy and Schwarz, 1994b) and their advantages and drawbacks will be analyzed. They are shown in Figures 7.2a to 7.2d. They do not represent an exhaustive list but they present the basic principles from which other antenna configurations can be derived. It has been assumed in the following that the spatial geometry of the vectors between the antennas is known in a suitably chosen body frame. It has also been assumed that all antennas are in one plane. This is not a necessary assumption but has been chosen for convenience.

Figure 7.2a shows the minimum configuration for fast ambiguity resolution. It uses four antennas, three along the main longitudinal axis and one on the transverse axis. Antennas 1 to 3 have to be approximately collinear and antennas 1 and 2 have to be less than half a cycle apart. The short baseline 1-2 is used to limit the search region for ambiguity resolution of baseline 1-3. Then, the known geometry is used to resolve the ambiguities of baseline 1-4. This configuration has two limitations. First, the distance 1-3 should not be longer than about 5m. Otherwise, the search region will get larger and larger, and the advantage of using this method will soon be lost. Second, the roll of the vehicle should be within a few degrees, as is the case for most land vehicle applications. If changes in roll of more than 10 degrees occur, the configuration has to be modified to obtain reliable roll determination.

Figure 7.2b shows this modification. It adds another antenna to the axis orthogonal to the main axis 1-3. This antenna is again within half a cycle of one of the other antennas along the orthogonal axis and the principle is then the same as for the main axis. This configuration will result in fast ambiguity resolution independent of the magnitude of roll.

Figure 7.2c shows a possible configuration for the case when the main axis exceeds the 5m-limit considerably. The same basic principle is now applied sequentially. The search range for baseline 1-3 is again determined by using vector components obtained from the vector 1-2. Once the ambiguities of the baseline 1-3 have been determined, its vector components can be used to determine the initial estimate of the main baseline 1-4. In this case, the distance 1-4 can be extended to about 25-30 metres without losing the capability of epoch to epoch ambiguity resolution.

Figure 7.2d shows another configuration. In this case, a pair of closely spaced antennas is used at each end of the main axis, allowing two independent determinations of the axis. This adds reliability to the procedure, and gives a unique solution for the ambiguities of the shorter baselines when baseline lengths are more than half a cycle, but less than a full one. It also allows an independent test for the estimated ambiguities. All configurations shown in Figures 7.2a to 7.2d were tested and their feasibility shown.

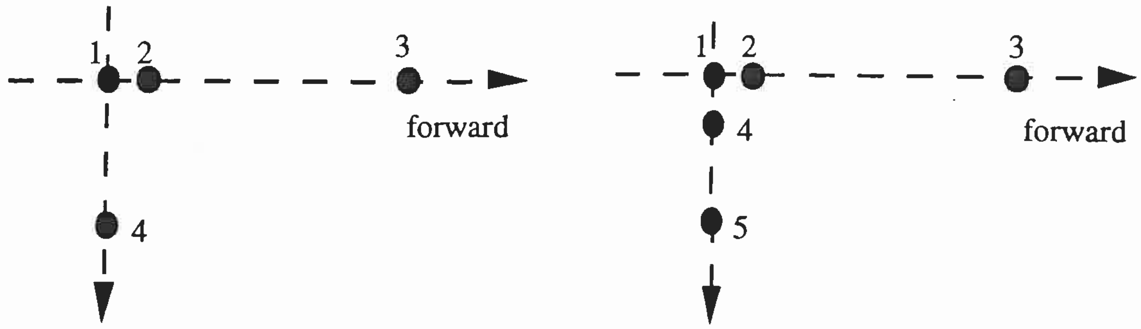

Fig. 7.2a Minimum antenna configuration with small roll angle

Fig. 7.2b Roll-independent antenna configuration

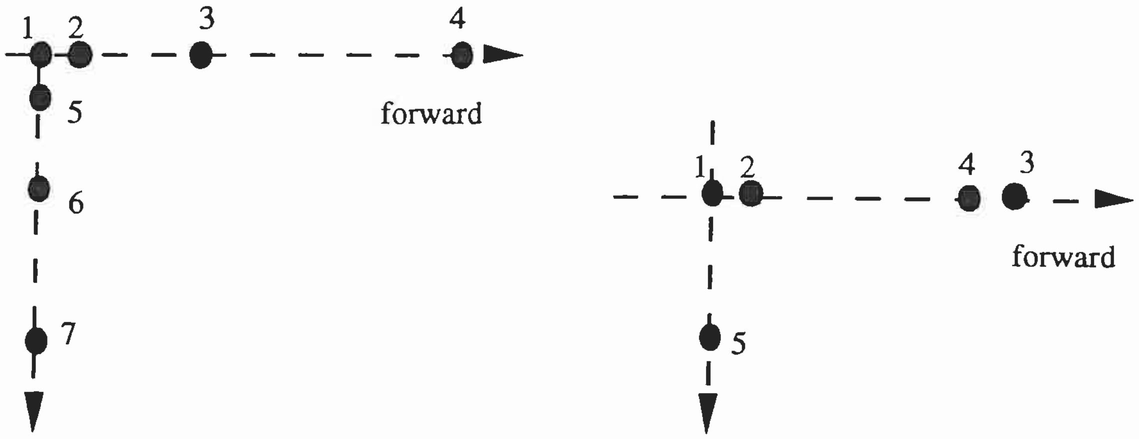

Fig. 7.2c Sequential antenna configuration for large baselines

Fig. 7.2d Overdetermined attitude estimation with small roll angle

Fig. 7.2 Antenna configurations for fast ambiguity resolution

To show the role of the selected antenna configurations in achieving a good approximation of the primary baselines, the case shown in Figure 7.2d is considered. The four antennas (1,2,3 and 4) are chosen as collinear. Taking into consideration that errors in collinearity will be reflected as errors in the estimated approximate vector components, collinearity errors should not be allowed to exceed a few millimetres. The baseline lengths are also assumed known, as they can be accurately measured. The known lengths play a vital role in estimating the approximate components of the vector 1-3.

As mentioned in Section 7.2, to use phase double differences, single differences have first to be determined. Single difference phase ambiguities of the short baselines can be estimated as the integer part of the differenced phase measurement if the baseline is within half a cycle. In that case, the maximum phase single differences measured will be a fraction of a cycle and will not exceed the baseline length. To achieve unique ambiguity estimation in practice, it is recommended that the baseline length is chosen less than half a cycle by an amount equivalent to the combined effect of all errors affecting the phase single difference measurements (see Chapter 4). When the baseline length exceeds half a cycle, but is still less than a full one, each ambiguity has potentially two solutions and thus becomes non-unique. The first solution results from taking the ambiguity single difference as the direct integer part of the phase single difference. The second solution results from considering the ambiguity as the integer part with one cycle added or subtracted, whichever gives an absolute value of the phase single difference of less than the baseline length.

If antennas cannot be placed within a distance of half a cycle, but can be placed at a distance of less than a cycle, a special technique can be utilized to estimate unique ambiguity single differences (El-Mowafy and Schwarz,1994b). In the first step, four satellites of good geometry are chosen as the primary satellites. By using measurements to only four satellites, vector components can be unambiguously determined. The possible sets of ambiguity single differences of the primary satellites for each of the baselines 1-2 and 3-4 are identified as mentioned above. In this case, there will be 8 different primary single difference ambiguity combinations for each of the two baselines. For each of the possible ambiguity sets, double difference ambiguities are computed. The vectors and the heading of the two baselines are then determined independently. Among these combinations, at least one heading of the first baseline will agree with a heading of the second baseline within a few degrees. The ambiguities generating these vectors are identified as the correct ones. If more than one pair of ambiguities pass this test, the one with the minimum sum of variances is taken as the correct one.

Once the ambiguity double differences of the four primary satellites are identified, the vector components of the two baselines computed from these ambiguities can be used to identify the correct ambiguities of the remaining satellites. The procedure starts by computing the misclosure of the remaining phase single differences after subtracting the integer part. If the misclosure is larger than the baseline length, one cycle is added or subtracted to guarantee that the single difference measurement does not exceed the baseline length. After estimating all double differenced ambiguities, their values are subtracted from double differenced phase measurements, and these measurements are used to estimate the vector components of baselines 1-2 and 3-4 using a least-squares approach.

Once the components of baselines 1-2 and 3-4 have been determined in the WGS-84 frame, the approximate components of baseline 1-3 can be estimated from the ratio of the known baseline lengths as follows:

$$\Delta X_{13} = (\Delta X_{12} + \Delta X_{34}) \frac{L_{13}}{L_{12} + L_{34}} \tag{7.4}$$

$$\Delta Y_{13} = (\Delta Y_{12} + \Delta Y_{34}) \frac{L_{13}}{L_{12} + L_{34}} \tag{7.5}$$

$$\Delta Z_{13} = (\Delta Z_{12} + \Delta Z_{34}) \frac{L_{13}}{L_{12} + L_{34}} \tag{7.6}$$

Typically, baselines 1-2 and 4-3 have lengths in the range of 9 to 15 cm, while baseline 1-3 will be one to five metres in length. The ratio of the baseline length 1-3 to the combined length of baselines 1-2 and 4-3 will usually be in the range of 3 to 25. Errors in the short baselines 1-2 and 4-3 will be at the level of 2 mm to 5 mm if their vector components are determined from only one epoch of data. Consequently, the components of the vector 1-3, as estimated from equations (7.4) to (7.6), will have the same error multiplied by the length ratio of the baselines. In the worst case, when the errors in the components of the vectors 1-2 and 4-3 lie in the same direction and reach 5 mm, the maximum error for each component of the vector 1-3 can be 25 cm. These approximate components of the vector 1-3 will be used to generate the initial ambiguities (El-Mowafy and Schwarz,1994b).

7.5 Least-Squares Ambiguity Determination with An Optimum Search Region

The method used for ambiguity resolution applies a search technique that follows the principles given in Hatch (1989 and 1991). However, the search region is much smaller and the resolution is therefore much faster. The search starts by determining an initial set of ambiguities estimated from an approximate solution of the antenna vector as described in the previous section. Estimation of the initial ambiguity set is done by using equations (7.1) and (7.3). Searching for the correct ambiguities is then performed by testing different possible ambiguity combinations defined by the range of accuracy of the initial solution.

If more than four satellites are observed, the set of four satellites giving the best geometry is chosen as a primary group of satellites, for which the search is conducted. In the next step, three initial double difference ambiguities associated with the four primary satellites are estimated from the approximate solution of the vector components and different possible combinations of ambiguities around the initial set are tested. For each set of ambiguities, new vector components are determined to best fit the tested set. The secondary group of satellites, consisting of the remaining satellites in view, are used to check the reliability of each solution. For each set, the variance of all primary and secondary satellite measurements is computed, and the set that gives minimum variance is chosen as the correct one. If only four satellites are visible, the combination of those three

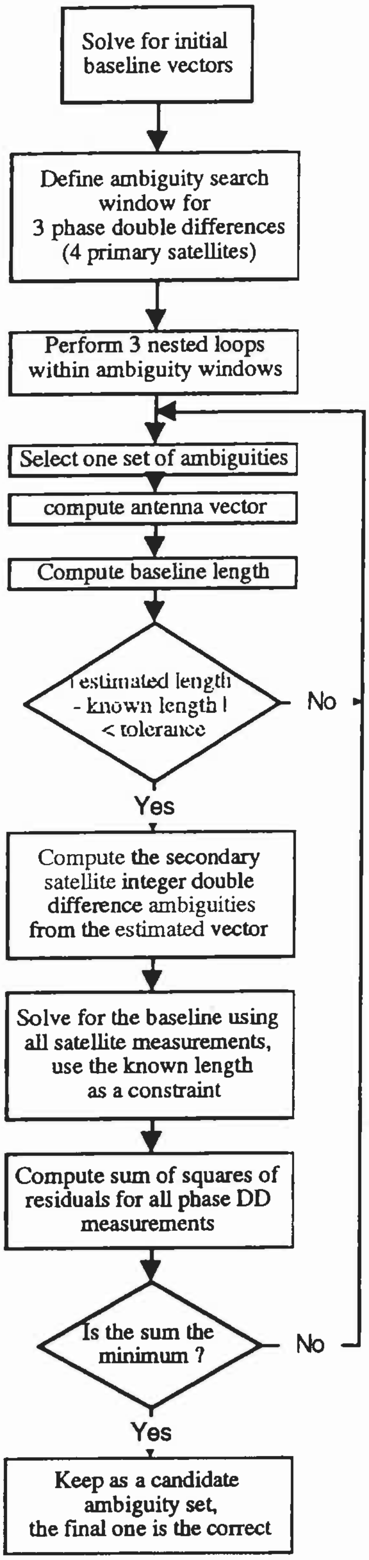
Solve for initial baseline vectors
Define ambiguity search window for 3 phase double differences (4 primary satellites)
Perform 3 nested loops within ambiguity windows
Select one set of ambiguities
compute antenna vector
Compute baseline length
I estimated length - known length I < tolerance
No
Yes
Compute the secondary satellite integer double difference ambiguities from the estimated vector
Solve for the baseline using all satellite measurements, use the known length as a constraint
Compute sum of squares of residuals for all phase DD measurements
Is the sum the minimum ?
No
Yes
Keep as a candidate ambiguity set, the final one is the correct

Fig. 7.3 Flowchart of ambiguity search procedure

double difference ambiguities which have the minimum variance is chosen as the correct one. Figure 7.3 shows the ambiguity determination procedure in form of a flowchart.

Since the approximate (X,Y,Z) vector components have maximum errors of 25 cm or less, the projection of these errors on the baseline length will give a maximum error of 43.3 cm. As Figure 7.1 shows, the single difference measurement can be computed from the equation:

$$\Delta\phi_{12} = b \cos\theta. \tag{7.7}$$

The maximum error of the single difference will be 42.6 cm, i.e. approximately two L1 cycles, for an angle (θ) ranging between 10 and 90 degrees. This means that with these approximate vector components, the number of possible ambiguity combinations to be searched is restricted to $2\text{x}2^4$ ($\pm 2^4$), when using single difference phase measurements. If double difference measurements are used, the error is multiplied by a factor of $\sqrt{2}$ due to the application of the variance law. However, since we are dealing with integers, the maximum search region will be $2\text{x}4^3$ ($\pm 4^3$).

For the multi-antenna system, the antennas are connected to the same receiver, which has one clock, and the receiver clock error is virtually eliminated when applying single differencing. In this case, the number of tested ambiguity sets will be $\pm 2^4$. However, in practice, a small amount of receiver clock error still exists, see Section 3.1.3. Therefore, to achieve a reliable solution, one should apply double differencing. In this case the maximum number of tested sets of ambiguities is $\pm 4^3$; with a computer such as a 486 DX with a 50 MHz clock rate, the search can be executed in about half a second (El-Mowafy and Schwarz,1994b). The number of ambiguities to be searched by the adopted technique is very small compared to the number required by the existing techniques. For instance, for a baseline of three metres in length, the proposed technique searches in $2\text{x}4^3$ ($\pm 4^3$) sets, while existing techniques would search in $2\text{x}15^3$ ($\pm 15^3$) sets (Knight,1994). Thus, the proposed technique reduces the computation time by a factor of about 40 for the given example.

7.6 Using a Primary Group Consisting of Measurements of Two Phase Double Differences and the Baseline Length

In the search approach described above, the search is conducted within three phase double differences, i.e. by performing three nested loops. For instance, if the search envelope is defined by ± 4 cycles from an initial value, the total number of trials required will be 9^3. Searching within three primary phase double difference measurements was originally developed for traditional GPS surveys. In attitude determination, the relative spatial positions of the antennas do hardly change and the antenna baseline lengths can be pre-determined in static mode. Thus, to limit the number of searches, the measured distances can be treated as measurements with standard deviations computed from the static survey, instead of treating them as constraints with virtual zero standard deviations.

Determining antenna baselines one at a time, the minimum number of measurements needed to unambiguously determine each baseline vector is three. Instead of using three phase double differences, as has been done in the previous section, the three measurements can be chosen as two phase double differences and the measured baseline length. The three measurements will define a primary group of measurements, used for ambiguity testing. Since ambiguity determination from data of a single epoch is of particular concern in this study, the two double differences are best chosen from the three satellites giving the best geometry. Having an initial vector estimate, the search can be conducted only within the two phase double differences. In any of the tests, the baseline length remains the same. The number of tests will then only be the square of the number of ambiguities in the search region. For the example given above, the total number of tests needed will be 9^2. As a result, computation time required to perform the ambiguity search is significantly reduced.

The remaining satellites in view are used to check the reliability of the solution as in the approach described in the previous section. A detailed flowchart of the search procedure is given in Figure 7.4. Note that the two approaches, described in this section and the previous section, will have identical performance in finding the correct ambiguities. This is due to the fact that the criterion used for correct ambiguity identification is the same for both approaches, where the set giving minimum variance from all visible satellite measurements, will be considered as the correct one.

However, one should realize that reduction of the computation time between the two approaches is not governed by the ratio $(\pm n)^2/(\pm n)^3$, where n is the number of cycles defined in the search window. In the method described in Section 7.5, which will be referred to as the first method, the measured length is treated as a constraint. Checking the estimated baseline length against the known length becomes an efficient tool to eliminate most of the incorrect sets at an early stage of each test, see next section for more details. In the method described in this section, which will be referred to as the second method, the initial baseline vector at the same level of computations is estimated from two phase double differences and the vector length as a measurement. The estimated vector components are then determined to best fit the length measurement. As a result, length checking becomes invalid, and the complete computational cycle, up to computing the variance of all visible satellite measurements, must be performed for each test.

To achieve the two goals of searching within only two phase double differences and of applying the baseline check, an alternative approach is suggested. In this approach the search proceeds by iterating within only two phase double difference measurements and

considering the length as a measurement. Vector components estimated from these measurements are then used to give an estimate for the integer ambiguity of a third phase double difference measurement. The three phase double difference measurements, including the two tested double difference ambiguities and the estimated one, are used in a following step to give a new estimate of the baseline. The measured length is excluded in this process. Hence, the new baseline estimate becomes independent of the measured baseline length, and its estimated length can be tested against the known one to eliminate wrong ambiguity sets. The new estimate is not necessarily close to the previous one, as wrong ambiguity combinations are used and vector estimation is affected by the presence of measurement noise of the third phase double difference. The process continues as described in the first approach, but with the basic difference that only two nested loops are executed. Figure 7.5 illustrates this process by a flowchart. In the sequel, this method will be refereed to as the third method.

7.7 Enhancing the Speed of Ambiguity Resolution

The search technique can be considerably accelerated by streamlining computational techniques. Factors to be considered are: computing the normal equation matrix in the least squares approach only once for all test sets at the same epoch, performing only one iteration of the least-squares solution, and testing the antenna vector magnitude, produced from each test ambiguity set, against the known baseline length.

In the least-squares approach, the observation coefficient matrix A is computed from the coordinates of the satellites and the receiver. Satellite coordinates are obtained from the broadcast ephemeris. Receiver coordinates can be determined in many ways, the easiest is to use a point positioning solution utilizing pseudorange measurements. In this case, the

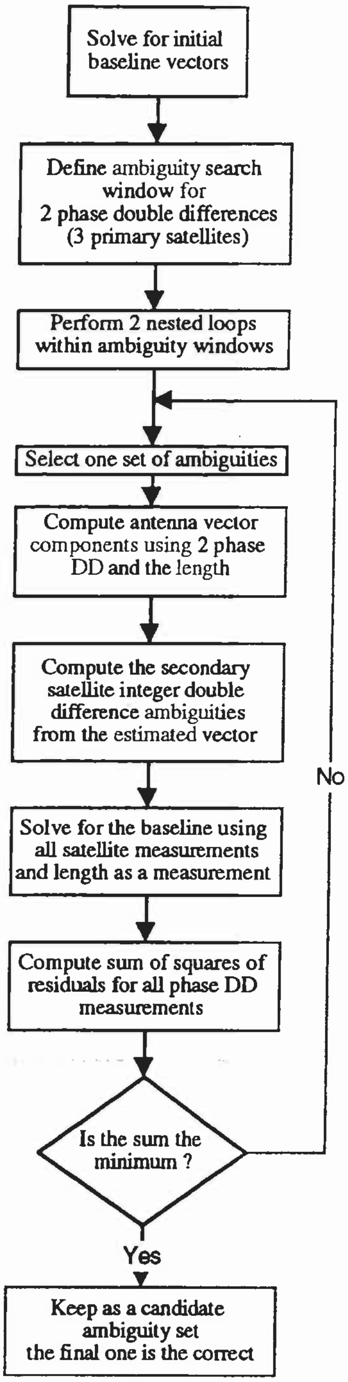
Solve for initial baseline vectors
Define ambiguity search window for 2 phase double differences (3 primary satellites)
Perform 2 nested loops within ambiguity windows
Select one set of ambiguities
Compute antenna vector components using 2 phase DD and the length
Compute the secondary satellite integer double difference ambiguities from the estimated vector
Solve for the baseline using all satellite measurements and length as a measurement
Compute sum of squares of residuals for all phase DD measurements
Is the sum the minimum ?
No
Yes
Keep as a candidate ambiguity set the final one is the correct

Fig. 7.4 Flowchart of the second method

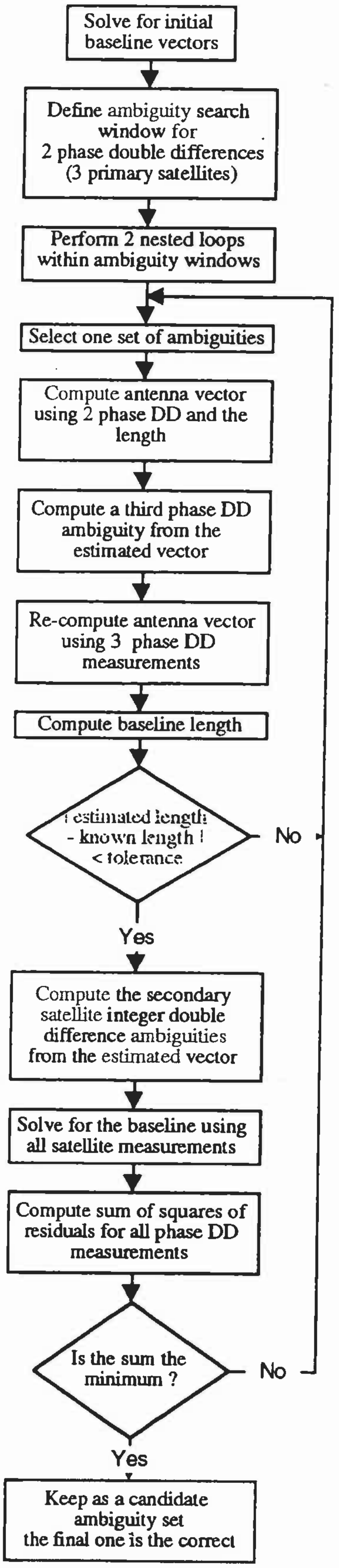
Solve for initial baseline vectors
Define ambiguity search window for 2 phase double differences (3 primary satellites)
Perform 2 nested loops within ambiguity windows
Select one set of ambiguities
Compute antenna vector using 2 phase DD and the length
Compute a third phase DD ambiguity from the estimated vector
Re-compute antenna vector using 3 phase DD measurements
Compute baseline length
| estimated length - known length | < tolerance
No
Yes
Compute the secondary satellite integer double difference ambiguities from the estimated vector
Solve for the baseline using all satellite measurements
Compute sum of squares of residuals for all phase DD measurements
Is the sum the minimum ?
No
Yes
Keep as a candidate ambiguity set the final one is the correct

Fig. 7.5 Flowchart of the third method

computed A matrix is independent of the ambiguity computation, and consequently it is the same for all tested ambiguity combinations.

The unknown corrections ($\hat{\delta}$) in the least-squares approach are computed from the equation:

$$\hat{\delta} = (A^T P A)^{-1} A^T P w \tag{7.8}$$

Since the matrix A is similar for all ambiguity combinations, the term $[(A^T P A)^{-1} A^T P]$ will have the same value for all ambiguity sets and thus is only computed once at each epoch. This limits the computations between different ambiguity candidates to estimating the misclosure vector, which is an easy task and not time consuming. Measurement residuals are computed from the equation:

$$v = A \hat{\delta} + w \tag{7.9}$$

The variance, which is the criterion used to assess the ambiguity combination, is computed from the measurement residuals using equation (3.30).

Usually, the least-squares approach is performed iteratively, with three to four iterations, to accommodate the non-linearity of the solution model. In the ambiguity search approach, this iterative procedure is not required. Since both receiver and satellite coordinates are assumed known, the observation model is linear. One iteration is therefore sufficient.

Determining the baseline length in advance facilitates fast elimination of most of the incorrect ambiguity candidates. This is done by testing the difference between the known baseline length and the estimated length computed from each trial set. If the difference exceeds a pre-defined tolerance, the corresponding ambiguity set is automatically rejected. This leaves fewer ambiguity sets to be tested, and the ones to be further examined will only be 15% to 20% of the total. The test takes the form:

$$L_{known} - L_{computed} < \text{pre-defined tolerance} \qquad (7.10)$$

The tolerance will be around a few centimetres for the correct set as it represents errors of estimation mainly due to receiver and multipath noise. However, choosing the tolerance value is a sensitive operation. A small tolerance accelerates the search process considerably, but has the inherent risk that the correct set might be rejected if the tolerance is chosen too small. Experience indicates that the tolerance should be in the range of 5 centimetres (El-Mowafy and Schwarz,1994b). Such a conservative tolerance is sufficient for rejecting most of the wrong ambiguities and maintaining the confidence of finding the correct ambiguity set.

It should be mentioned that in the above test, the known length should not be used as a measurement or constraint in the least-squares procedure. If it is included, the adjustment will give vector components with a baseline length as close as possible to the correct value; hence, the test becomes meaningless. However, after performing the length test, the known length can be included as an additional measurement or constraint for the next stage.

A fast ambiguity search can also be achieved in cases where short baselines are aligned with the main ones. In those cases, the direction (azimuth and pitch) of the short baseline can be used to chose the correct ambiguities of the longer baselines. Errors in estimating the short baselines are usually limited to few millimetres. Their azimuth and pitch may differ from that of the longer baselines by a few degrees. Experience indicates that the difference is in the range of 10 degrees, depending on the magnitude of the error, baseline lengths, alignment, and baseline orientation in the local-level frame. Therefore, the tested ambiguity combination can be rejected if the estimated azimuth and pitch of the longer baseline are outside the tolerance of 10 degrees.

7.8 Enhancing Robustness of Finding the Correct Ambiguities Using Known Ones

In kinematic positioning, cycle slips can occur, either through physical obstruction of the signals or bandwidth problems in a high dynamics environment. If four satellites or more are observed, cycle slips do not represent a problem in the epoch-by-epoch ambiguity resolution technique, as the ambiguities at each epoch are estimated independently. On the other hand, when the ambiguities are re-initialized after passing through a period of tracking less than four satellites, some of the ambiguities are known, namely those of satellites which have been continuously tracked. All the existing ambiguity determination techniques take the satellites with known ambiguities as a sub-set of the primary group of satellites. Such a choice minimizes the number of sets to be tested, and this is preferred when long times are needed to search among numerous possible ambiguity sets.

Unlike the existing techniques, the technique presented here has a limited number of test sets. Thus, instantaneous ambiguity resolution can always be achieved. An easy and reliable approach to find the correct ambiguities is to determine the single difference ambiguities for all satellites from the baseline solution, and to keep tracking them in time. If satellite blockage occurs such that one or more satellites are still visible, it is best to put one of the satellites with known ambiguities in the secondary group of satellites whenever complete visibility is regained. At the same epoch, the tested candidate double difference ambiguity sets generate possible solutions for the baseline, from which, estimated values for the known ambiguity can be determined. The correct ambiguity set is therefore determined as the one gives an ambiguity estimate equals to the known ambiguity.

If more than one ambiguity is known, it is enough to put one known ambiguity in the secondary group and to put the others in the primary group. In this case both goals are achieved: the search is faster with a minimum of trial sets, and a correct solution is guaranteed. The same procedure can be applied for any of the existing search techniques. In post mission or real-time, the idea holds, and correct ambiguity re-initialization can be made using data of one epoch only.

7.9 Acceptance of the Correct Ambiguity Set

In real-time positioning, where the data considered are those of one epoch, the number of measurements used is always limited and is usually less than 10. As a consequence, the statistical information available becomes dependent on relatively small sample sizes. Hence, it can happen that the set giving minimum variance is not necessarily the correct one. Although this phenomenon is not often encountered, its existence will lead to wrong ambiguity resolution, and hence incorrect estimation of the antenna vector. In addition, if the ambiguities are incorrectly computed at one epoch and are considered fixed for the rest of the trajectory, serious errors can result. Therefore, efficient strategies must be implemented to safeguard against this problem. Three of them have been investigated in this thesis, namely, statistical tests, conjugate ambiguity test, and ambiguity moving average.

7.9.1 Statistical Tests

Commonly used statistical tests to identify the correct ambiguity set are the chi-square test and the F-test. In the first one, the estimated variance factor (σ^2) of a particular ambiguity set is compared to *a priori* variance factor (σ^2_o). The test acceptance criterion is given as:

$$\chi^2_{df,\alpha/2} \leq \frac{\sigma^2}{\sigma^2_o} \leq \chi^2_{df,1-\alpha/2} \qquad (7.11)$$

see (Hamilton,1964), where $\chi^2_{df,\alpha/2}$ and $\chi^2_{df,1-\alpha/2}$ is the chi-square percentiles for the degrees of freedom df, and the confidence interval $\alpha/2$ and $1-\alpha/2$, respectively, and α is the significance level. The test rejects an integer ambiguity combination if the computed ratio is larger than the acceptance criterion. Among the sets that pass the chi-square test, the one that gives minimum variance is usually chosen as the correct one (Lachapelle et al., 1992a). It is unlikely that this test will work well in real-time applications because the sample from which χ^2 is computed is very small (one epoch only).

The second test to identify the correct ambiguity set is the F-test, which tests the ratio between the two smallest variances (Erickson,1992b). The acceptance criterion is:

$$\frac{\sigma^2_2}{\sigma^2_1} \geq F_{df,\alpha} \qquad (7.12)$$

where σ^2_1 is the smallest variance and σ^2_2 is the second smallest variance. If the test passes, the ambiguities given by the smallest variance are accepted as the correct ones. If it fails, the data used is deemed to be insufficient to correctly resolve the ambiguities and further testing in following epochs is needed. An approximate method of applying this test has been given in (Lachapelle et al.,1992b) and (Landau and Euler,1992) where $F_{df,\alpha}$ has been set to 2, and in (Cannon and Haverland,1993) where $F_{df,\alpha}$ has been set to 3. These values are taken based on empirical results. In attitude determination from data of a single epoch, when examining the measurement variances generated by different ambiguity sets, many small variances can lie within the same population containing the smallest variance (El-Mowafy and Schwarz,1994b). The test then, will ignore the set giving the smallest variance, even though it might be the correct one.

Since the chi-square test and the F-test are based on the assumption that the residuals are normally distributed, this assumption must also be tested. When resolving the ambiguities in a single epoch, the number of measurements are small and from the statistical point of view, the sample size is not large enough to give a detailed picture of the residual distribution. Therefore, statistical testing may not be helpful or reliable in rejecting false ambiguity sets in real-time attitude determination.

7.9.2 Conjugate Ambiguity Test

This test is only available in case of using redundant antennas collinear with the main ones as given in Figure 7.2. For example, consider the case given in Section 7.4, which is shown in Figure 7.2d. For any of the tested ambiguities of the baseline 1-3, a conjugate set can be computed for the baseline 2-4 through a simple process of ambiguity transition. Since only the correct ambiguity set of the baseline 1-3 can give a correct (conjugate) ambiguity set for the baseline 2-4, the ambiguity set of the baseline 2-4 that gives the minimum variance should be generated from the set that gives a minimum variance for the baseline 1-3. Thus, their combined variance should be a minimum.

The transition process can be summarized as follows. Referring to Figure 7.2d, and neglecting the error terms, the phase double difference equation for baseline 1-3 is given as:

$$\begin{aligned}(\vec{e}^A - \vec{e}^B) \,.\, \vec{b}_{13} &= \nabla\Delta\phi^{AB}{}_{13} - \lambda\nabla\Delta n^{AB}{}_{13} \\ &= (\phi^A{}_1 - \phi^A{}_3) - (\phi^B{}_1 - \phi^B{}_3) - \lambda\,[\,(n^A{}_1 - n^A{}_3) - (n^B{}_1 - n^B{}_3)\,] \qquad (7.13)\end{aligned}$$

where ϕ is taken in length units (metres). Similarly, for the baseline 2-4, the phase double difference equation will be:

$$\begin{aligned}(\vec{e}^A - \vec{e}^B) \,.\, \vec{b}_{24} &= \nabla\Delta\phi^{AB}{}_{24} - \lambda\nabla\Delta n^{AB}{}_{24} \\ &= (\phi^A{}_2 - \phi^A{}_4) - (\phi^B{}_2 - \phi^B{}_4) - \lambda\,[\,(n^A{}_2 - n^A{}_4) - (n^B{}_2 - n^B{}_4)\,] \qquad (7.14)\end{aligned}$$

Subtracting equation (7.14) from (7.13), and ignoring $\nabla\Delta\phi^{AB}{}_{13}$ and $\nabla\Delta\phi^{AB}{}_{24}$ since they are fractions of a cycle, one obtains:

$$\nabla\Delta n^{AB}{}_{13} - \nabla\Delta n^{AB}{}_{24} = \\ [\ (n^{A}{}_{1} - n^{A}{}_{2}) - (n^{B}{}_{1} - n^{B}{}_{2}) - (n^{A}{}_{3} - n^{A}{}_{4}) - (n^{B}{}_{3} - n^{B}{}_{4})\ ] \qquad (7.15)$$

which is nothing but the differenced double difference ambiguities between the baselines 1-2 and 3-4. These ambiguities can be determined directly from the phase integer cycle measurements. In cycle units, the double difference ambiguities are given as:

$$\nabla\Delta n^{AB}{}_{12} = \nabla\Delta\phi^{AB}{}_{12} \qquad (7.16)$$

$$\nabla\Delta n^{AB}{}_{34} = \nabla\Delta\phi^{AB}{}_{34} \qquad (7.17)$$

Finally, a double difference ambiguity for the baseline 2-4 is directly produced from a conjugate tested ambiguity of the baseline 1-3, as follows:

$$\nabla\Delta n^{AB}{}_{24} = \nabla\Delta n^{AB}{}_{13} - [\ \nabla\Delta n^{AB}{}_{12} + \nabla\Delta n^{AB}{}_{34}\ ] \qquad (7.18)$$

The baseline 2-4 can then be estimated, and the measurement variance is determined. The combined variance of the two baselines 1-3 and 2-4 can be taken, for simplicity, as the sum of the variances. The set of the baseline 1-3 ambiguities that gives the minimum combined variance can then be chosen as the correct one.

Existence of the baseline 2-4 adds reliability to the attitude determination process. If one or both of the primary antennas (number 1 and 3) are subject to electronic problems or cycle slips, such that less than four satellites are being tracked, the attitude can be instantaneously recovered by automatically switching to antennas 2 and 4, provided that the antennas 2 and 4 are free from the mentioned problems. Recovery of the attitude becomes then feasible using the independent baseline 2-4.

7.9.3 Testing Ambiguity Consistency Using A Moving Average Technique

Another strategy to identify the correct ambiguity set is a check on the consistency of the estimated ambiguities epoch by epoch. The basic principle is: unless the satellite-to-receiver signal path has been interrupted, phase ambiguities should be the same. To correct the ambiguities at the epochs of incorrect ambiguity resolution, an ambiguity moving average technique is used (El-Mowafy and Schwarz,1994a). A moving average for each double difference ambiguity is computed at each epoch, starting from a reset point. It is updated with the ambiguity values at the current epoch, using the ambiguity set that has minimum variance. Before considering the current ambiguity in the computation of the moving average, a simple test is made for checking the presence of cycle slips above the selected ambiguity window (4 cycles). The current ambiguity based on data of one epoch is checked against the moving average derived from previous epochs. If the difference is less than the preset value (±4 cycles), no cycle slip is assumed. However, if the difference is larger than this envelope, it is assumed that a cycle slip has occurred and the moving average is reset accordingly.

To compute the moving average, the only parameters to be stored and transferred from one epoch to another are the ambiguity average and an index of the epoch, counted from the last reset epoch. The moving average of any of the double difference ambiguities is computed as follows:

$$avr_n = \frac{(n-1)\, avr_{n-1} + amb}{n} \tag{7.19}$$

where (n) is the current epoch time index, (n-1) is the previous time index, (amb) is the current computed ambiguity, avr_{n-1} is the previous ambiguity average and avr_n is the current one. Once the current average has been computed, the ambiguity of the set giving minimum variance is compared to it. If they agree, the ambiguity is considered as the correct one. If not, the moving average is taken as the correct ambiguity (El-Mowafy and Schwarz, 1994a).

Comparing the computed ambiguities to the moving average should start not earlier than 10 seconds after the reset, in order to allow for a reliable computation of the moving average. The choice of this time period is highly dependent on the amount of noise expected and 10 seconds apply to a low noise situation. For high noise situations, periods of up to one minute may be needed. During this period of estimating the moving average, the ambiguities giving the minimum variance are taken as the correct ones.

If epoch-by-epoch ambiguity resolution is not required during the complete mission, a simple strategy can be applied. A moving average of the epoch by epoch computed ambiguities is estimated, as described above, after a sufficient initialization period. Once the moving average has been computed reliably, it is taken as the correct ambiguity for the rest of the survey route. No further ambiguity computations are required until the signal pass is interrupted. Checking cycle slips, however, is necessary at each epoch, and this can be done by testing the computed baseline lengths against the known ones. It should be clearly understood that one does not need to wait until the final moving average is computed and then start working. Instead, during the process of computing the final average, the ambiguities are computed at each epoch, and can then be immediately used at their epochs. Only in a high noise environment, there is a limited risk that some of these ambiguities might not be the correct ones. This means that the system gives the required parameters at all epochs, but with higher reliability after the ambiguity average has been computed.

7.10 Ambiguity Resolution Using the Known Baseline Geometry

Attitude determination using the multi-antenna system has the advantage that the antennas are closely spaced. Moreover, for many applications, antenna positions in the body frame, if chosen properly, can be satisfactorily considered as fixed along the whole survey route. Therefore, if antenna geometry is determined, for instance, in a pre-survey static mode, the known geometric elements such as baseline lengths and the spatial angles between the baselines can be used to identify the correct ambiguities. The main principle is that all baseline vectors estimated from the correct ambiguities should satisfy the known spatial geometry of the antenna configuration.

For the determination of a 3D attitude, the minimum number of antennas required is three. Therefore, the technique will be presented assuming, for simplicity, that only three antennas are used, keeping in mind that the same principles can be applied when redundant antennas exist. Figure 7.6 illustrates a general antenna configuration using three antennas.

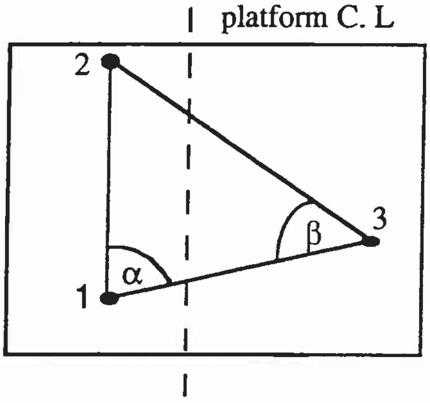

Fig. 7.6 General antenna layout

For each of the baselines 1-2 and 1-3, the search is conducted within a pre-defined window, determined from the expected accuracy of the initial baseline estimate. The search can be performed within three primary phase double differences (the first method) or within two primary phase double differences and an estimated value for a third one (the third method), see Sections 7.5 and 7.6. For any of the ambiguity combinations passing the length check, double differenced ambiguities of the secondary group of satellites are computed from the estimated baseline vector. A new estimate of the baseline is then determined, for each ambiguity combination, based on measurements of all satellites. The candidate baseline estimates along with their corresponding ambiguities for both baselines (1-2 and 1-3) are stored for further testing. If the main baselines are approximately determined from short ones aligned with them, ambiguity combinations that are further tested can be significantly reduced if only those having directions (heading and pitch) close to the known ones are considered.

To give a complete picture of the geometry of the figure, an estimate of the baseline 2-3 should first be found. That requires the definition of the ambiguity double differences for the baseline 2-3. They can be directly computed from the tested ones, by subtracting each possible ambiguity set of the baseline 1-2 from a candidate one of the baseline 1-3. Thus, if there are n estimates for the baseline 1-2 and m estimates for the baseline 1-3, there will be nxm ambiguity estimates for the baseline 2-3. The equation for the ambiguity double difference of the baseline 2-3, for satellites A and B, is given as:

$$(\nabla\Delta\, n_{23}^{AB})_{1..nxm} = (\nabla\Delta\, n_{13}^{AB})_{1..n} - (\nabla\Delta\, n_{12}^{AB})_{1..m} \qquad (7.20)$$

Note that, estimated values of the baseline vector 2-3 will be similar to differencing the baseline vectors 1-3 and 1-2 only when the correct ambiguities are used.

The geometry derived from the three baseline estimates is tested against the known geometry, to check the correctness of the candidate ambiguities. Consecutive tests are applied for this purpose. Figure 7.7 illustrates the sequence of these tests for the case when the search is conducted within three ambiguity double differences. First, since the three baselines form a closed loop, the sum of each component (X, Y, Z) should be zero. In practice, due to the presence of noise in the measurements, small tolerances can be accepted, depending on the expected noise level.

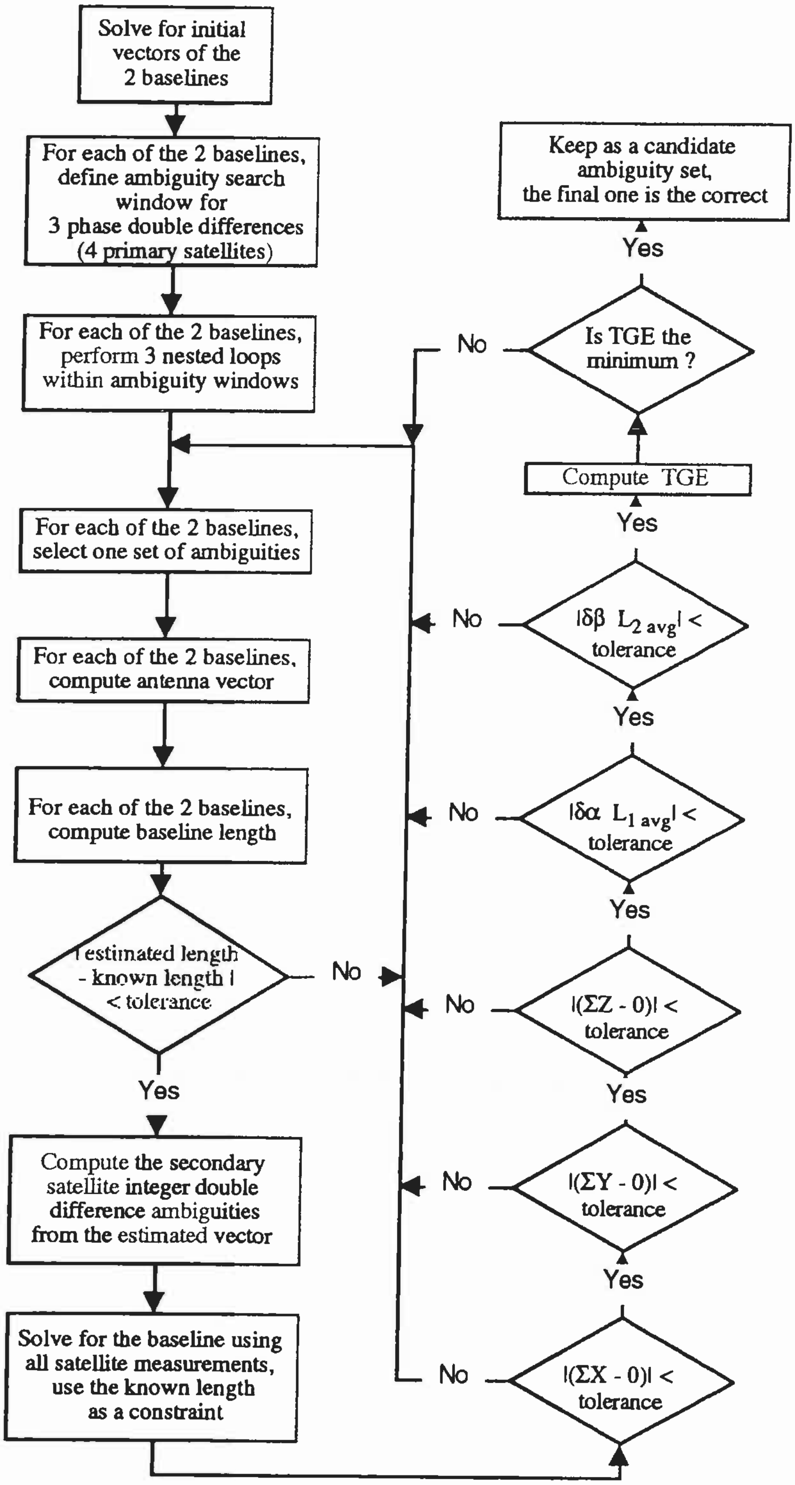
Solve for initial vectors of the 2 baselines
For each of the 2 baselines, define ambiguity search window for 3 phase double differences (4 primary satellites)
For each of the 2 baselines, perform 3 nested loops within ambiguity windows
For each of the 2 baselines, select one set of ambiguities
For each of the 2 baselines, compute antenna vector
For each of the 2 baselines, compute baseline length
| estimated length - known length | < tolerance
No
Yes
Compute the secondary satellite integer double difference ambiguities from the estimated vector
Solve for the baseline using all satellite measurements, use the known length as a constraint
$|(\Sigma X - 0)| <$ tolerance
No
Yes
$|(\Sigma Y - 0)| <$ tolerance
No
Yes
$|(\Sigma Z - 0)| <$ tolerance
No
Yes
$|\delta\alpha\ L_{1\,avg}| <$ tolerance
No
Yes
$|\delta\beta\ L_{2\,avg}| <$ tolerance
No
Yes
Compute TGE
Is TGE the minimum ?
No
Yes
Keep as a candidate ambiguity set, the final one is the correct

Fig. 7.7 Flowchart of the ambiguity search using the known geometry

The closure tests, although essential, are not enough to prove compatibility between the geometry derived from baseline estimates and known antenna geometry. Therefore, ambiguity candidates passing the closure tests are next subjected to additional tests for the shape of the figure. This can be accomplished by comparing the estimated and the known spatial angles contained between the baselines of the antenna triad. The two independent angles α and β, shown in figure 7.6, can be used for this purpose. To determine the two angles from vector components, the following equations are used:

$$\alpha = \cos^{-1} \frac{\vec{b}_{12}.\vec{b}_{13}}{\| b_{12} \| \| b_{13} \|} \tag{7.21}$$

$$\beta = \cos^{-1} \frac{\vec{b}_{31}.\vec{b}_{32}}{\| b_{31} \| \| b_{32} \|} \tag{7.22}$$

If more than one group of baseline estimates and ambiguity combinations pass the given tests, although this is not very likely, a final check can be performed. In this test, the total closure and shape errors are combined in one error term, and the baselines and ambiguity set giving the least total error will be taken as the correct one. The total error, defined as the Total Geometric Error (TGE), represents the overall compatibility error between the estimated and the correct antenna spatial geometry. The TGE can be written as:

$$\mathrm{TGE} = \sqrt{|\Sigma\Delta X - 0|^2 + |\Sigma\Delta Y - 0|^2 + |\Sigma\Delta Z - 0|^2 + |\delta\alpha\, L_{1\,avg}|^2 + |\delta\beta\, L_{2\,avg}|^2} \tag{7.23}$$

Where:

$\delta\alpha$ and $\delta\beta$ are the error (within tolerance) of estimating the angles α and β, respectively.

$\Sigma\Delta X$, $\Sigma\Delta Y$, and $\Sigma\Delta Z$ are the closure errors (within tolerance) in the X,Y,Z directions.

$L_{1\,avg}$ is the average length of the baselines 1-2 and 1-3.

$L_{2\,avg}$ is the average length of the baselines 3-1 and 3-2.

CHAPTER 8

TESTING THE MULTI-ANTENNA SYSTEM

In this chapter, field tests are analyzed to evaluate the performance of the techniques discussed in previous chapters. the theoretical developments are verified in a number of field tests. Testing was mainly performed in a kinematic mode, in land using a van and in an airborne mode. Static tests will be used as a base for the assessment of kinematic results.

The chapter starts by stating test objectives and methodology. Then, a detailed description of different tests is given, including operational conditions. The results of instantaneous ambiguity resolution are analyzed in detail. Finally, accuracy performance of attitude determination for the van and aircraft tests will be investigated and compared.

8.1 Test Objectives and Methodology

The kinematic tests have been performed with two main objectives in mind, namely:

- to test the performance of the different ambiguity determination techniques presented in Chapter 7,
- to assess the overall performance and accuracy of attitude determination under different operating conditions, in land and airborne mode.

The multi-antenna system used for attitude determination is the Ashtech Three-Dimensional Direction Finding (3DF) system. To check results of attitude determination, the output is compared to that of the Litton LTN 90/100 strapdown inertial system. The correctness of the determined ambiguities was checked by comparing attitude results of both systems. If they agree within a tolerance of 0.5 degrees, the 3DF attitude is considered correct, and therefore the ambiguities generating attitude solution are also considered correct. The 0.5 degree tolerance is based on 2σ value of the expected error between the two systems, derived from previous experience.

8.2 Test Design

Three sets of tests have been performed. In the first two series a van was used, in the last, a fixed wing aircraft.

In the first series of van tests, redundant antennas were used to create short baselines, collinear with the main one, for a fast initial estimate of the main baselines as described in Section 7.4. Only one baseline was tested in this case. Therefore, heading and pitch on the one hand, and heading and roll on the other were determined in independent tests. A statistical criterion (minimum variance) was used to find the correct ambiguities. Attitude parameters were determined using the direct approach given in Section 3.4.

In the second set of van tests the 3D attitude was determined using a general antenna configuration. Feasibility of instantaneous ambiguity resolution using the known spatial geometry of the antennas was analyzed.

In the last set of tests the attitude of an aircraft was determined. Attitude determination in airborne mode differs from that on land because the aircraft undergoes considerable changes in dynamics within short time periods. Also, during turns of the airplane, satellite blockage is possible, which highlights the problem of instantaneous re-initialization of the ambiguities and cycle slips detection and recovery. The chosen antenna configuration is similar, in principle, to the one given for the first series of van tests. The technique used for attitude determination is also the same. Thus, a head-to-head comparison between attitude results will show the performance of attitude determination in the two operational environments.

8.3 Test Description

8.3.1 Description of the First Series of Van Tests

In the first series of van tests, the redundant antennas were collinear with the main ones. Micro strip antennas of the "geodetic type" made by Sensors Inc. were used. The antennas are square, with side lengths of 0.14 m. With such dimensions, it is not possible to establish short baselines of less than half a cycle. A configuration similar to that in Figure 7.2d was therefore chosen. With two pairs of antennas, where each pair consisted of two antennas mounted at about a 15 cm spacing, the phase ambiguities of the short baselines could readily be determined by applying the technique described in Section 7.4. Each antenna pair was mounted on a trapezoidal frame, fixed to the roof rack. This allows the antennas to be elevated about 17 cm above the roof of the vehicle to minimize multipath due to reflection of the signals from the vehicle's roof. The heading and pitch were computed in one series of tests, the roll in another. This was necessary because only four antennas were available. For the computation of heading and pitch, one pair was mounted at the front of the vehicle and the other at the rear, see Figure 8.1. The distance between the centre points of the two farthest antennas was 2.975 metres.

For roll determination, the same two pairs were used in independent tests, but in this case, their baseline was oriented orthogonal to the vehicle's forward direction. Only one roof rack was mounted in the middle of the vehicle. The two pairs were mounted on the left and right ends of the roof rack, such that the line connecting the antennas is in the transverse direction, see Figure 8.2. The distance between the centre points of the farthest two antenna was 1.572 metres.

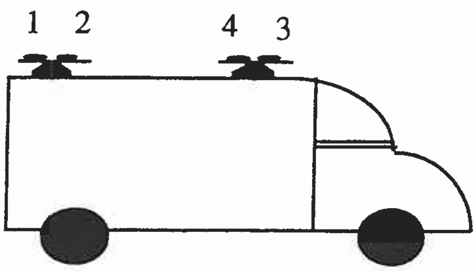

Fig. 8.1 Layout of the antennas for heading and pitch

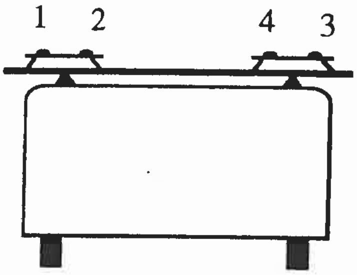

Fig. 8.2 Layout of the antennas for roll determination

The tests were conducted on a well-surveyed test traverse close to Calgary with east-west and north-south direction legs. Figure 8.3 shows the test traverse. Two series of tests were performed. The first was conducted on June 24, 1993 and the second on June 25. In each series, a static test was first performed, followed by a kinematic test. On August 9, 1993, another series of tests was conducted. This series started with a static test, followed by two independent kinematic tests. The tests were performed for periods ranging from 15 to 37 minutes.

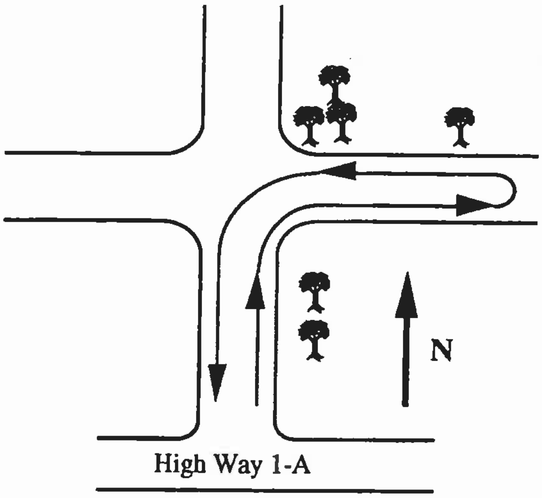

Fig. 8.3 Test traverse of the first van test

The number of satellites observed during these tests ranges from four to six, the PDOP ranges from 2.0 to 6.0. The AZDOP was between 1.0 to 3.1, and the El-DOP was between 0.8 to 3.6. The maximum acceleration determined from the tests was 1.73 m/s^2, and the maximum velocity was 64 km/h, while the average velocity was 58 km/h. All runs were preceded by a stationary period during which the inertial system was aligned. All kinematic runs include a stationary period of about 20 seconds each three to four minutes for zero velocity updates of the INS.

8.3.2 Description of the Second Series of Van Tests

The second series of van tests was performed in the same area, but with a different antenna configuration. Again, a static test followed by a kinematic one were executed. The antenna configuration used is illustrated in Figure 8.4, and the antenna spacing and baseline lengths are shown in Figure 8.5. Antennas 1, 2 and 3 were collinear, while antenna 4 was at a distance of 1.616 m. The antennas used were of the type known as "aircraft antennas", made by Sensor Inc. These antennas are compact with small dimensions (the diameter is approximately 8.8 cm). They also have a microstrip patch design. The selected antenna configuration is similar to the one given in Figure 7.2b. Because of the small size of the antennas, it was possible to put antennas 1 and 2 at a distance that is smaller than half a cycle (0.094 m). Thus, phase double difference ambiguities of the short baseline can be directly determined as the integer part of the measured phase double differences. The short baseline 1-2 can then be used to give an approximate estimate of the main baseline (1-3), from which initial ambiguity values can be calculated. After determination of the correct baseline ambiguities, attitude parameters are determined from baselines 1-3 and 1-4.

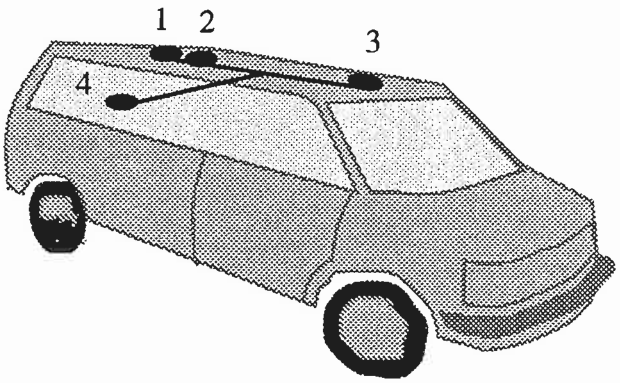

Fig. 8.4 Test van

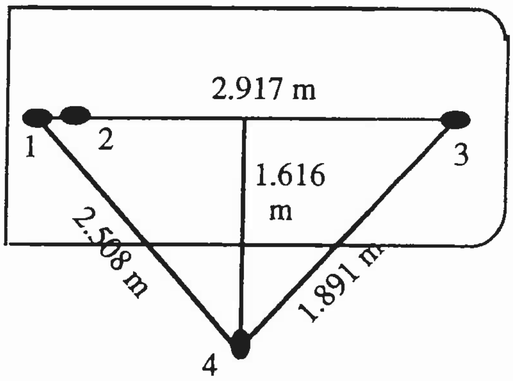

Fig. 8.5 Antenna configuration

Figure 8.6 shows the outline of the test traverse. The tests were performed on September 10, 1994. The static test took about 14 minutes, while the kinematic one took approximately 16 minutes. The number of satellites observed was four to six, giving PDOP between 3 and 6, AZDOP between 0.9 to 2.0, and El-DOP between 1.0 to 2.1. The acceleration and velocity encountered in the kinematic test were similar to the ones given in the first series of van tests. During the test, the inertial system had periods of malfunctioning.

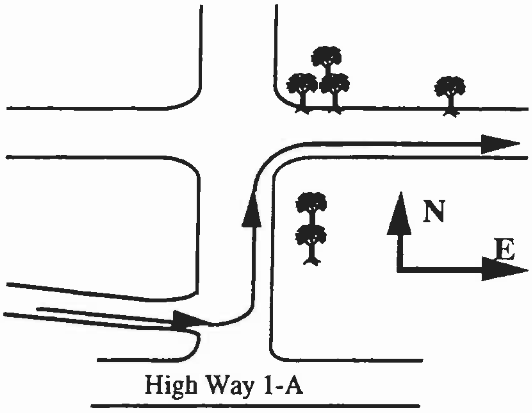

Fig. 8.6 Test traverse of the second segment of van tests

8.3.3 Description of the Airborne Test

In the airborne test, a KING AIR 90 airplane was used, which is a small airplane with twin turbo engines. Figure 8.7 shows the airplane. No antennas were permitted to be mounted on the wings. Since the fuselage is curved and narrow in the transverse direction, it was not practically possible to put the antennas such that a baseline in transverse direction could be created. Consequently, only the heading and pitch were determined in this test. Three collinear antennas were used for this purpose. Figure 8.8 illustrates the antenna configuration on the airplane. Antenna 1 was located on a 2.502 m away from antenna 3, and antennas 2 and 3 were placed within a distance of 0.093 m. The given configuration, allowed fast ambiguity determination because results of the short baseline could be used to limit the search region for the longer baseline. After estimation of the ambiguities, phase measurements of baseline 1-3 were used for attitude determination.

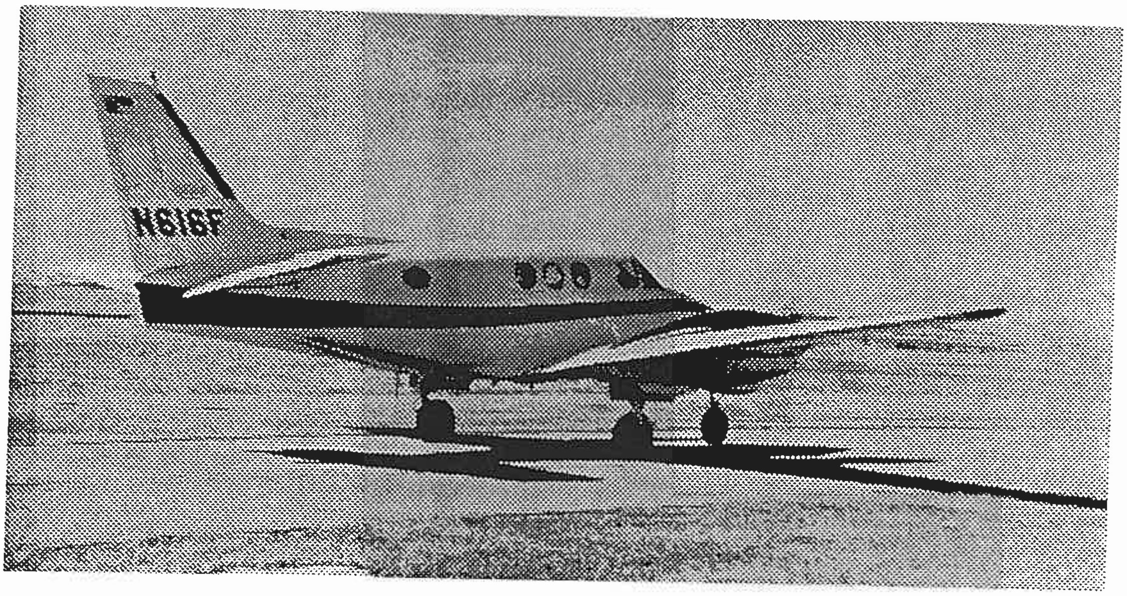

Fig. 8.7 Airplane used in test (KING AIR 90)

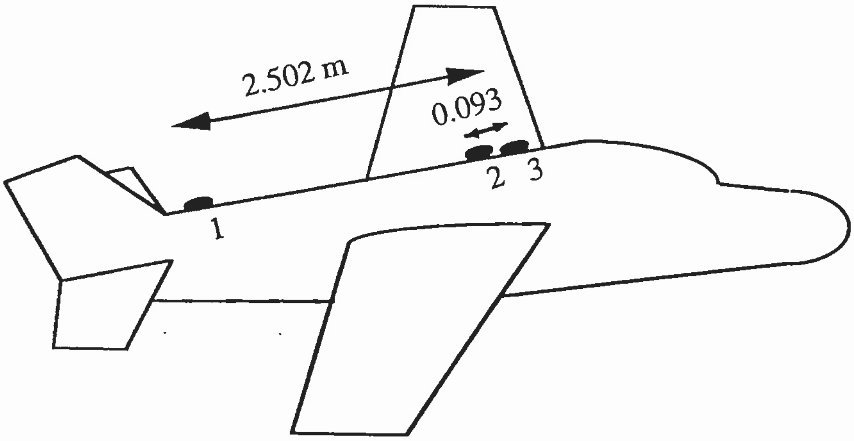

Fig. 8.8 Antenna configuration on the airplane

The test was conducted on March 29, 1994 close to Calgary. The trajectory of the flight is shown in Figure 8.9. The test starts by a static run of 26 minutes, followed by a kinematic one. The static test was performed when the airplane was on the runway, ready to fly. The engines were running to provide power to the inertial system. When the airplane started to accelerate and move on the runway, the kinematic test began. During the static test the number of satellites observed was 5 to 6, giving PDOPs between 2 and 4, AZDOPs between 1.0 to 1.6, and El-DOPs between 1.0 and 2.7.

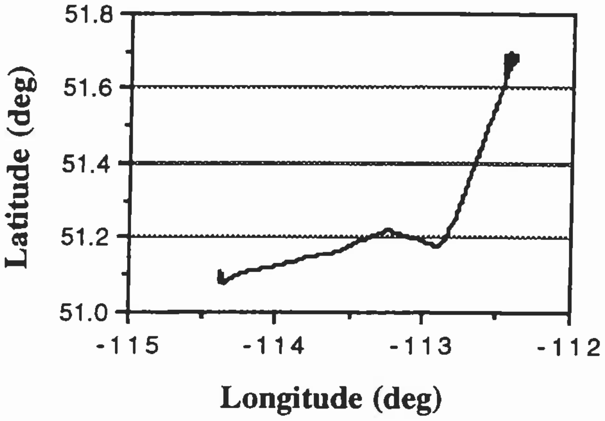

Fig. 8.9 Flight trajectory

For the kinematic test, the number of satellites observed by all antennas changed between 3 and 6, but not in a typical descending or ascending order. For instance, during some periods the number was 6, changing to 5 or 4 and then came back to 6. This is due to blockage of signals of some satellites during flying maneuvers. For approximately 42.5 minutes of flight (2554 epochs), a minimum of 3 satellites were observed; thus, ambiguity resolution and attitude determination were possible. After that, the number of satellites dropped to 2 and attitude determination had to be stopped. The PDOPs values vary between 4 and 8 when tracking more than 3 satellites. The corresponding AZDOPs were 1.4 to 3.2, and El-DOPs were 1.1 and 3.0. These values increased considerably when the number of satellites dropped to 3, reaching values of up to 30 for PDOP in some cases.

During some periods, the aircraft experienced strong vibrations due to flight conditions. At few epochs, the acceleration reached 9 m/s^2, while it was less than 1.5 m/s^2 during normal flight conditions. In addition, problems related to the tracking of satellite phase measurements in the receiver channels occurred during the flight. Some satellites were received at one antenna, while they were not received at another. This reduced the number of useful data to 2554 epochs. However, the number is sufficient to test the ambiguity resolution technique and assess attitude determination in a statistically meaningful way.

8.4 Analysis of Ambiguity Resolution

Since attitude determination in real-time is of main concern in this study, the ambiguities were determined epoch-by-epoch where the search was performed independently during each epoch, i.e. the data used were those of a single epoch. Results of instantaneous ambiguity resolution are given in the following.

8.4.1 Ambiguity Resolution in the First Series of Van Tests

Results for the first method of ambiguity resolution given in Chapter 7 are given in table 8.1. A statistical criterion (minimum variance) was used to identify the correct ambiguity set. The main criteria of the proposed technique are: applying an optimized search region, streamlining the computations, and applying algorithms that enhance correct ambiguity determination. Computation time needed did not exceed half a second at any epoch. Table 8.1 shows the number of epochs and the success percentile of finding the correct ambiguities, for all static and kinematic tests performed in the first series of van tests. Results show that the adopted epoch-by-epoch ambiguity resolution approach is efficient and has an overall success rate of about 99%.

Attitude Component	Static			Kinematic			
	Run 1	Run 2	Run 3	Run 1	Run 2	Run 3	Run 4
Heading & Pitch	1865 99.1%	1478 98.7%	2144 99.8%	1871 98.7%	2201 99.7%	1778 98.8%	1575 99.2%
Roll	905 98.4%	--	--	1482 98.1%	--	--	--

Table 8.1 Number of epochs and ambiguity success rate

In the epochs where the ambiguities were incorrectly determined (about 1% of the total), the correct ambiguities were those with the second smallest variance in 80% of the cases. To investigate the relation between the two smallest variances, ratio testing was performed using both the rigorous and the approximate F-test. As expected, neither of these tests gave a definite answer at all epochs. In some cases the variance ratio did not pass the test and, according to the test methodology, further testing in the following epoch is required. In other cases the smallest variance did not result in the correct ambiguities, even though the tested ratio was significant, leading to a false "statistically satisfactory" solution. This is most likely due to the small number of events that are available at one epoch to compute test statistics.

The chi-square test does not improve performance for ambiguity resolution. This is mainly due to the fact that the data used are from a single epoch, see details in Section 7.9.1. It appears therefore that statistical testing does not help in identifying the correct ambiguity set. The conjugate ambiguity test gave, in most of the cases, the same results as those determined when using the baseline 1-3 only. Thus, this test does not add significant information. At the few epochs where the results differed, the difference seems to be due to different noise levels experienced at different antennas.

When the moving average approach is used, the number of epochs of incorrect ambiguity resolution drops dramatically, typically by a factor of 3 to 4. For instance, in the first static test, only 2 of the 20 epochs of incorrect ambiguity resolution remain. This means that the percentage of finding the correct ambiguities increases from 98.7% to 99.86%. Similar results are obtained in kinematic tests. For instance, for the kinematic test of the first run, the epochs experiencing wrong ambiguity resolution drops from 25 epochs to 7. The percentage improves from 98.7% to 99.6%. The remaining epochs of erroneous ambiguity resolution were scattered along the survey course; therefore, their effect was insignificant. Usually they are found in the early period of building the moving average.

The performance of different techniques that can be used to reject the incorrect ambiguity sets are given in Table 8.2. The percentiles given are the overall percentage of correctly determining the ambiguities from all static and kinematic tests. As shown, the ambiguity moving average technique is the only one that improves correct ambiguity identification.

Technique Employed	Ambiguity resolution without test	Ambiguity resolution with test	Usefulness of test procedure
Chi-square test	98.94%	98.94%	no difference
F-test	98.94%	93.03%	degraded
Conjugate ambiguity	98.94%	98.51%	slightly degraded
Moving average	98.94%	99.62%	improved

Table 8.2 Overall performance of different techniques of testing for correct ambiguity resolution

The computer time needed to perform ambiguity search using the three methods given in Sections 7.5 and 7.6 was investigated. Table 8.3 summarizes the basic differences between these methods. Comparisons are made on the basis of attitude determination from one epoch of data using a 486 DX computer with a 50 MHz clock rate. The compared values are of the average computation time needed by each method to perform the search in all tests. The computation time for the first method is used as the standard to compare the second and third methods. The ratios are shown in Table 8.4. Different ambiguity search windows were tried. The search region of ±2 cycles was only used for the static tests. Results show that the first method is the poorest while, in general, the second method performs best. Only for a search window of ±2 cycles, there is some advantage of using the third method. As Table 8.4 shows, the reduction in computation time compared to the first method improves with the increase in the size of the search window.

Reduction of search time is important when processing data in real-time. It also matters when less accurate initial estimates of the baseline have to be used. As an example, the computation time required by the first method to search in a window of ±4 cycles is close to searching in a window of ±8 cycles when the second method is used. This means that if an array of additional antennas is used, applying the second approach allows for longer baselines between the antennas because initial accuracy is not that crucial. Also, a smaller number of additional antennas will be needed if the sequential approach described in Section 7.4 is employed.

Method No.	No. of DD ambiguities to be searched	Perform baseline check	Ambiguity selection criterion
1	3	yes	minimum variance of all meas.
2	2	no	same
3	2	yes	same

Table 8.3 Basic differences in the search approach between different techniques

Search Window (cycles)	Time ratio between the second and first methods	Time ratio between the third and first methods
±2	0.482	0.357
±4	0.322	0.358
±6	0.246	0.282
±8	0.186	0.222

Table 8.4 Ambiguity computation time ratio between the first method and the second and the third

8.4.2 Ambiguity Resolution in the Second Series of Van Tests

The antenna configuration used is a general one in this case, and ambiguity resolution can be obtained in the same manner as presented in Section 7.10, where the correct ambiguity set is chosen based only on the condition that it gives antenna geometry that matches the known one. The correct ambiguity set is the one that passes the tests that the components of the baselines in X, Y, Z directions should sum to zero and that the spatial angles of the antenna configuration, computed from the baseline estimates, should match the known ones. Considering test conditions on hand, a tolerance of 3 cm for the X, Y, Z sums, and 2.5 arcminutes for angle comparison was chosen. These values were selected based on a 2 σ value of the residuals of the tested values in the static case and by multiplying the static values by an empirical factor of 1.5 in the kinematic case, to compensate for errors due to changes in the dynamics. It must be emphasized that the given values apply only to the limited dynamic changes expected in this test. For other levels of dynamics, the tolerance should be modified to give optimum performance.

During the test, the inertial system had periods of malfunctioning. Since, the two main roads used in the test (A and B in Figure 8.6) are well aligned in the north-south and east-west directions, the correctness of ambiguity resolution during periods of malfunctioning of the INS was possible by comparing the resulting heading of the 3DF system to the known direction of the roads. One would expect heading differences within a few degrees due to steering, therefore if heading results are close, the ambiguities are considered correct. No accuracy is lost in this case, since from experience, wrong ambiguity estimation would generate a heading differences considerably larger than a few degrees.

The ambiguity search approach using the known antenna geometry was applied epoch-by-epoch. Table 8.5 gives the total number of epochs of the static and kinematic tests and the number of epochs where the ambiguities were unsuccessfully determined. In the static test, the adopted approach succeeded in finding the correct ambiguity sets in all epochs. Not a single epoch was missed. In the kinematic case, only three out of 954 epochs had wrong ambiguity estimation. It comes as a surprise that some wrong baseline estimates at these epochs gave a geometry that was close to the correct one. The static and kinematic results show that this geometric ambiguity search approach is very efficient. It is more selective than statistical tests which examine a hypothesis, which is based on assumptions that may or may not be true. However, results are preliminary at this point because testing of this new approach has been limited to one test. More tests are needed, at different levels of dynamics and satellite geometry, before a final assessment can be made.

Test	Static	Kinematic
number of epochs	841	954
wrong ambiguity resolution	0	3

Table 8.5 Performance of ambiguity resolution using the known geometry of the antenna configuration

8.4.3 Ambiguity Resolution in the Airborne Test

The heading and pitch were determined from vector components of the baseline 1-3. For estimation of the initial ambiguities, the short baseline 2-3 was used to give an approximate estimation of the longer baseline (1-3). Since the length of the short baseline 1-2 is less than half a cycle, no ambiguity search was needed. After estimating the components of the baseline 1-2, they are used to determine the approximate components of the baseline 1-3. From the approximate baseline solution, the initial values of the ambiguities can be estimated. Searching for the correct ambiguity set of the baseline 1-3 and identifying it epoch-by-epoch follows the procedure described in Chapter 7.

During the flight, some satellites were blocked, resulting in a number of cycle slips. The ambiguity moving average technique proved to be a powerful approach in finding these cycle slips. However, when sudden changes in dynamics occur, cycle slips of one or two cycles may appear. The most likely cause of this phenomenon is non-optimality of changing the tracking phase loop bandwidth in the Ashtech 3DF to accommodate rapid changes in acceleration. The ambiguity moving average technique does not allow for detection of cycle slips as low as one or two cycles. In fact, in the presence of these small cycle slips, the ambiguity moving average may assume that the newly estimated instantaneous ambiguity, which differs by one or two cycles from the moving average is false and thus shift it incorrectly. To safeguard against this problem, the ambiguity moving average approach should be preceded by another approach, capable of detecting smaller cycle slips.

Different techniques for cycle slip detection are used in DGPS when using GPS data only, see for instance (Westrop et al.,1989), (Lu and Lachapelle,1990) and (Hofmann-Wellenhof et al.,1992). Cycle slip detection in the multi-antenna system is easier than for DGPS, because the atmospheric errors are negligible when differencing phase measurements on very short baselines. Suspected cycle slips are easier to identify since they cannot be mixed up with errors due to atmospheric propagation. In addition, the antenna baselines in the multi-antenna system can be accurately measured. Thus, by computing the baseline length, using phase measurement including in one case the current ambiguity resolution, and in another case the moving average, and comparing the estimated baseline length in each case to its true value, a decision can be made whether the estimated ambiguity is correct or whether it should be shifted to the moving average.

Another useful feature of the multi-antenna system is that all antennas are mounted on the same surface, and thus are subject to the same changes in dynamics. In addition, all channels have the same design, and therefore, behave consistently. Thus, most of the small cycle slips cancel in differencing the phase measurements between antennas. To illustrate this phenomenon, let us consider a simple approach that compares the measured carrier phase with a predicted one, determined from the measured Doppler frequency, to assess the occurrence of cycle slips. In this technique, the predicted carrier phase at time t_{k+1} can be determined as (Cannon,1991):

$$\phi_{k+1} = \phi_k + \frac{\dot{\phi}_{k+1} + \dot{\phi}_k}{2} \Delta t \tag{9.1}$$

where ϕ_{k+1} is the predicted phase measurement at t_{k+1}

ϕ_k is the phase measurement at t_k

$\dot{\phi}_{k+1}$ and $\dot{\phi}_k$ are the Doppler frequency measurement at t_{k+1} and t_k, respectively

Δt is the time difference between t_{k+1} and t_k.

Figures 8.10 and 8.11 show, as an example, the difference between the predicted and measured phase at antenna 1 and 3 for satellite 19, using the test data on hand. Figure 8.12 and 8.13 show similar results for satellite 31. The differences shown are due to changes in the dynamics, as equation (8.1) assumes constant acceleration during Δt. Comparing Figure 8.10 to Figure 8.11, and Figure 8.12 to Figure 8.13, shows clearly that the changes are similar for antennas 1 and 3. When using double differences, all common differences are canceled and only small random cycle slips are left, which are mainly attributed to differences in performance between carrier tracking loops of receiver channels. This is depicted in Figure 8.14. The spikes shown are due to cycle slips at these epochs, which can be easily detected using the moving average approach. The cycle slips of one cycle shown, are the only ones that would appear in the solution. The same cycle slips were detected when using the baseline length to check for cycle slips.

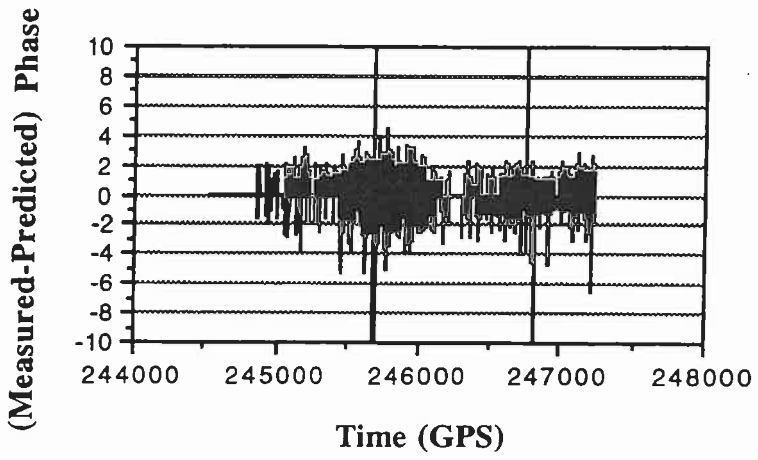

Fig. 8.10 Phase difference of satellite 19 at antenna 1

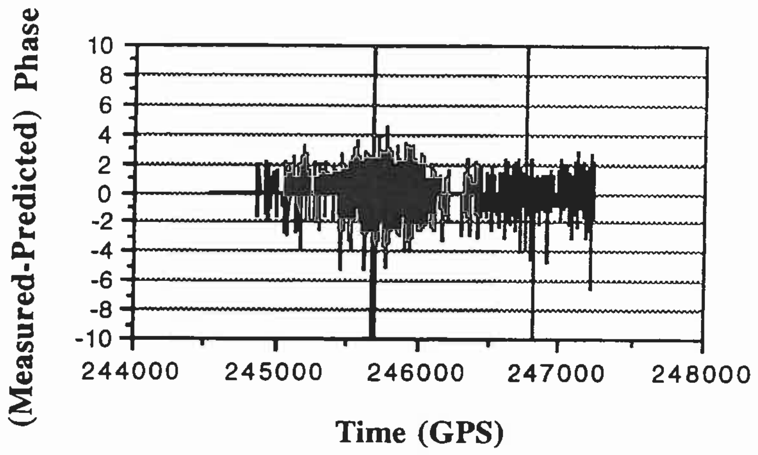

Fig. 8.11 Phase difference of satellite 19 at antenna 3

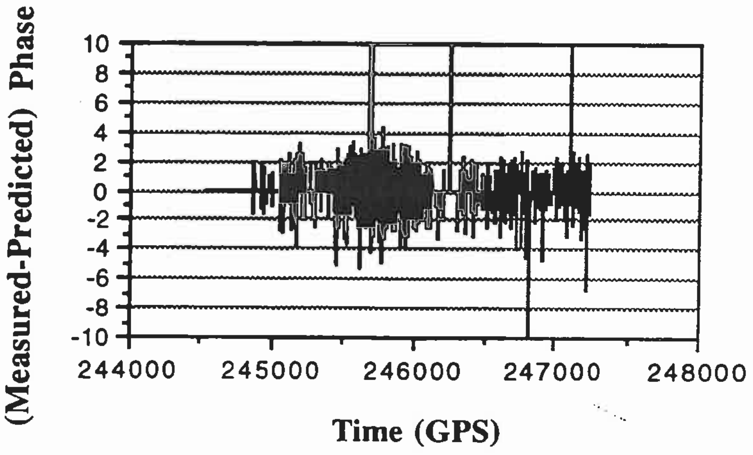

Fig. 8.12 Phase difference of satellite 31 at antenna 1

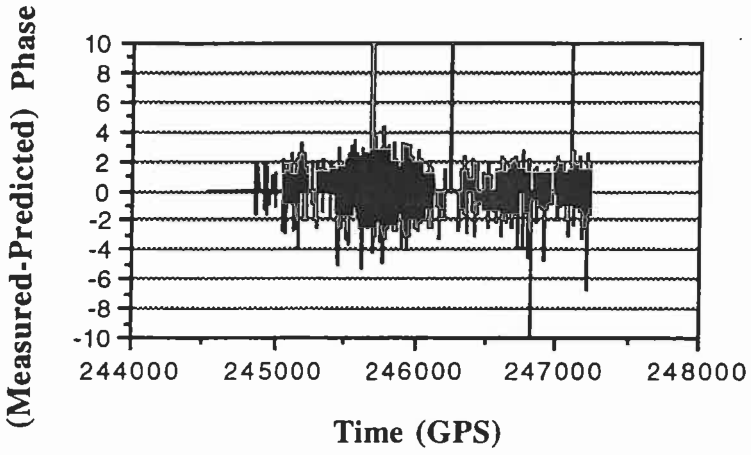

Fig. 8.13 Phase difference of satellite 31 at antenna 3

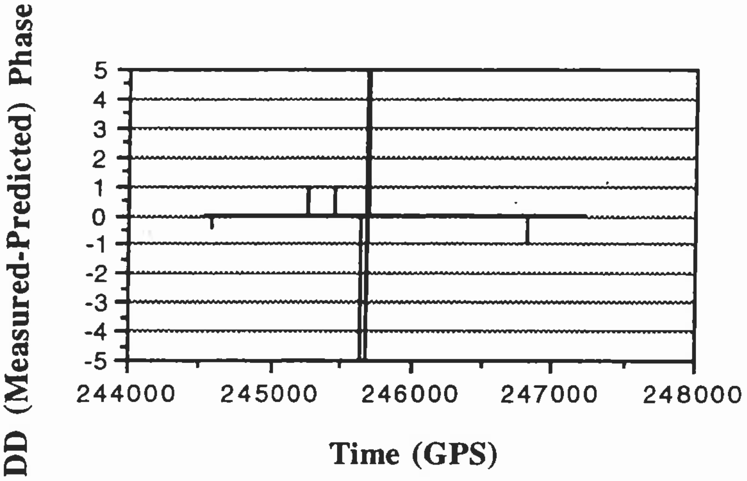

Fig. 8.14 Difference of phase double difference between satellites 19 and 31

Table 8.6 show results of instantaneous ambiguity resolution for both static and kinematic tests. Out of 1555 epochs in the static case, only two epochs had wrong ambiguity estimation. In the kinematic case, the epoch-by-epoch ambiguity resolution gave very good results in the periods of good satellite visibility, the success rate was about 95%. This result shows that the adopted technique is very reliable when considering the high level of dynamics experienced by the aircraft. During the period of bad satellite geometry with 3 satellites, the success rate drops to 74%. This is expected as there is no redundant measurement available in this case, and poor satellite geometry has a profound impact on ambiguity resolution. It should be noted that these results are specific to the multi-antenna system used and may change when other receivers are used.

Test	Static Test	Kinematic using 4-6 satellites	Kinematic using 3 satellites
number of epochs	1555	2002	552
wrong ambiguity resolution	2	87	144

Table 8.6 Performance of ambiguity resolution in airborne mode

8.5 Analysis of Attitude Determination Performance

Antenna configuration and attitude determination technique used in the first series of van tests and in the airborne tests are similar. Therefore, analysis of attitude results will be given for both cases, and their performance will be compared.

8.5.1 Attitude Results in the First Series of Van Tests

8.5.1.1 Static Test Results

Figures 8.15a and 8.15b show, as an example, pitch results of one of the static tests as determined independently by the 3DF and the INS systems, respectively. Complete attitude results of the two systems are given in Appendix C. The comparison of the two figures (8.15a and 8.15b) clearly shows the presence of multipath in the 3DF data. Its period is about 10 minutes and its amplitude 0.15 degrees. All other static 3DF data sets show multipath with similar trend and magnitude. Considering that the test area was chosen for low multipath, it appears that this phenomenon cannot be avoided in the static case.

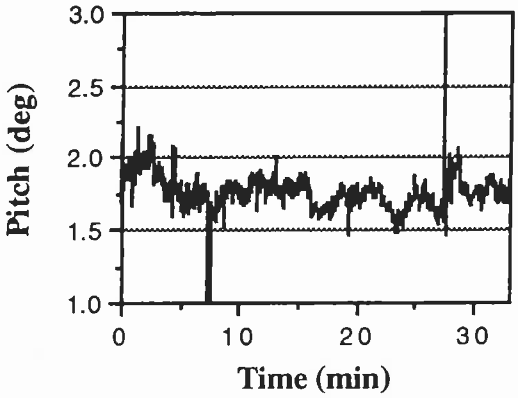

Fig. 8.15a Static 3DF pitch

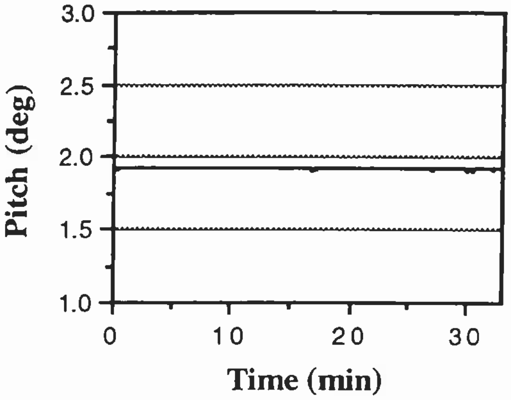

Fig. 8.15b Static INS pitch

Heading and roll variation patterns are similar to those of pitch, but with different amplitudes. The (INS-3DF) differences are shown in Figures 8.16 and 8.17 for heading and pitch of the first test, and in Figures 8.18 and 8.19 for the second test. The differences in roll are depicted in Figure 8.20. The large spikes shown are due to erroneous ambiguity determination. Table 8.7 gives the statistical results (rms) for all tests performed. The smaller error amplitude in heading is very typical for all static results and is due to the fact that the height component does not enter into the computation. Note that the difference in baseline lengths for pitch and roll does not result in a difference in the static error rms. This is due to the fact that the satellite geometry was better for the roll test than for the pitch test.

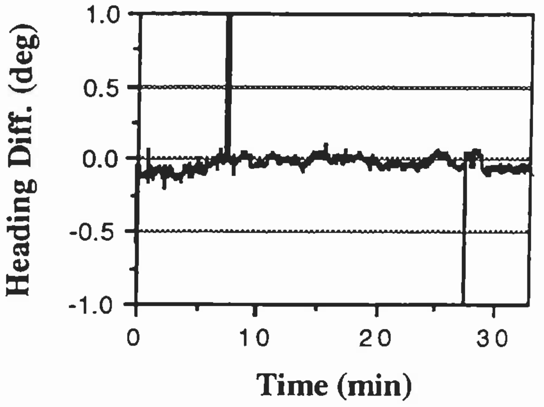

Fig. 8.16 Static heading difference test (1)

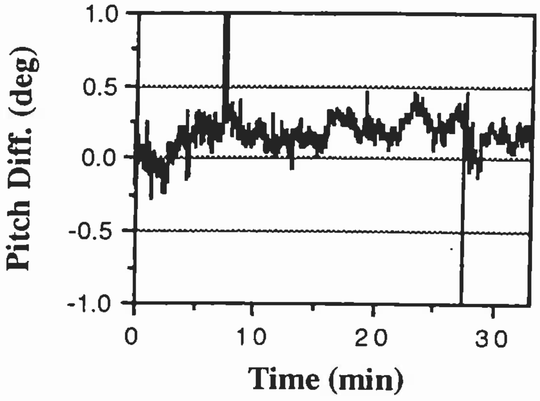

Fig. 8.17 Static pitch difference test (1)

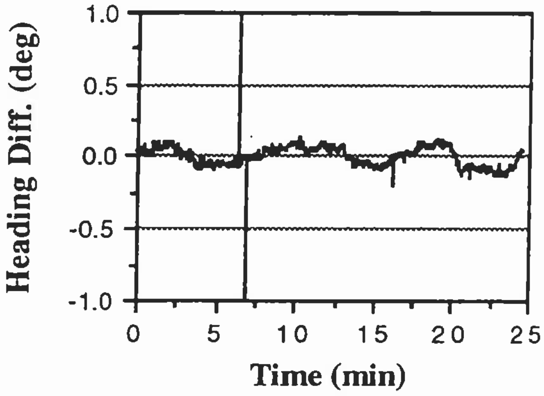

Fig. 8.18 Static heading difference test (2)

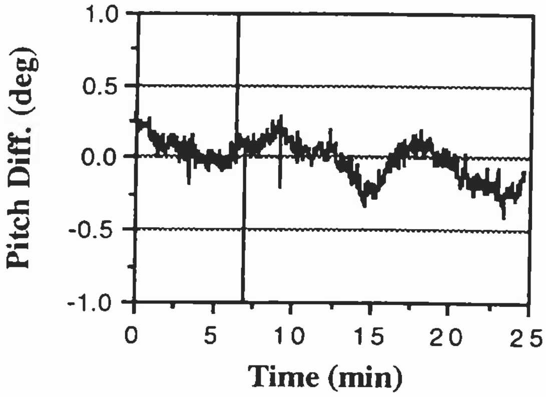

Fig. 8.19 Static pitch difference test (2)

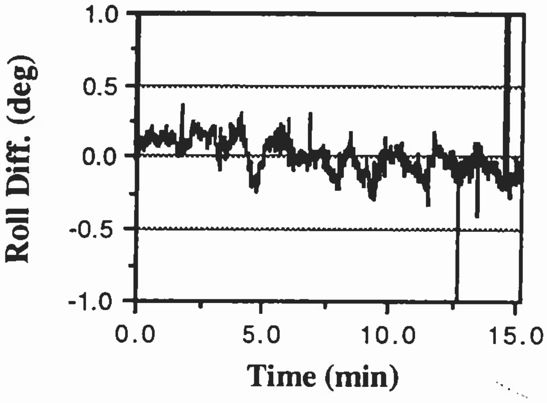

Fig. 8.20 Static roll difference

Attitude Component	Static			Kinematic			
	Run 1	Run 2	Run 3	Run 1	Run 2	Run 3	Run 4
Heading	0.052	0.045	0.064	0.058	0.047	0.057	0.086
Pitch	0.105	0.111	0.133	0.091	0.098	0.113	0.120
Roll	0.110	--	--	0.171	--	--	--

Table 8.7 rms of attitude differences for the static and kinematic runs (deg)

8.5.1.2 Kinematic Test Results

Figures 8.21a and 8.21b show results of the pitch for the first kinematic test as a typical example. The first figure gives the 3DF results, and the second shows the INS results. The agreement between the two system outputs is very good at the scale given. For detailed attitude results of the two systems, refer to Appendix C. To give a head-to-head comparison with the presented static results, the difference between the 3DF and the INS estimated attitude in heading and pitch from the first and second tests are shown in Figures 8.22 to 8.25. The difference in roll is illustrated in Figure 8.26. The estimated error level of the ranges from less than 0.05 degree in heading to approximately 0.17 degree in roll. The spikes shown in the figures are due to erroneous ambiguity resolution.

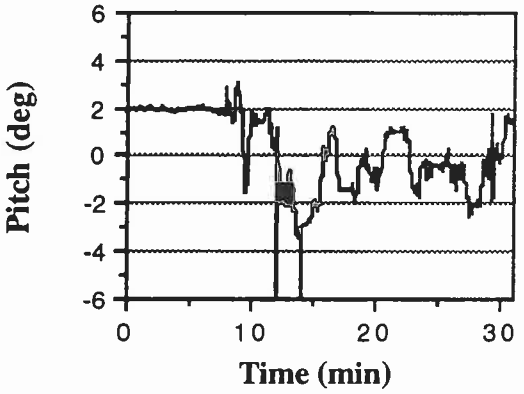

Fig. 8.21a Kinematic 3DF pitch

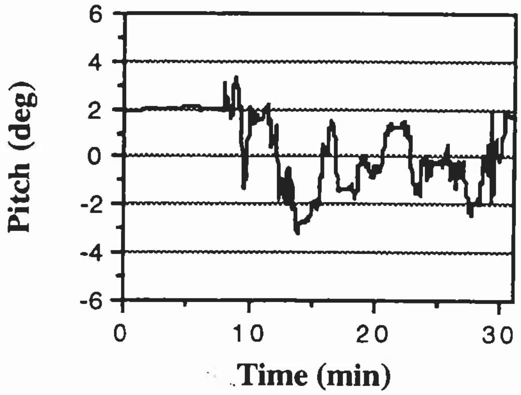

Fig. 8.21b Kinematic INS pitch

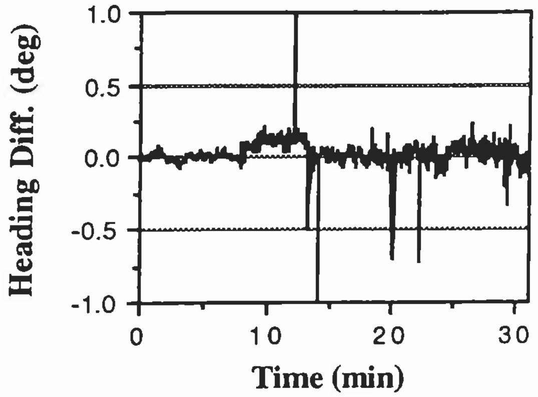

Fig. 8.22 Kinematic heading difference test(1)

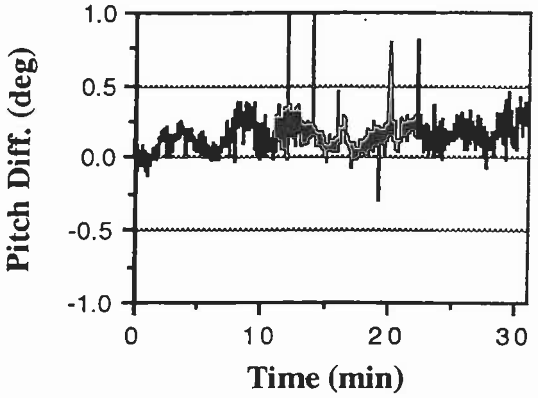

Fig. 8.23 Kinematic pitch difference test(1)

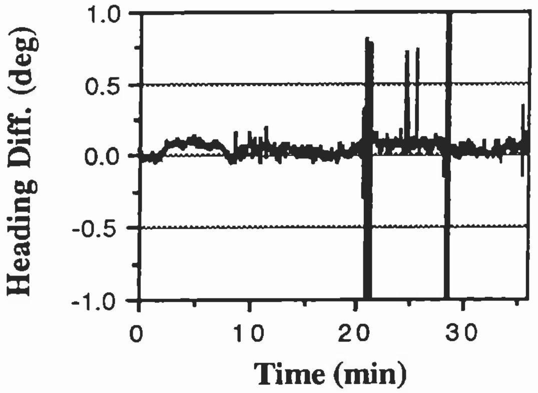

Fig. 8.24 Kinematic heading difference test(2)

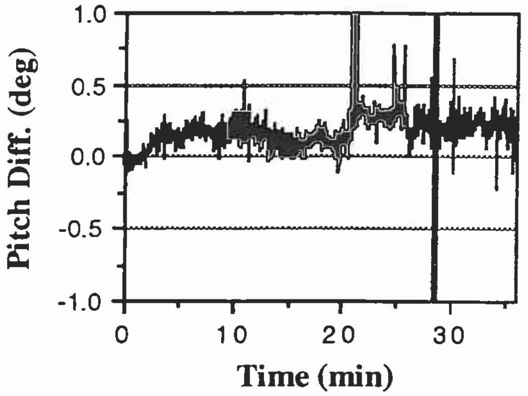

Fig. 8.25 Kinematic pitch difference test(2)

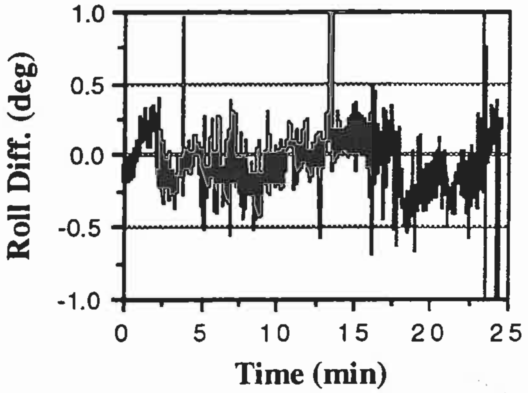

Fig. 8.26 Kinematic roll difference

Roll results show a higher multipath level than heading and pitch. This is mainly due to a difference in satellite geometry between the heading and pitch tests on the one hand, and the roll test on the other. When comparing the rms values given in Table 8.7, the roll has a larger rms than the pitch. This is due to using a shorter baseline length when estimating the roll (1.572 m compared to 2.975 m). The difference between the static and kinematic roll results is due to the fact that the satellite number and geometry employed in the kinematic case are much poorer than those used in the static case. In the kinematic test, 4 or 5 satellites with a PDOP of about 6 were used, giving El-DOPs of about 2.3. In the static test 6 satellites were available and the PDOP was 2, and the El-DOP was 1.2.

When comparing the kinematic results to the static ones, two conclusions can be drawn. First, the multipath error is less significant in the kinematic case. This is mainly due to the continuous geometry changes between satellites, reflecting objects and antennas, and also due to antenna vibrations; see for instance Braasch and Van Grass (1991). It is also confirmed by independent results recently published in Schwarz and Wei (1994). The second important observation is that the general noise level is almost the same in the static and kinematic modes. It is approximately 3 arcminutes for heading and 6 arcminutes for pitch. These results were achieved with a baseline of 2.975 metre. Better accuracy is obtained when longer baselines are used, see for instance (Lachapelle et al., 1994). Taking baseline lengths into account, the accuracy achieved is close to the one shown in the tests given in Chapter 5.

8.5.2 Attitude Results in the Airborne Test

8.5.2.1 Static Results

Figures 8.27a and 8.27b illustrate the 3DF heading and pitch results of the static test, respectively. As shown, multipath is clearly visible. Since the airplane was not in the vicinity of big buildings or hills, the body of the airplane and the ground have to be considered multipath sources. The inertial system attitude parameters were very stable during the static test. The difference between the 3DF and the INS outputs are shown in Figures 8.28 and 8.29. Errors in heading were smaller than in pitch, and this can be attributed to the inclusion of the height component in estimating pitch. This is also reflected in the rms of attitude differences between the two systems, given in Table 8.8. The rms for heading is four times smaller than that for pitch. Previous tests (Section 8.5.1.1) show that this ratio was only two before. Major factors that may have caused this variation are the airplane vibration, where the engines were running to provide power to the INS system, and the change of satellite geometry and multipath effects from one test to the other.

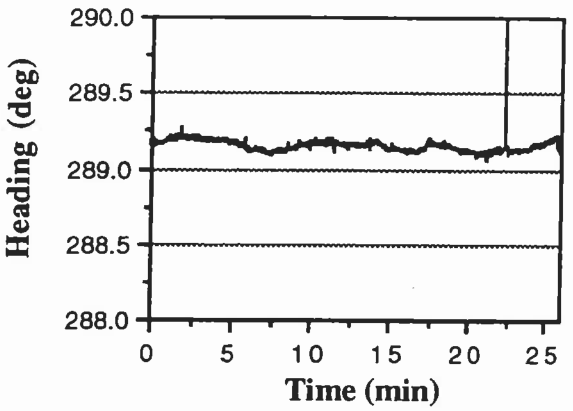

Fig. 8.27a 3DF static heading results

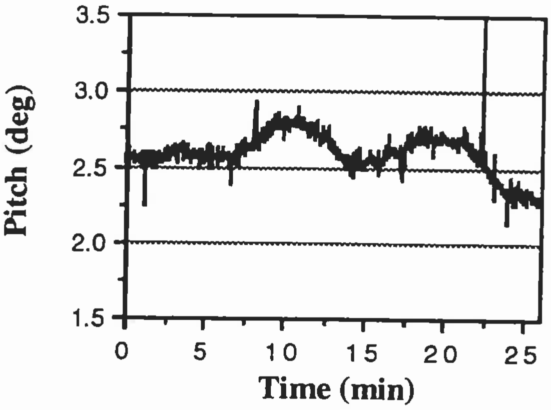

Fig. 8.27b 3DF static pitch results

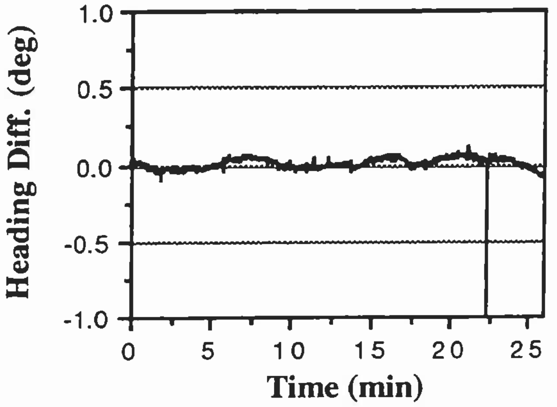

Fig. 8.28 Static (INS-3DF) heading

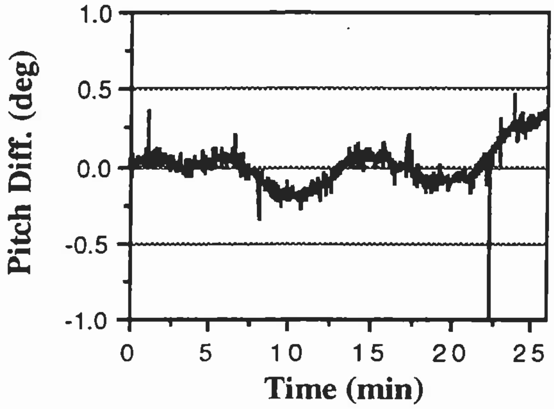

Fig. 8.29 Static (INS-3DF) pitch

Attitude Component	Static Test	Kinematic using 4-6 satellites	Kinematic Including 3 satellites
Heading	0.032	0.118	0.273
Pitch	0.127	0.138	0.433

Table 8.8 rms of attitude components in static and kinematic tests (deg)

8.5.2.2 Kinematic Results

Figure 8.30a and 8.30b illustrate the kinematic results of the 3DF system for heading and pitch, respectively. Appendix C gives the INS heading and pitch results. When the aircraft was heading north, differences in steering generated jumps from 0 to 360 degrees, which are visible in the heading figure. The differences between the output of the 3DF and the INS are shown in Figure 8.31 for heading and in Figure 8.32 for pitch. In contrast to the static case, there is no clear indication of multipath errors in the kinematic test. This is most likely due to randomization of these errors due to orientation changes of the aircraft, as well as vibration of the aircraft which dampens the multipath (see Chapter 4). One should also consider the possibility that multipath errors in this high dynamic environment may be partially masked by other errors. On the other hand, since the airplane body, as a reflecting source, exists in both the static and kinematic tests, this difference in multipath behaviour indicates that the ground may have been the major multipath error source in the static test.

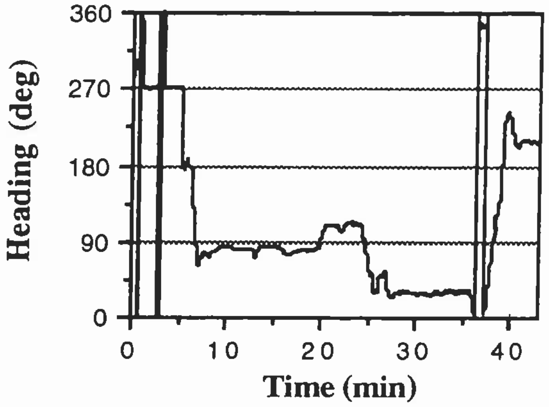

Fig. 8.30a 3DF kinematic heading results

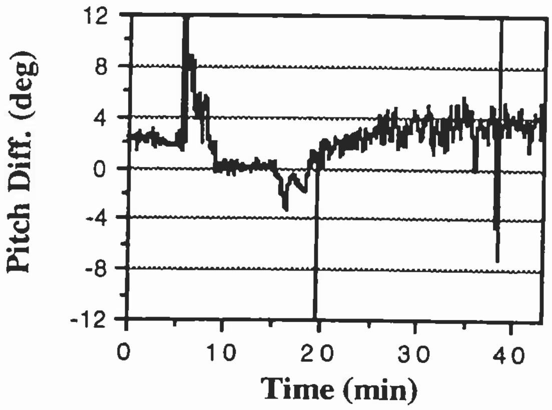

Fig. 8.30b 3DF kinematic pitch results

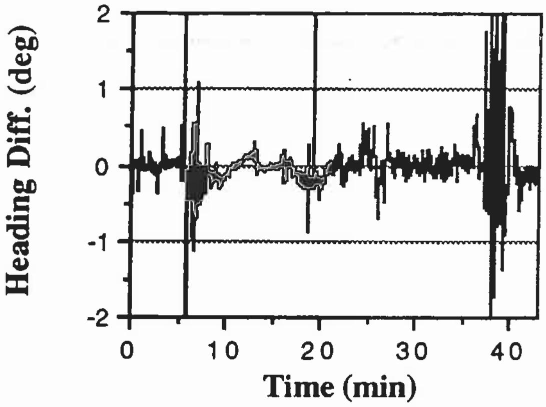

Fig. 8.31 Kinematic (INS-3DF) heading

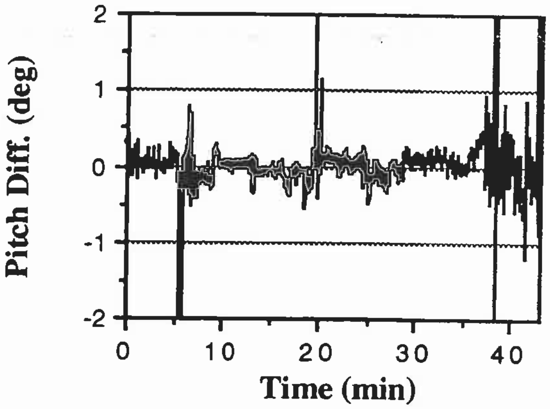

Fig. 8.32 Kinematic (INS-3DF) pitch

Changes in satellite visibility and geometry described before have a direct effect on the final output. Periods with good satellite geometry showed more stable and consistent errors, while those with bad geometry showed large errors of inconsistent pattern. This is clear when comparing, for instance, the third quarter of the data to the fourth. In the former, 5 to 6 satellites with good geometry were observed, resulting in errors bounded in a range usually expected under these favorable conditions. In the fourth quarter of the data, poor satellite visibility was encountered with mostly 3 satellites. During this period, the level of errors was magnified considerably. This is reflected in the estimation of the rms of the differences between the 3DF and the INS outputs given in Table 8.8. The third column of the table shows the rms for periods when 4 to 6 satellites were observed giving geometry that varies between normal to good. The fourth column shows the rms values when periods of bad satellite geometry were included. As shown, the rms values were magnified by a factor of two to three.

The results extracted from the periods of normal to good satellite geometry compare well with the ones given in Cohen et al. (1994) and Cannon et al.(1994), when taking the baseline length ratio into consideration. In both studies, the attitude of a GPS based system was compared to that of an accurate inertial system. In the first test, an rms of about 3 arcminutes in attitude difference was reported for all components using a baseline length of 7.92 m. In the second study, averaged accuracy, from two tests, of 3.5 and 5.8 arcminutes were reported for heading and pitch respectively, using a baseline length of 6.93 m.

When considering the case of good satellite geometry, one notices that heading and pitch results are very close, which contradicts results shown in the previous tests (Section 8.5.1.1). This is most likely due to aircraft vibrations.

8.5.3 Comparison between Attitude Determination Performance on Land and in Airborne Tests

Comparison of the attitude determination results on land and in the airborne show two important features. First, attitude determination is less accurate in the airborne mode than on land. Second, multipath effects in flight are less of a problem than on land. The first feature is mainly due to effects of vehicle dynamics on attitude determination. Low dynamics do not change attitude accuracy significantly, as is clear when comparing static and kinematic results of the van tests, where the level of accuracy achieved almost did hardly change. The difference of dynamics between the land and airborne modes is, however, large, because more vibrations are expected in airborne mode. In addition, during turns and maneuvering in flight, satellite shading may occur. In these cases, attitude accuracy may degrade by a factor of about 2.

Multipath sources in kinematic airborne mode are limited to the aircraft body, and during normal flight its effect is minimal. In addition, vibration of the airplane dampens multipath effects. In turns and maneuvering, some multipath may appear from the wings due to tilting of the airplane. On land, a multitude of multipath sources exist. Even with changes in the geometry of the satellites and the moving antennas, some multipath effects remain.

Test results also show that with a baseline of 3 m, the achievable accuracy in heading is between 3 and 6 arcminutes, and in pitch and roll is between 5 and 8 arcminutes, depending on factors discussed in Chapter 4. More accuracy is expected when the baseline length is increased.

CHAPTER 9

CONCLUSIONS AND RECOMMENDATIONS

The emphasis of this research was on the development and testing of techniques for reliable attitude determination and ambiguity resolution in kinematic GPS applications. Major contributions were made in three areas. First of all, the geometry of the antenna configuration was used to enhance the accuracy of attitude determination by a network approach and to introduce a new methodology of ambiguity resolution by geometrical constraints. Second, instantaneous ambiguity determination algorithms were developed, and methods of enhancing speed and robustness of finding the correct ambiguities were presented. These algorithms were extensively tested in different operational modes. Finally, a new approach for direct attitude determination from phase measurements was developed and extensively compared to existing methods. The comparison included operational factors, such as computational time, number of antennas and antenna configuration, as well as an accuracy analysis. Detailed conclusions resulting from this research are given in the following.

9.1 Conclusions

The following conclusions can be drawn from these investigations.

1) Solving the multi-antenna baselines in a network solution, in general, improves attitude determination as compared to a baseline-by-baseline approach. This is because the network approach includes additional geometric information (baseline lengths and angles), and considers the correlation between baselines. The additional computational time needed to

apply the network approach is a few milliseconds for each epoch. The network approach can therefore be used in real time.

2) Three methods are presented for attitude determination. They are: indirect attitude determination using the transformation matrix between the body frame and the local-level frame, attitude determination from vector orientation in the local-level frame, direct determination of attitude parameters from phase measurements. All three methods have been tested under different operational conditions and perform well. Using a baseline of 3 metres length, heading accuracies of 3-7 arcminutes, and pitch and roll accuracies of 5-8 arcminutes can be achieved, depending on factors, such as magnitude of multipath, satellite geometry and level of dynamics and vibrations.

3) If attitude parameters are determined from the transformation matrix between the body frame and the local-level frame, they cannot be determined directly from the elements of the transformation matrix because the rotation sequence is unknown. Instead, an adjustment approach is used. Because of the non-linearity of the observation equations, the method is not compatible with the other techniques. Differences in the solution are usually less than 1.5 arcminute; however, they can reach 5 arcminutes, especially when rapid changes in the orientation occur. The direction of a line cannot be determined with this method, it works only for 3D attitude determination. It also needs an initialization period to determine baseline components in the body frame. The method, however, is advantageous in terms of the antenna configuration because the antennas can be located anywhere and at any height above the moving carrier. When using redundant antennas the algorithm does not change.

4) The direct approach and the method of attitude determination from vector orientation in the local-level frame are very compatible, and show no significant difference in attitude determination. Also, the computational time needed is almost the same. The direct method,

however, is straightforward and simple in principle. Both methods can be used for direction finding or 3D attitude determination, as long as all baselines are in one plane. However, both approaches are not flexible regarding antenna distribution. At least two antennas have to be parallel with the longitudinal axis of the moving body. In addition, redundant antennas can only be used if they are in the same plane as the three primary ones, otherwise a transformation matrix is needed, which essentially results in a solution similar to the first approach.

5) Instantaneous ambiguity resolution is the key element in achieving a reliable attitude solution in kinematic applications. If the correct ambiguities are determined using a search approach around the initial estimate of the baseline, additional antennas will speed up ambiguity resolution by estimating the initial baseline within a small range of uncertainty. For baselines between 3 and 5 metres the search can be conducted in a region of 9 cycles. For longer baselines the additional antennas can be added sequentially to generate the same search region. Additional antennas increase the total cost of the system, however.

6) The search can be performed within two phase double differences taking the measured baseline length into consideration. This information is enough to produce a unique baseline solution that can be tested to define the correct ambiguities. This approach replaces a widely used method of searching within three phase double differences for the same purpose. The reduction of the search time when using the proposed approach is significant. The reduction time ratio increases with the increase of the search region.

7) Other features that can be used to speed up the ambiguity search procedure are: computing the normal equation matrix in the least-squares approach only once for all test sets at the same epoch, performing only one iteration of the least-squares solution, and

testing the antenna vector magnitude, produced from each test ambiguity set, against the known baseline length.

8) Ambiguity resolution using the known antenna geometry appears to be an efficient technique with a high reliability of determining the correct ambiguities. The main principle is that all baseline vectors estimated from the correct ambiguities should satisfy the known spatial geometry of the antenna configuration. This technique is more selective than statistical tests. Results are preliminary at this point because testing of this new approach has been limited to one test.

9) The use of the ambiguity moving average approach increases the probability of correct ambiguity resolution. It can be also be used for detection of cycle slips.

10) Ambiguity re-initialization can be performed more reliably if one single difference ambiguity is known. This is performed by estimating values for the known ambiguity, from baseline solutions based on tested sets of ambiguities. The correct ambiguity set is then determined as the one giving an ambiguity estimate equal to the known ambiguity.

11) The adopted ambiguity resolution techniques use an epoch-by-epoch solution approach. In this scheme, wrong attitude determination are limited to the epochs of erroneous ambiguity determination and will not propagate into the following epochs.

12) Van and aircraft tests show clearly the feasibility and high reliability of achieving instantaneous ambiguity resolution in different dynamic environments. Field tests using a van indicate that the ambiguities can be resolved in real-time in 99% of the cases. The performance is similar for the low dynamics and static tests. In a high dynamic environment, such as in airborne mode, where the aircraft is subjected to vibrations and

sudden changes in dynamics, performance of correct ambiguity determination was about 95%. In cases of poor satellite geometry, it could drop to 74% of the total. In all approaches, the ambiguities are resolved and the attitude is computed in less than half a second, using a 486 DX computer with 50 MHz clock rate.

13) For a baseline of 3 m length, one millimetre error in the relative positions between the antennas will produce an error of about one arcminute in baseline orientation. To maximize system accuracy, errors at the millimetre level have to be minimized. For the multi-antenna system, common receiver, antenna and atmospheric errors are canceled through phase measurement differencing, and the major errors remaining that can produce relative errors at this level are multipath, carrier tracking noise and antenna phase centre variation. Field tests show that multipath is almost unavoidable in the static case. Errors in attitude due to multipath can reach 9 arcminutes. In the kinematic case, multipath effects are minimized due to randomization of the satellite-multipath source-antenna geometry, and vibrations. Phase noise and antenna phase centre variation can also produce a few millimetre errors in relative positioning. In high dynamics, phase noise is the major error source. Phase noise can be minimized by enhancing receiver design, and antenna phase centre variation can be reduced by using antennas of rugged and consistent design, and orienting the antennas in the same direction.

14) In general, accuracy of attitude determination increases with the increase in baseline length. However, errors, such as uncorrelated multipath and surface flexing, will lead to a diminishing gain when the baseline exceeds a certain length.

15) To determine the attitude of a moving vehicle reliably, the antennas should be rugged and should be mounted in such a way that the rigid body assumption, upon which the attitude model is based, is approximated as well as possible. Even small errors in the rigid

body assumption can lead to large errors in attitude determination if short baselines are used. Antenna locations should therefore be chosen to avoid as much as possible changes in the body of the moving vehicle due to torsion, bending, and flexing.

16) Some limited studies on optimal antenna configurations are not conclusive. Antennas with significant height differences produce phase double differences of high signal-to-noise ratio, which is an advantage. However, the signal-to-noise ratio is also dependent on satellite geometry. Moreover, an inverted orthogonal antenna triad is theoretically more advantageous than antennas distributed in the same plane. Limited field testing has not confirmed this result.

9.2 Recommendations

Based on the results of this research, the following recommendations regarding improved performance of GPS multi-antenna attitude determination system can be made:

1) An improved oscillator and hardware design for a common receiver operating multi-antennas will make single differencing the preferred differencing technique replacing double differencing. This will result in improved measurement accuracy.

2) Further testing of the instantaneous ambiguity resolution approach using the known geometry of the antenna configuration is needed. The tests should include shipborne and airborne modes.

3) Additional tests are required to assess performance of attitude determination methods when increasing baseline length. This will be important for some commercial applications,

as for instance big air carriers and ships, where flexing, bending, and torsion modeling may also be needed.

4) The inverted orthogonal antenna triad should be further tested under different dynamic environments to give a final assessment of its performance.

5) A comprehensive analysis of multipath effects on attitude determination in the kinematic case, and its minimization is needed.

6) Integration of the system with a medium accuracy inertial system is an attractive option for kinematic applications. While a GPS multi-antenna system with short baselines has accuracy in the arcminutes range, it does not drift with time as the inertial system does. The inertial system on the other-hand has a high output rate, good accuracy in the short term and does not have the problem of satellite shading or ambiguity initialization. It can provide initial values for attitude parameters that can be used to achieve instantaneous ambiguity resolution without the need for additional antennas. If multipath problems have been solved, the integrated system will be an attractive alternative to the more expensive and accurate inertial systems currently used.

REFERENCES

Ashtech (1991), Three-Dimensional Attitude Determination with the Ashtech 3DF 24-Channel GPS Measurement System, Company Publication.

Balanis, C. (1982), Antenna Theory: Analysis and Design, Harper & Row Publishers Inc., New York, 1982.

Beck N., J.R. Duval and P.T. Taylor, (1989), GPS Processing Methods: Comparison with Precise Trilateration, Journal of Surveying Engineering, 1989.

Blais, J.A.R. (1979), Least-Squares Block Adjustment of Stereoscopic Models and Error Analysis, Ph. D. Thesis, UCGE Report number 30001, Department of Geomatics Engineering, The University of Calgary, 1979.

Blomenhofer, H., G. W. Hein and D. Walsh (1993), On-The-Fly Carrier Phase Ambiguity Resolution for Precise Aircraft Landing, Proc. ION GPS-93, Salt Lake city, Utah, September 22-24, 1993.

Braasch, M. and F. Van Graas (1991), Guidance Accuracy Considerations for Real-time GPS Interferometry, Proc. ION GPS-91, Albuquerque, New Mexico, September 11-13, 1991.

Braasch, M. (1992), Characterization of GPS Multipath Errors in the Final Approach Environment, Proc. ION GPS-92, Albuquerque, New Mexico, September 16-18, 1992.

Brown, R. and P. Ward (1990), A GPS Receiver with Built-In Precision Pointing Capability, Proc. of the IEEE PLANS (1990), Las Vegas, Nevada, March 20-23, 1990.

Brown, R. and A. Evans (1990), GPS Pointing System Performance, Proc. ION GPS-90, Colorado Springs, Colorado, September 1990.

Brown, R.A. (1992), Instantaneous GPS Attitude Determination, Proc. of the IEEE PLANS, 1992.

Cannon, M.E. (1991), Airborne GPS/INS with an Application to Aerotriangulation, Ph. D. Thesis, UCGE Report number 20040, Department of Geomatics Engineering, The University of Calgary, 1991.

Cannon, M.E., J. Schleppe, J.F. Mclellan and T.E. Ollevier (1992), Real-Time Heading Determination Using An Integrated GPS-Dead Reckoning System, Proc. ION GPS-92, Albuquerque, New Mexico, September 16-18, 1992.

Cannon, M.E. and M. Haverland (1993), Experiences of GPS Attitude Determination within a Helicopter Pod, Proc. ION GPS-93, Salt Lake City, Utah, September 22-24, 1993.

Cannon, M.E., H. Sun, T.E. Owen and M.A. Meindl (1994), Assessment of a Non-Dedicated GPS Receiver System for Precise Airborne Attitude Determination, Proc. ION GPS-94, Salt Lake city, Utah, September 20-23, 1994.

Cohen, C.E. and B.W. Parkinson (1991), Expanding the Performance Envelope of GPS-Based Attitude determination. Proc. ION GPS-91, Albuquerque, New Mexico, September 11-13,1991.

Cohen, C.E. and B.W. Parkinson (1992), Aircraft Applications of GPS-Based Attitude Determination, Proc. ION GPS-92, Albuquerque, New Mexico, September 16-18, 1992.

Cohen, C.E., H. S. Cobb and B. W. Parkinson (1992), Generalizing Wahba's Problem for High Output Rates and Evaluation of Static Accuracy Using a Theodolite, Proc. ION GPS-92, Albuquerque, New Mexico, September 16-18,1992.

Cohen, C.E., B.W. Parkinson and B. D. Mcnally (1994), Flight Tests of Attitude Determination Using GPS Compared Against an Inertial Navigation Unit, Navigation, Journal of The Institute of Navigation, Vol. 41, No. 1, Spring,1994.

Comp, C. J. (1993), Optimal Antenna Configuration for GPS Based Attitude Determination, Proc. ION GPS-93, Salt Lake city, Utah, September 22-24, 1993.

Comrey, A.L., P.A. Bott and H.B. Lee (1989), Elementary Statistics: A Problem-Solving Approach, WM. C. Brown Publishers, Dubuque, Iowa, 1989.

Corbett, S. (1993), GPS for Attitude Determination and Positioning in Airborne Remote Sensing, Proc. ION GPS-93, Salt Lake city, Utah, September 22-24, 1993.

Diefes, D.L., L.C. Fan and C. E. Rodgers (1993a), Dynamic GPS Attitude Determination System (ADS) for Marine Applications, Concept Design and Developmental Test Results, Proc. ION National Technical Meeting, San Francisco, January 20-22, 1993.

Diefes, D. L., G. G. Hazel and D. F. Greenlee (1993b), GPS Attitude Determination System for Marine Navigation, Proc. ION GPS-93, Salt Lake city, Utah, September 22-24, 1993.

DMA (1991), World Geodetic System 1984: Its Definition and Relationships with Local Geodetic Systems, The Defense Mapping Agency Technical Report 8350.2, Second Edition, September, 1991.

El-Mowafy, A. and K.P. Schwarz (1994a), Epoch by Epoch Attitude Determination Using A Multi-Antenna System in Kinematic Mode, Proc. KIS-94, Banff, Canada, August 30 - September 2, 1994.

El-Mowafy, A. and K.P. Schwarz (1994b), Epoch by Epoch Ambiguity Resolution for Real-Time Attitude Determination Using a GPS Multi-Antenna System, Accepted for Publication in Navigation, Journal of the US Institute of Navigation, 1994.

Erickson, C. (1992a), Investigations of C/A Code and Carrier Measurements and Techniques for Rapid Static GPS Survey, M.Sc. Thesis, UCGE Report number 20044, Department of Geomatics Engineering, The University of Calgary, 1992.

Erickson, C. (1992b), An Analysis of Ambiguity Resolution Techniques for Rapid Static GPS Surveys Using Single Frequency Data, Proc. ION GPS-92, Albuquerque, New Mexico, September 16-18, 1992.

Ferguson, K., J. Kosmalska, M. Kuhl, J.M. Eichner, K. Kepski and R. Abtahi (1991a), Three-Dimensional Attitude Determination with the Ashtech 3DF 24-Channel GPS Measurement System, Proc. ION National Technical Meeting, Phoenix, Arizona, January 22-25, 1991.

Ferguson, K., S. Gourevitch, M. Kuhl and X. Qin (1991b), Attitude Determination with The Ashtech Three-Dimensional Direction Finding System, Presented at the ASCE Surveying Engineering Division, Transportation Applications of GPS Positioning Strategy, GPS '91, Sacramento, September 18-21, 1991.

Frei, E., J. Yau and D. Sauer (1993), Ambiguity Resolution on the Fly (AROF): Results, Facts, Limitations, Proc. ION GPS-93, Salt Lake city, Utah, September 22-24, 1993.

Georgiadou, Y. and A. Kleusberg (1988), On Carrier Signal Multipath Effects in Relative GPS Positioning, Manuscripta Geodaetica, Vol. 13, 1988.

Georgiadou, Y. and A. Kleusberg (1989), Multipath effects in Static and Kinematic GPS Surveying, Proc. IAG, Symposium 102, Edinburgh, Scotland, August 7-8, 1989.

Goad, C. and M. Yang (1993), On Automatic Precision Airborne GPS Positioning, Proc. KIS-94, Banff, Canada, August 30 - September 2, 1994.

Goldstein, H. (1980), Classical Mechanics, 2nd Edition, Addison-Wesley, Reading, Massachusetts, USA, 1980.

Grafarend, E.W. and S. Frenando (1985), Optimization and Design of Geodetic Networks, Springer-Verlag, Berlin, Germany, 1985.

Hamilton, W.C. (1964), Statistics in Physical Science, The Ronald Press Company, New York, 1964.

Hatch , R. (1989), Ambiguity Resolution in the Fast Lane, Proc. ION GPS-89, Colorado Springs, Colorado, September 27-29, 1989.

Hatch, R. (1991), Instantaneous Ambiguity Resolution, Proc. of IAG International Symposium 107 on Kinematic Systems in Geodesy, Surveying and Remote Sensing, Springer Verlag, New York, 1991.

Hazel, G. and S. L. Smith (1994), Instantaneous GPS Attitude Tests: Cycle Ambiguity Resolved, Proc. ION GPS-94, Salt Lake city, Utah, September 20-23, 1994.

Hofmann-Wellenhof, B., H. Lichtenegger and J. Collins (1992), Global Positioning System: Theory and Practice, Springer-Verlag, Wien, 1992.

Hwang, P.Y.C. and R.G. Brown (1989), GPS Navigation: Combining Pseudorange with Continuos Carrier Phase Using a Kalman Filter, Proc. ION GPS-92, Colorado Springs, Colorado, September 27-29, 1989.

Hwang, P.Y. (1990), A Near-Instantaneous Initialization Method for Attitude Determination, Proc. ION GPS-90, Colorado Springs, Colorado, September 1990.

Jonge, P.J. and C. C. Tiberius (1994), A New GPS Ambiguity Estimation Method Based on Integer Least Squares, Proc. KIS-94, Banff, Canada, August 30 - September 2, 1994.

Jurgens, R., C.E. Rodgers and L.C. Fan (1991), Advances in GPS Attitude Determining Technology as Developed for The Strategic Defense Command, Proc. ION GPS-91, Albuquerque, New Mexico, September 11-13, 1991.

Jurgens, R., L. Fan, D. Diefes and C. Rodgers (1992), Measurement of Errors in GPS Attitude Determining Systems, Proc. ION GPS-92, Albuquerque, New Mexico, September 16-18, 1992.

Knight, J. and R. Hatch (1990), Attitude Determination Via GPS, Proc. KIS 1990 Symposium No. 107, Banff, September 10-13, 1990.

Knight, D. (1994), A New Method of Instantaneous Ambiguity Resolution, Proc. ION GPS-94, Salt Lake city, Utah, September 20-23, 1994.

Kruczynski, L.R., P.C. Li, A.G. Evans and B.R. Hermann (1989), Using GPS to Determine Vehicle Attitude: U.S.S. Yorktown Test Results. Proc. ION GPS-89, Colorado Springs, Colorado, September 27-29, 1989.

Kuhl, M., X. Qin and Cottrell (1994), Design Considerations and Operational Results of a GPS Attitude Determination Unit, Proc. ION GPS-94, Salt Lake city, Utah, September 20-23, 1994.

Lachapelle, G., M.E. Cannon and G. Lu (1992a), High Precision GPS Navigation with Emphasis on Carrier Phase Ambiguity Resolution, Marine Geodesy, April, 1992.

Lachapelle, G., M.E. Cannon and G. Lu (1992b), Ambiguity Resolution on the Fly - A Comparison of P Code and High Performance C/A Code Receiver Technologies, Proc. ION GPS-92, Albuquerque, New Mexico, September 16-18, 1992.

Lachapelle, G. (1993), Navstar GPS Theory and Applications, Dept. of Geomatics Engineering, The University of Calgary, Lectures Notes, ENGO 625, 1993.

Lachapelle, G., H. Sun, M.E. Cannon and G. Lu (1994a), Precise Aircraft-to-Aircraft Positioning Using A Multiple Receiver Configuration, Canadian Aeronautics and Space Journal, Vol. 40, No. 2, June, 1994.

Lachapelle, G., G. Lu and B. Loncarevic (1994b), Precise Shipborne Attitude Determination Using Wide Antenna Spacing, Proc. KIS-94, Banff, Canada, August 30 - September 2, 1994.

Landau, H. and H-J. Euler (1992), On-the-Fly Ambiguity Resolution for Precise Differential Positioning, Proc. ION GPS-92, Albuquerque, New Mexico, September 16-18, 1992.

Leick, A. (1990), GPS Satellite Surveying, A Willey-Interscience Publication, John Wiley & Sons, New York, 1990.

Lu, G. and G. Lachapelle (1990), Reliability Analysis Applied to Kinematic GPS Positioning and Velocity Estimation, Proc. of the International Symposium on Kinematic Positioning for Geodesy, Surveying and Remote Sensing, Springer Verlag, New York, 1990.

Lu, G., M.E. Cannon, G. Lachapelle and P. Kielland (1993), Attitude Determination in a Survey Launch Using Multi-Antenna GPS Technologies, Proc. ION National Technical Meeting, San Francisco, January 20-22, 1993.

Mader, G.L. (1990), Ambiguity Function Techniques for GPS Phase Initialization and Kinematic Solutions, Proc. of the Second International Symposium on Precise Positioning with the Global Positioning System, Ottawa, Sept. 3-7, 1990.

Malys, S. and J.A. Slater (1994), Maintenance and Enhancement of the World Geodetic System 1984, Proc. ION GPS-94, Salt Lake city, Utah, September 20-23, 1994.

McMillan, J.C. (1994), A GPS Attitude Error Model for Kalman Filtering, Proc. ION GPS-94, Salt Lake city, Utah, September 20-23, 1994.

Mikhail, E.M. and F. Ackermann (1977), Observations and Least Squares, IEP-A Don Donnelley Publisher, New York, 1977.

Milliken, R.J. and C.J. Zoller (1980), Principle of Operation of NAVSTAR and System Characteristics, Published in Navigation, the Institute of Navigation, Washington, D.C., 1980.

Pratt, A. (1993), Mathematical and Physical Modelling of Multipath Interference, Proc. ION GPS-93, Salt Lake city, Utah, September 22-24, 1993.

Qiu, W. (1993), An Analysis of Some Critical Error Sources in Static GPS Surveying, UCGE Report number 20054, Department of Geomatics Engineering, The University of Calgary, 1993.

Remondi, B.W. (1984), Using the Global Positioing System (GPS) Phase Observable for Relative Geodesy: Modeling, Processing, and Results, Ph.D. Disseratation, Centre for Space Research, The University of Texas at Austin, Austin, 1984.

Remondi, B.W. (1990), Pseudo-Kinematic GPS Results Using the Ambiguity Function Method, NOAA Technical Memorandum NOS NGS-52, Rockville, MD, 1990.

Richardus, P. (1966), Project Surveying, North-Holland Publishing House, Amsterdam, 1966.

Rodgers, C. (1992), Multipath Simulation software developed for the design of a low multipath DGPS Antenna for the U.S. Coast Guard, Proc. ION GPS-92, Albuquerque, New Mexico, September 16-18, 1992.

Rodgers, C. and A. R. Gardner (1993), Statistical Testing and Analysis of Performance Factors in GPS Attitude Determination Systems, Proc. ION GPS-93, Salt Lake city, Utah, September 22-24, 1993.

Sauermann K., M.H. Becker and K.Mathes (1993) Ambiguity Resolution “On-The-Fly” Using The Latest Generation of GPS-Receivers, Proc. ION GPS-93, Salt Lake city, Utah, September 22-24, 1993.

Schade, H.and M. Cramer (1994), Airborne Kinematic Attitude Determination with GPS for Photogrammetry and Remote Sensing, Proc. KIS-94, Banff, Canada, August 30 - September 2, 1994.

Schwarz, K.P., A. El-Mowafy and M. Wei (1992), Testing A GPS Attitude System in Kinematic Mode, Proc. ION GPS-92, Albuquerque, New Mexico, September 16-18, 1992.

Schwarz, K.P., Z. Li and A. El-Mowafy (1993), GPS Multipath Detection and Reduction Using Spectral Technique”, Presented at The International Association of Geodesy General Meeting, Beijing, P. R. of China, August 9-13, 1993.

Schwarz, K.P. and M. Wei (1994), Some Unsolved Problems in Airborne Gravimetry, Presented at The Symposium, Gravity and Geoid, Graz, Austria, September 11-17, 1994.

Schwarz, K.P., M.A. Chapman, M.E. Cannon, P. Gong and D. Cosandier (1994), A Precise Positioning/Attitude System in Support of airborne Remote Sensing, Presented at the GIS/ISPPRS Conference, Ottawa, Canada, June 6-10, 1994.

Sherrer, R. (1985), The WM GPS Primer, Wild Heerbrugg, Geodesy Division, Switzerland, Company Publications, 1985.

Sims, M. (1989), Phase centre variation in the Geodetic TI4100 GPS receiver System's Conical Spiral Antenna, Proc. IAG, Symposium 102, Edinburgh, Scotland, August 7-8, 1989.

Slama, C., C. Theurer and S. Henriksen (1980), Manual of Photogrammetry, American Society of Photogrammetry, Virginia, 1980.

Spilker Jr., J., (1977), Digital Communications by Satellite, Prentice-Hall, Inc., Englewood Cliffs, New Jersey, 1977.

Sun, H. (1994), Integration of INS with Multiple GPS Antennas for Airborne Applications, Proc. ION GPS-94, Salt Lake city, Utah, September 20-23, 1994.

Teunissen, P.J. (1994), A New Method for Fast Carrier Phase Ambiguity Estimation, Proc. KIS-94, Banff, Canada, August 30 - September 2, 1994.

Tranquilla, J.M. and B.G. Colpitts (1988), GPS Antenna Design Characteristics for High Precision Applications, ASCE Specialty Conference GPS 88 Engineering Applications of GPS Satellite Surveying Technology, Nashville, TN, May 11-14, 1988.

Tranquilla, J.M. and J.P. Carr (1991), GPS Multipath Field Observations at Land and Water Sites, Navigation, Journal of the US Institute of Navigation, 1991.

Van Grass, F. and M.S. Braasch (1991), GPS Interferometric Attitude and Heading Determination: Flight Test Results, Proc. ION National Technical Meeting, Phoenix, Arizona, January 22-25, 1991.

Vaniček, P. and E.J. Krakiwsky (1982), Geodesy the Concepts, North-Holland Publishing Company, New York, N.Y., 1982.

Van Nee, D.J.R (1991), Multipath Effects on GPS Code Phase Measurements, Proc. ION GPS-91, Albuquerque, New Mexico, September 11-13, 1991.

Wells, D., N. Beck, D. Delikaraoglu, A. Kleusberg, E. Krakiwsky, G. Lachapelle, R. Langley, M. Nakiboglu, K.P. Schwarz, J. Tranquilla and P. Vanicek, (1986), Guide to GPS Positioning, The University of New Brunswick, Fredericton, New Brunswick, December, 1986.

Wertz, J.R. (1978), Spacecraft Attitude Determination and Control, Kluwer Academic Publishers, The Netherlands, 1978.

Westrop J., M.E. Napier and V. Ashkenazi (1989), Cycle Slips On the Move: Detection and Elimination, Proc. ION GPS-89, Colorado Springs, Colorado, September 27-29, 1989.

Wong, l. (1979), Mathematics Hand Book, Advanced Education Express, Beijing, China, 1979.

For a given attitude matrix T, Cayley axis and angle parameters can be determined as follows:

$$\cos\alpha = 1/2\ [\ \mathrm{trace}(T) - 1] \tag{A.4}$$

$$e_1 = (t_6 - t_8) / (2 \sin\alpha) \tag{A.5}$$

$$e_2 = (t_7 - t_3) / (2 \sin\alpha) \tag{A.6}$$

$$e_3 = (t_2 - t_4) / (2 \sin\alpha) \tag{A.7}$$

where:

$$T = \begin{bmatrix} t_1 & t_2 & t_3 \\ t_4 & t_5 & t_6 \\ t_7 & t_8 & t_9 \end{bmatrix} \tag{A.8}$$

A drawback of using Cayley axis and angle parameterization is that the components e_i cannot be determined when $\sin\alpha$ is equal to zero.

A.2 Euler Symmetric Parameters (quaternions)

Another representation of the attitude matrix can be giving using four mathematical parameters (q_1, q_2, q_3, and q_4) known as quaternions. They can be defined in terms of Cayley axis and angle parameters as follows:

$$q_1 = e_1 \sin\frac{\alpha}{2} \tag{A.9}$$

$$q_2 = e_2 \sin\frac{\alpha}{2} \tag{A.10}$$

$$q_3 = e_3 \sin\frac{\alpha}{2} \tag{A.11}$$

$$q_4 = \cos\frac{\alpha}{2} \tag{A.12}$$

Only three quaternions are independent, as they satisfy the equation:

$$q_1^2+q_2^2+q_3^2+q_4^2 = 1 \tag{A.13}$$

The attitude matrix can be expressed in terms of quaternions by:

APPENDIX A

ATTITUDE PARAMETERIZATION

A.1 Cayley Axis/angle

The attitude matrix is a proper real orthogonal matrix. This matrix must have at least one eigenvector with eigenvalue unity. That is, there exists a unit vector, $\bar{\mathbf{e}}$, which does not change when multiplied by the attitude matrix, i.e.,:

$$\mathrm{T}\,\bar{\mathbf{e}} = \bar{\mathbf{e}} \tag{A.1}$$

where T denotes the attitude matrix. This means that $\bar{\mathbf{e}}$ is a vector along the axis of rotation. If this axis is determined, vector transformation between the body frame and the reference frame can be accomplished by rotating the first frame about the single axis of rotation by only one angle (α). The attitude matrix T can then be given as:

$$\mathrm{T} = \begin{bmatrix} \cos\alpha + e_1^2\,(1-\cos\alpha) & e_1e_2\,(1-\cos\alpha) + e_3\sin\alpha & e_1e_3\,(1-\cos\alpha) - e_2\sin\alpha \\ e_1e_2\,(1-\cos\alpha) - e_3\sin\alpha & \cos\alpha + e_2^2\,(1-\cos\alpha) & e_2e_2\,(1-\cos\alpha) + e_1\sin\alpha \\ e_1e_3\,(1-\cos\alpha) + e_2\sin\alpha & e_2e_3\,(1-\cos\alpha) - e_1\sin\alpha & \cos\alpha + e_3^2\,(1-\cos\alpha) \end{bmatrix} \tag{A.2}$$

(Wertz,1978), where e_1, e_2, e_3 are the components of the axis of rotation in the reference frame. This representation of the rigid body orientation is called the Cayley axis and angle parameterization. Since e_1, e_2, e_3 are related by:

$$e_1^2+e_2^2+e_3^2 = 1 \tag{A.3}$$

Cayley axis and angle parameterization only depends on three parameters.

$$T = \begin{bmatrix} q_1^2-q_2^2-q_3^2+q_4^2 & 2(q_1q_2+q_3q_4) & 2(q_1q_3-q_2q_4) \\ 2(q_1q_2-q_3q_4) & -q_1^2+q_2^2-q_3^2+q_4^2 & 2(q_2q_3+q_1q_4) \\ 2(q_1q_3+q_2q_4) & 2(q_2q_3-q_1q_4) & -q_1^2-q_2^2+q_3^2+q_4^2 \end{bmatrix} \tag{A.14}$$

Knowing the elements of a specific attitude matrix, the quaternions can be derived as follows (Wertz,1978):

$$q_4 = \pm\frac{1}{2}\sqrt{1+t_1+t_5+t_9} \tag{A.15}$$

$$q_1 = \frac{1}{4q_4}(t_6 - t_8) \tag{A.16}$$

$$q_2 = \frac{1}{4q_4}(t_7 - t_3) \tag{A.17}$$

$$q_3 = \frac{1}{4q_4}(t_2 - t_4) \tag{A.18}$$

The use of equation (A.15) to (A.18) is not the only method for determining quaternions from the attitude matrix, other methods are also available. All of them are mathematically equivalent.

Using quaternions for attitude parameterization is more convenient than using the attitude matrix because only three independent parameters are needed rather than nine. Also, determination of quaternions is mathematically more efficient than computing Cayley axis and angle parameters since no trigonometric functions are involved. The quaternions are not widely used for attitude parameterization in navigation with GPS mainly because they do not represent physical quantities.

A.3 Gibbs Vector

Another approach for attitude parameterization is given by the Gibbs vector. The number of parameters needed for attitude determination using this approach is three, defined as: g_1, g_2, and g_3. The attitude matrix is given in terms of Gibbs parameters as follows:

$$T = \frac{1}{1+g_1^2+g_2^2+g_3^2}\begin{bmatrix} 1+g_1^2-g_2^2-g_3^2 & 2(g_1g_2+g_3) & 2(g_1g_3-g_2) \\ 2(g_1g_2-g_3) & 1-g_1^2+g_2^2-g_3^2 & 2(g_2g_3+g_1) \\ 2(g_1g_3+g_2) & 2(g_2g_3-g_1) & 1-g_1^2-g_2^2+g_3^2 \end{bmatrix} \quad \text{(A.19)}$$

Gibbs parameters can also be related to Cayley axis/angle parameters and quaternions by the following equations (Wertz,1978):

$$g_1 = q_1/q_4 = e_1 \tan \frac{\alpha}{2} \quad \text{(A.20)}$$

$$g_2 = q_2/q_4 = e_2 \tan \frac{\alpha}{2} \quad \text{(A.21)}$$

$$g_3 = q_3/q_4 = e_3 \tan \frac{\alpha}{2} \quad \text{(A.22)}$$

As equation (A.20) to (A.22) show, Gibbs parameters become infinite when the rotation angle (α) is an odd multiple of 180 degree

If the rotation matrix is given, Gibbs parameters can be determined as follows:

$$g_1 = \frac{t_6 - t_8}{1+ t_1 + t_5 + t_9} \quad \text{(A.23)}$$

$$g_2 = \frac{t_7 - t_3}{1+ t_1 + t_5 + t_9} \quad \text{(A.24)}$$

$$g_3 = \frac{t_2 - t_4}{1+ t_1 + t_5 + t_9} \quad \text{(A.25)}$$

A.4 Euler Angles

The attitude matrix is a coordinate transformation matrix between the body frame and the reference frame. Thus, it can be simply obtained by forming the matrix product of three matrices of successive rotations about the axes of the body frame. Since there is one rotation angle for each axis, the attitude matrix will be a function of three rotation angles. The attitude can then be parameterized by the three rotation angles, which can be taken as ψ_E, θ_E, and φ_E. Figure A.1 illustrates the rotation between the body frame (x,y,z), and the reference frame, expressed by the orthogonal triad (u,v,w). A simple representation of the transformation process can be obtained by performing a rotation about the axis y by the angle φ_E, followed by a rotation about the axis x by the angle θ_E, and finally a rotation about the axis z by the angle ψ_E. Because of this clear physical interpretation of Euler angles, they are widely used in navigation with GPS.

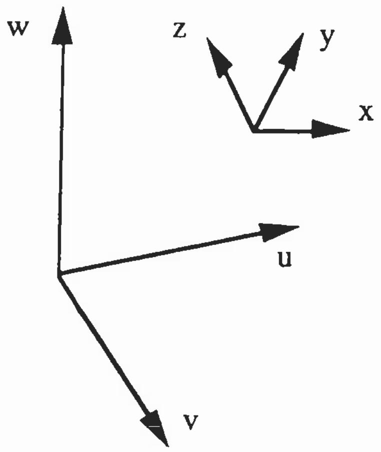

Fig. A.1 The body frame and the reference frame

Because Euler rotation angles are affected by the successive orientations of the body frame with respect to the local-level frame, which is dependent on the sequence used, Euler angles are, in general, not the same as the attitude parameters defined in Section 2.3. Therefore, these angles must be corrected using techniques similar to the one given in Section 2.3.

The sequence of rotations about the body axes can be performed in 12 distinct ways with the restriction that no successive rotations are permitted about the same axis because successive rotations are equivalent to one rotation by the sum of the rotation angles. Appendix B gives the transformation matrices for all the 12 possible Euler angle representations. They can be divided into two types:

Type I: In which the rotations take place successively about each of the three coordinate axes. This type has a singularity at $\theta_E = \pm 90$ degrees.

Type II: In this case, the first and third rotations take place about the same axis and the second rotation takes place about one of the other two axes. This type has a singularity when θ_E is zero or 180 degree.

The main obstacle in determining Euler angles directly from the attitude matrix is that the sequence of rotations is unknown. Thus, other techniques should be implemented instead of the direct approach.

Finally, transformation between one set of attitude parameterization to another is always possible. For instance, if Euler angles are determined and have been substituted in the rotation sequence z-y-z, the Euler symmetric parameters (quaternions) can be evaluated as follows (Wertz,1978):

$$q_1 = \sin\frac{\theta_E}{2}\cos\frac{(\varphi_E - \psi_E)}{2} \tag{A.26}$$

$$q_2 = \sin\frac{\theta_E}{2}\sin\frac{(\varphi_E - \psi_E)}{2} \tag{A.27}$$

$$q_3 = \cos\frac{\theta_E}{2}\sin\frac{(\varphi_E + \psi_E)}{2} \tag{A.28}$$

$$q_4 = \cos\frac{\theta_E}{2}\cos\frac{(\varphi_E + \psi_E)}{2}\,. \tag{A.29}$$

APPENDIX B

THE ATTITUDE MATRIX FOR THE 12 POSSIBLE EULER ANGLE REPRESENTATIONS

B.1 Type I Representation

In this type of the attitude matrix parameterization, the rotations take place successively about each of the three coordinate axes. Six rotation sequences can be performed. They are (Wertz,1978):

$$T_{y\text{-}x\text{-}z} = \begin{bmatrix} s(\psi_E)s(\theta_E)s(\varphi_E)+c(\psi_E)c(\varphi_E) & c(\theta_E)s(\psi_E) & s(\psi_E)s(\theta_E)c(\varphi_E)-c(\psi_E)s(\varphi_E) \\ s(\varphi_E)s(\theta_E)c(\psi_E)-c(\varphi_E)s(\psi_E) & c(\theta_E)c(\psi_E) & c(\psi_E)s(\theta_E)c(\varphi_E)+s(\psi_E)s(\varphi_E) \\ s(\varphi_E)c(\theta_E) & -s(\theta_E) & c(\varphi_E)c(\theta_E) \end{bmatrix}$$

$$T_{z\text{-}x\text{-}y} = \begin{bmatrix} c(\psi_E)c(\varphi_E)-s(\psi_E)s(\theta_E)s(\varphi_E) & s(\psi_E)s(\theta_E)c(\varphi_E)+c(\psi_E)s(\varphi_E) & -c(\theta_E)s(\psi_E) \\ -s(\varphi_E)c(\theta_E) & c(\varphi_E)c(\theta_E) & s(\theta_E) \\ s(\varphi_E)s(\theta_E)c(\psi_E)+c(\varphi_E)s(\psi_E) & s(\psi_E)s(\varphi_E)-c(\psi_E)s(\theta_E)c(\varphi_E) & c(\theta_E)c(\psi_E) \end{bmatrix}$$

$$T_{z\text{-}y\text{-}x} = \begin{bmatrix} c(\varphi_E)c(\theta_E) & s(\varphi_E)c(\theta_E) & -s(\theta_E) \\ s(\psi_E)s(\theta_E)c(\varphi_E)-c(\psi_E)s(\varphi_E) & c(\psi_E)c(\varphi_E)+s(\psi_E)s(\theta_E)s(\varphi_E) & c(\theta_E)s(\psi_E) \\ s(\psi_E)s(\varphi_E)+c(\psi_E)s(\theta_E)c(\varphi_E) & s(\varphi_E)s(\theta_E)c(\psi_E)-c(\varphi_E)s(\psi_E) & c(\theta_E)c(\psi_E) \end{bmatrix}$$

$$T_{x\text{-}y\text{-}z} = \begin{bmatrix} c(\theta_E)c(\psi_E) & s(\varphi_E)s(\theta_E)c(\psi_E)+c(\varphi_E)s(\psi_E) & s(\psi_E)s(\varphi_E)-c(\psi_E)s(\theta_E)c(\varphi_E) \\ -c(\theta_E)s(\psi_E) & c(\psi_E)c(\varphi_E)-s(\psi_E)s(\theta_E)s(\varphi_E) & s(\psi_E)s(\theta_E)c(\varphi_E)+c(\psi_E)s(\varphi_E) \\ s(\theta_E) & -s(\varphi_E)c(\theta_E) & c(\varphi_E)c(\theta_E) \end{bmatrix}$$

$$T_{x\text{-}z\text{-}y} = \begin{bmatrix} c(\theta_E)c(\psi_E) & s(\psi_E)s(\varphi_E)+c(\psi_E)s(\theta_E)c(\varphi_E) & s(\varphi_E)s(\theta_E)c(\psi_E)-c(\varphi_E)s(\psi_E) \\ -s(\theta_E) & c(\varphi_E)c(\theta_E) & s(\varphi_E)c(\theta_E) \\ c(\theta_E)s(\psi_E) & s(\psi_E)s(\theta_E)c(\varphi_E)-c(\psi_E)s(\varphi_E) & c(\psi_E)c(\varphi_E)+s(\psi_E)s(\theta_E)s(\varphi_E) \end{bmatrix}$$

$$T_{y\text{-}z\text{-}x} = \begin{bmatrix} c(\varphi_E)c(\theta_E) & s(\theta_E) & -s(\varphi_E)c(\theta_E) \\ s(\psi_E)s(\varphi_E)-c(\psi_E)s(\theta_E)c(\varphi_E) & c(\theta_E)c(\psi_E) & s(\varphi_E)s(\theta_E)c(\psi_E)+c(\varphi_E)s(\psi_E) \\ s(\psi_E)s(\theta_E)c(\varphi_E)+c(\psi_E)s(\varphi_E) & -c(\theta_E)s(\psi_E) & c(\psi_E)c(\varphi_E)-s(\psi_E)s(\theta_E)s(\varphi_E) \end{bmatrix}$$

where T is the attitude matrix, (x,y,z) are coordinate axes of the body frame, s and c denote the sine and cosine respectively. ψ_E, θ_E, φ_E are Euler angles, corresponding to the heading, pitch, and roll, respectively.

B.2 Type II Representation

In this case, the first and third rotations take place about the same axis and the second rotation takes place about one of the other two axes. Six rotation sequences can be used. They are (Wertz,1978):

$$T_{x\text{-}y\text{-}x} = \begin{bmatrix} c(\theta_E) & s(\varphi_E)s(\theta_E) & -s(\theta_E)c(\varphi_E) \\ s(\psi_E)s(\theta_E) & c(\psi_E)c(\varphi_E)-s(\psi_E)c(\theta_E)s(\varphi_E) & s(\psi_E)c(\theta_E)c(\varphi_E)+c(\psi_E)s(\varphi_E) \\ c(\psi_E)s(\theta_E) & -s(\psi_E)c(\varphi_E)-c(\psi_E)c(\theta_E)s(\varphi_E) & c(\varphi_E)c(\theta_E)c(\psi_E)-s(\varphi_E)s(\psi_E) \end{bmatrix}$$

$$T_{x\text{-}z\text{-}x} = \begin{bmatrix} c(\theta_E) & c(\varphi_E)s(\theta_E) & s(\theta_E)s(\varphi_E) \\ -c(\psi_E)s(\theta_E) & c(\varphi_E)c(\theta_E)c(\psi_E)-s(\varphi_E)s(\psi_E) & s(\varphi_E)c(\theta_E)c(\psi_E)+c(\varphi_E)s(\psi_E) \\ s(\psi_E)s(\theta_E) & -s(\psi_E)c(\theta_E)c(\varphi_E)-c(\psi_E)s(\varphi_E) & -s(\psi_E)c(\theta_E)s(\varphi_E)+c(\psi_E)c(\varphi_E) \end{bmatrix}$$

$$T_{y\text{-}x\text{-}y} = \begin{bmatrix} -s(\psi_E)c(\theta_E)s(\varphi_E)+c(\psi_E)c(\varphi_E) & s(\psi_E)s(\theta_E) & -s(\psi_E)c(\theta_E)c(\varphi_E)-c(\psi_E)s(\varphi_E) \\ s(\varphi_E)s(\theta_E) & c(\theta_E) & s(\theta_E)c(\varphi_E) \\ c(\psi_E)c(\theta_E)s(\varphi_E)+s(\psi_E)c(\varphi_E) & -c(\psi_E)s(\theta_E) & c(\varphi_E)c(\theta_E)c(\psi_E)-s(\varphi_E)s(\psi_E) \end{bmatrix}$$

$$T_{y\text{-}z\text{-}y} = \begin{bmatrix} c(\psi_E)c(\theta_E)c(\varphi_E)-s(\psi_E)s(\varphi_E) & c(\psi_E)s(\theta_E) & -c(\psi_E)c(\theta_E)s(\varphi_E)-s(\psi_E)c(\varphi_E) \\ -c(\varphi_E)s(\theta_E) & c(\theta_E) & s(\theta_E)s(\varphi_E) \\ s(\psi_E)c(\theta_E)c(\varphi_E)+c(\psi_E)s(\varphi_E) & s(\psi_E)s(\theta_E) & -s(\psi_E)c(\theta_E)s(\varphi_E)+c(\psi_E)c(\varphi_E) \end{bmatrix}$$

$$T_{z\text{-}x\text{-}z} = \begin{bmatrix} c(\psi_E)c(\varphi_E)-s(\psi_E)c(\theta_E)s(\varphi_E) & c(\psi_E)s(\varphi_E)+s(\psi_E)c(\theta_E)c(\varphi_E) & s(\psi_E)s(\theta_E) \\ -s(\psi_E)c(\varphi_E)-c(\psi_E)c(\theta_E)s(\varphi_E) & -s(\psi_E)s(\varphi_E)+c(\psi_E)c(\theta_E)c(\varphi_E) & c(\psi_E)s(\theta_E) \\ s(\theta_E)s(\varphi_E) & -s(\theta_E)c(\varphi_E) & c(\theta_E) \end{bmatrix}$$

$$T_{z\text{-}y\text{-}z} = \begin{bmatrix} -s(\psi_E)s(\varphi_E)+c(\psi_E)c(\theta_E)c(\varphi_E) & s(\psi_E)c(\varphi_E)+c(\psi_E)c(\theta_E)s(\varphi_E) & -c(\psi_E)s(\theta_E) \\ -c(\psi_E)s(\varphi_E)-s(\psi_E)c(\theta_E)c(\varphi_E) & c(\psi_E)c(\varphi_E)-s(\psi_E)c(\theta_E)s(\varphi_E) & s(\psi_E)s(\theta_E) \\ s(\theta_E)c(\varphi_E) & s(\theta_E)s(\varphi_E) & c(\theta_E) \end{bmatrix}$$

APPENDIX C

DETAILED ATTITUDE RESULTS

In this appendix, complete attitude results are given for all tests, mentioned in this thesis, in which the attitude outputs of the multi-antenna system (3DF) were referenced to simultaneous outputs of the Litton 90/100 inertial system (INS). The differences of the outputs between the two systems are given in the main text. Since in the static case the results of the inertial system are usually constants at the plotting scale, only 3DF results are given. In the kinematic case, both 3DF and INS results are presented since they change with time.

C.1 Truck Results

This section gives the attitude results (heading, pitch, roll) of the truck test described in Chapter 5.

C.1.1 Static Results

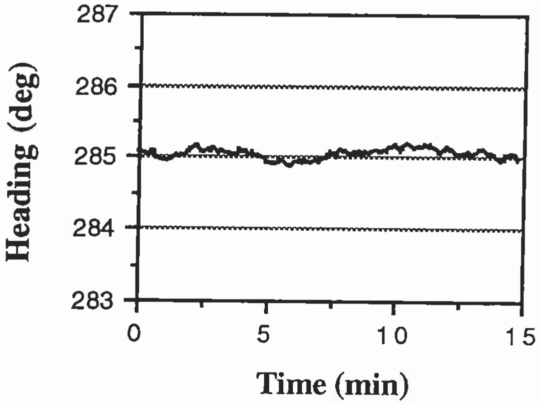

Fig C.1 3DF heading

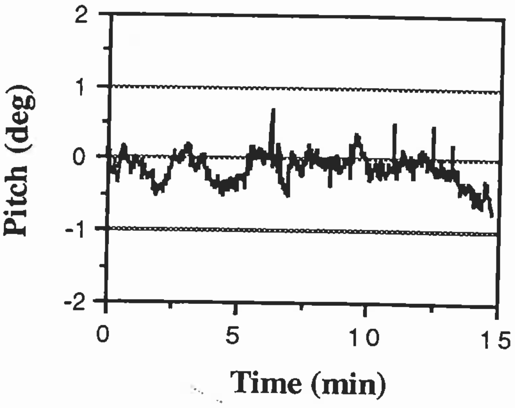

Fig C.2 3DF pitch

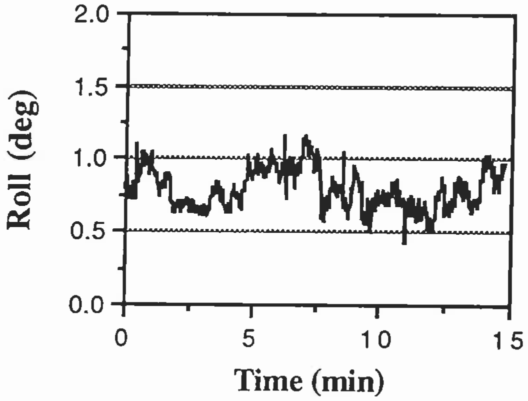

Fig. C.3 3DF roll

C.1.2 Kinematic Results

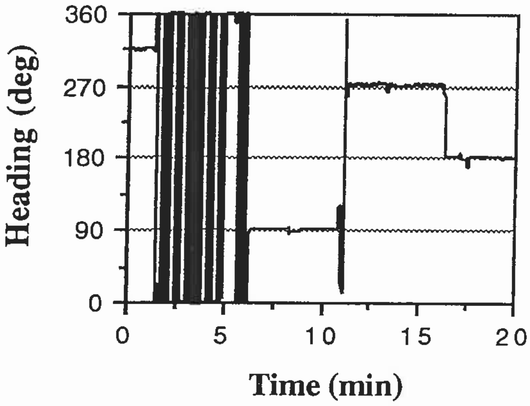

Fig C.4 3DF heading

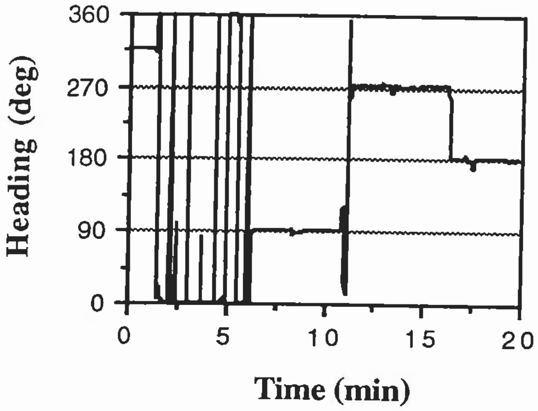

Fig C.5 INS heading

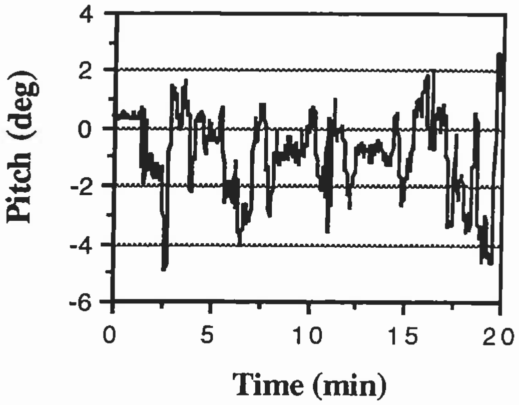

Fig C.6 3DF pitch

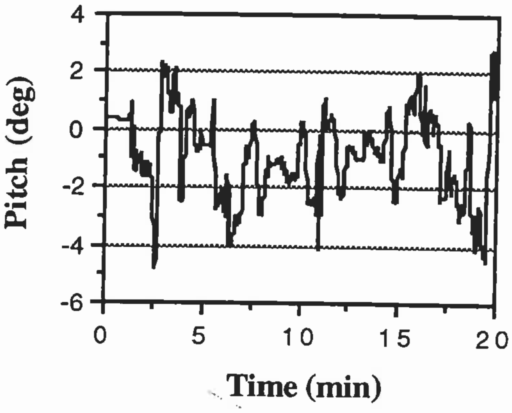

Fig C.7 INS pitch

The jumps shown in heading figure (from 0 to 360 degrees) are due to differences in steering when heading north.

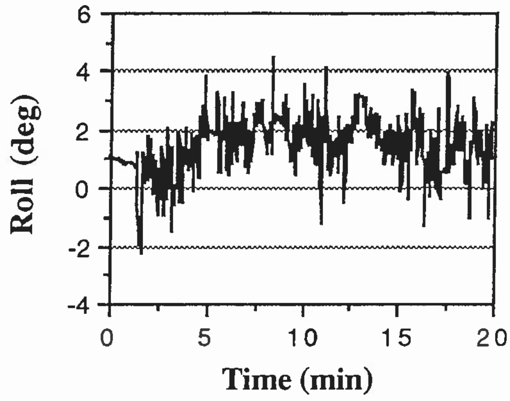

Fig C.8 3DF roll

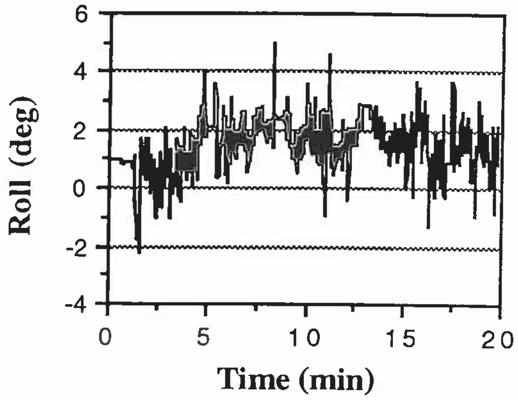

Fig C.9 INS roll

C.2 First Series of Van Tests

The following are attitude results of the first series of van tests described in Section 8.3.1.

C.2.1 Static Results

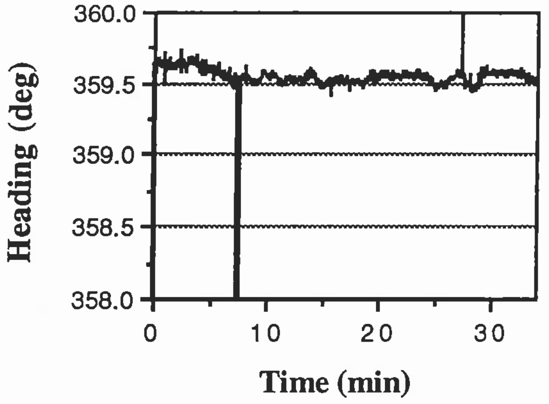

Fig C.10 3DF heading - test (1)

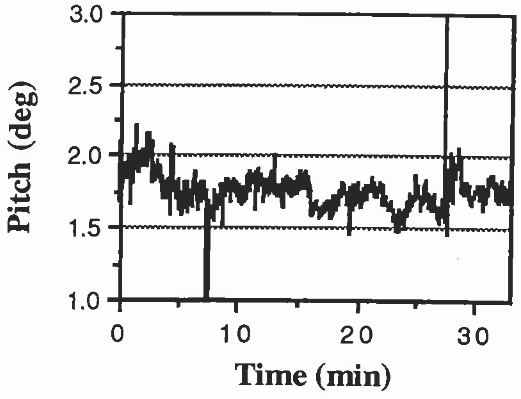

Fig C.11 3DF pitch - test (1)

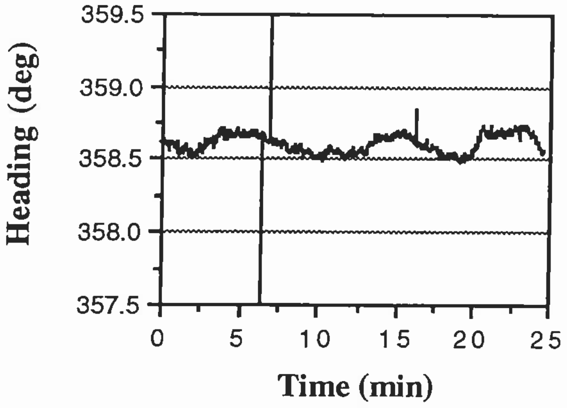

Fig C.12 3DF heading - test (1)

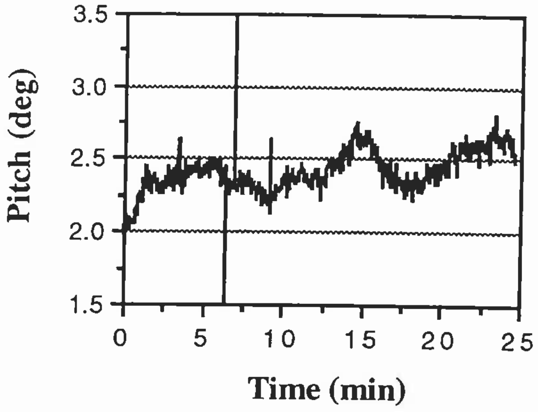

Fig C.13 3DF pitch - test (2)

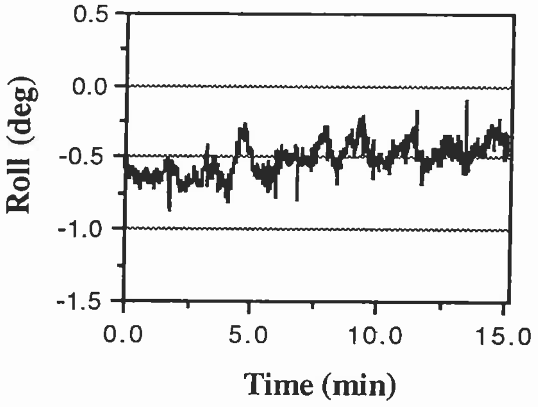

Fig. C.14 3DF roll

C.2.2 Kinematic Results

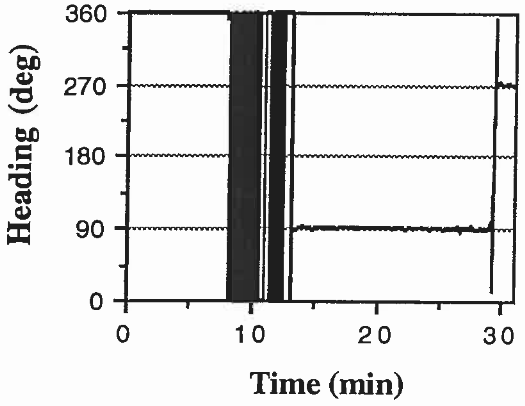

Fig C.15 3DF heading - test (1)

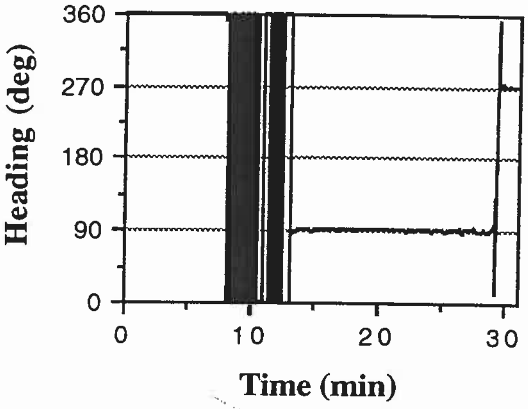

Fig C.16 INS heading - test (1)

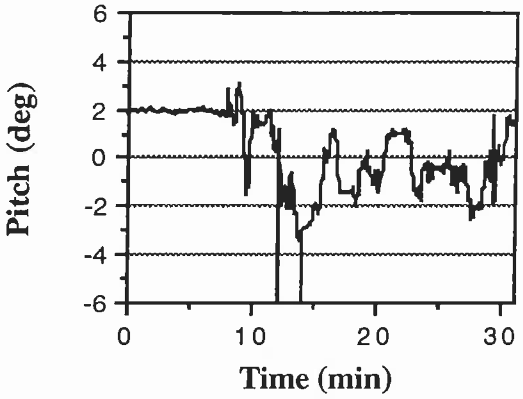

Fig. C.17 3DF pitch - test (1)

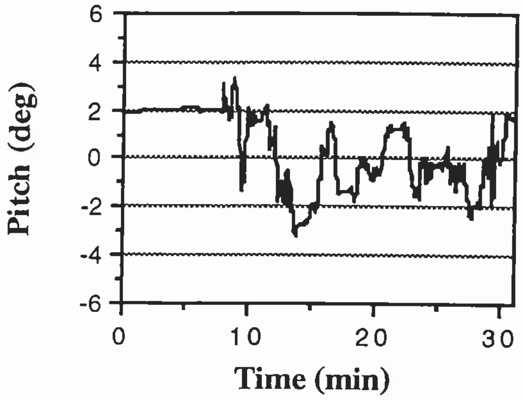

Fig. C.18 INS pitch - test (1)

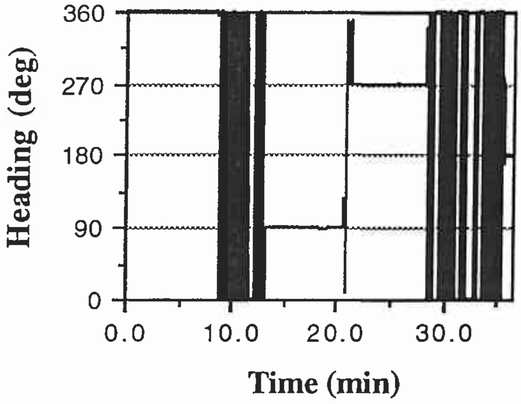

Fig C.19 3DF heading - test (2)

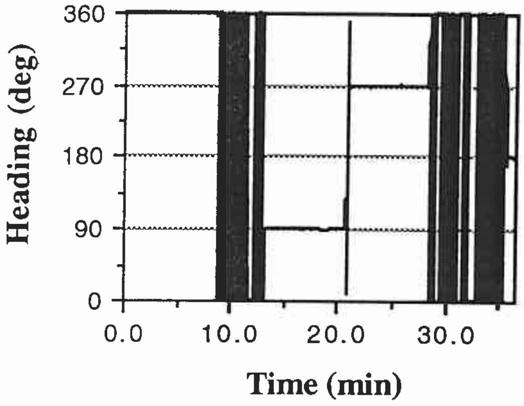

Fig C.20 INS heading - test (2)

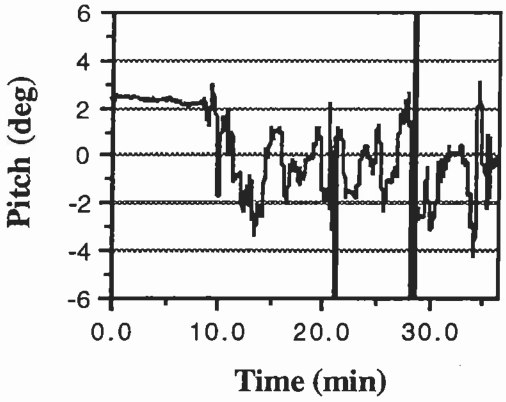

Fig. C.21 3DF pitch - test (2)

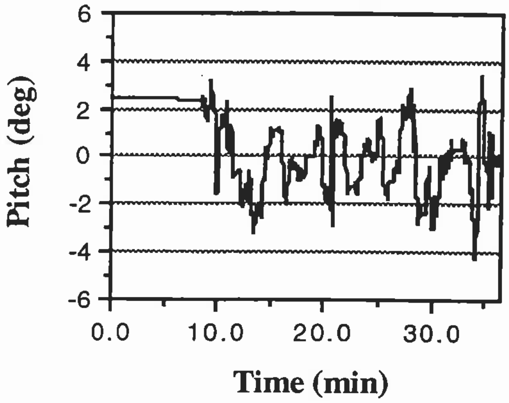

Fig. C.22 INS pitch - test (2)

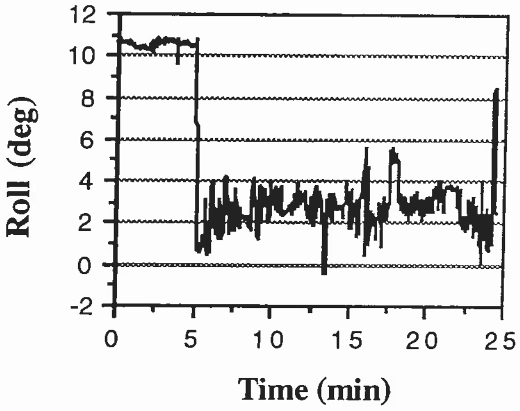

Fig. C.23 3DF roll

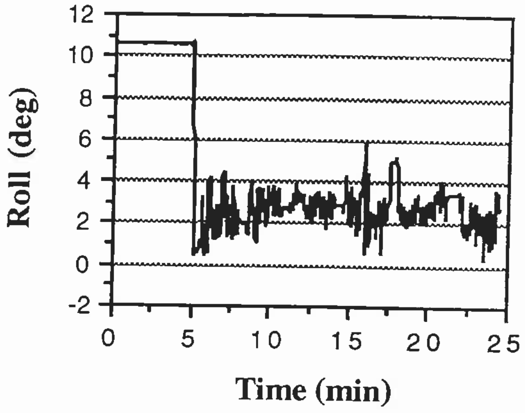

Fig. C.24 INS roll

C.3 Second Series of Van Tests

In this section, the 3DF attitude results of the second series of van tests, described in Section 8.3.2, are given. Static and kinematic results are shown in the same plots.

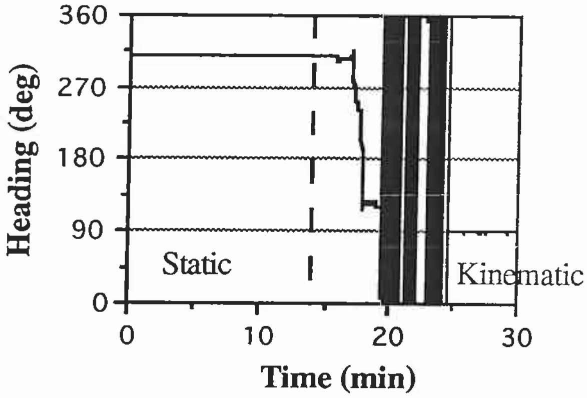

Fig. C.25 3DF heading

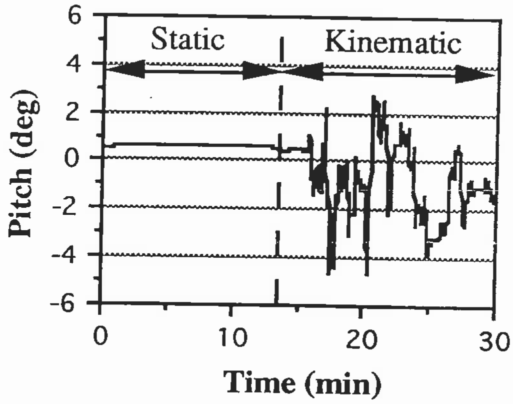

Fig. C.26 3DF pitch

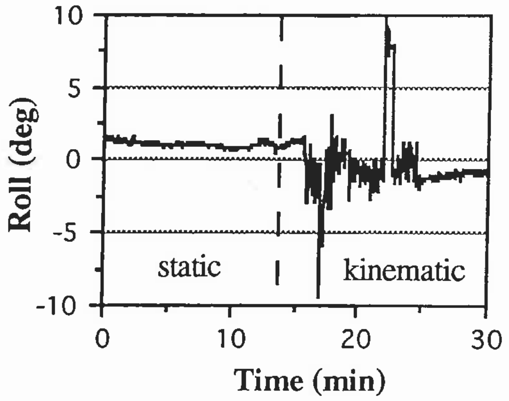

Fig. C.27 3DF roll

C.4 Airborne Results

Complete attitude results of the aircraft tests described in Section 8.3.3 are given in this section.

C.4.1 Static Results

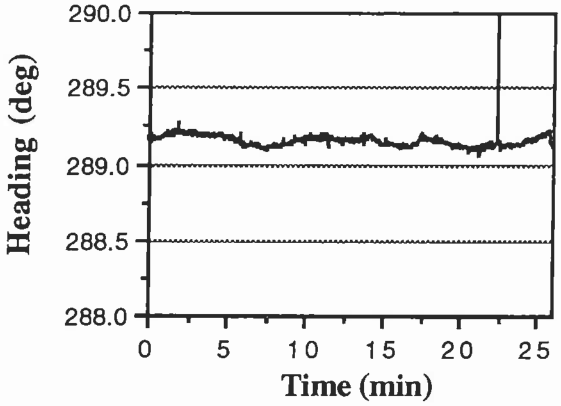

Fig. C.28 3DF heading

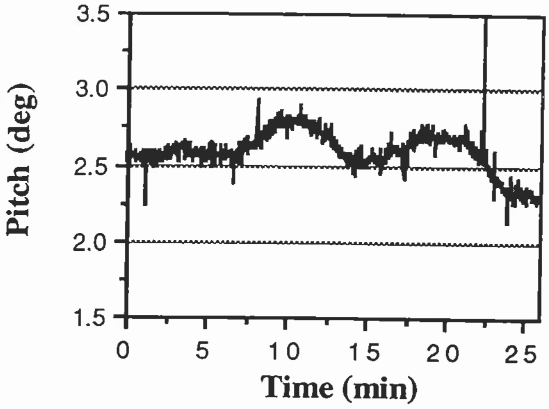

Fig. C.29 3DF pitch

C.4.2 Kinematic Results

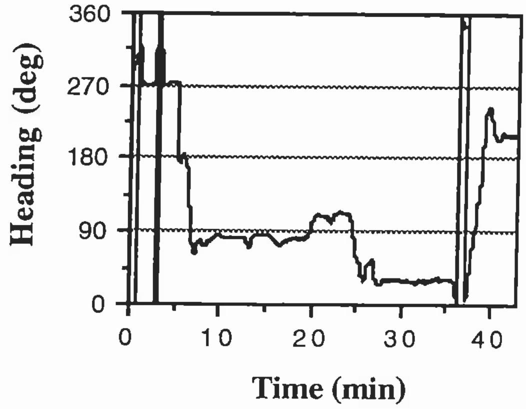

Fig. C.30 3DF heading

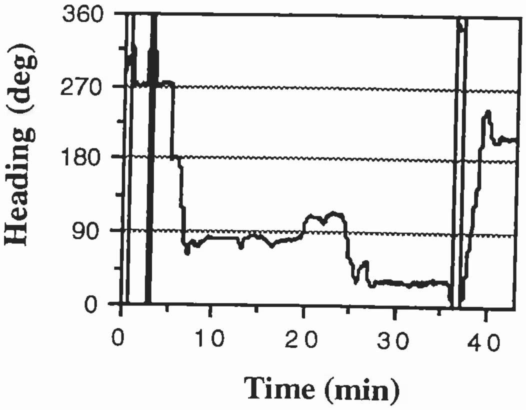

Fig. C.31 INS heading

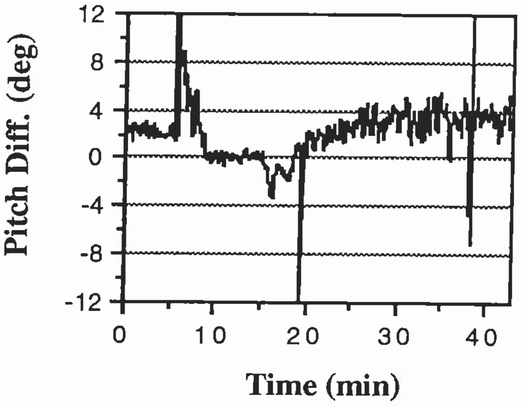

Fig. C.32 3DF pitch

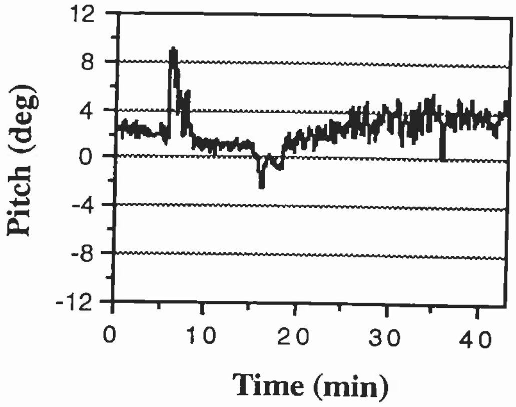

Fig. C.33 INS pitch